UNIVERSITY OF OKLAHOMA
GRADUATE COLLEGE

EXPLORING SOUTHEAST UNITED STATES SEVERE ENVIRONMENTS USING ATMOSPHERIC SOUNDINGS

A DISSERTATION
SUBMITTED TO THE GRADUATE FACULTY
in partial fulfillment of the requirements for the
Degree of
DOCTOR OF PHILOSOPHY

by LAUREN E. POUNDS
Norman, Oklahoma
2026

Downloaded from SHAREOK. Persistent Handle URL: https://hdl.handle.net/11244/342790

EXPLORING SOUTHEAST UNITED STATES SEVERE ENVIRONMENTS USING ATMOSPHERIC SOUNDINGS

A DISSERTATION APPROVED FOR THE
SCHOOL OF METEOROLOGY

BY THE COMMITTEE CONSISTING OF

Dr. Michael Coniglio (Chair)

Dr. Matthew Flournoy

Dr. David Bodine

Dr. Stacey Hitchcock

Dr. Cameron Homeyer

Dr. Joseph Ripberger

©Copyright by LAUREN E. POUNDS 2026

All Rights Reserved.

Acknowledgments

I first want to acknowledge the funding source for this work, Weather Program Office VORTEX-USA award, NA23OAR4590344, and the NOAA/Office of Oceanic and Atmospheric Research under NOAA-University of Oklahoma Cooperative Agreement NA21OAR4320204. The School of Meteorology at OU, CIWRO, and NSSL have all provided me with the resources and support necessary to complete my degree. I am thankful for all the opportunities I was given as a graduate student at OU/CIWRO/NSSL from flying on the NOAA P-3 aircraft around supercells in South Dakota, to serving as the student representative for the colloquium committee and getting to organization many lunches and have thoughtful conversations with renowned scientists, to driving a mobile mesonet truck towards an ongoing EF–4 tornado in the Mississippi Delta (safely, for science), to spending hours in a truck on field-campaigns with scientists I always looked up to, to attending conferences to present my work in my hometown and in new states I got to check off my list, to being able to lead a paper discussion group where we both talk science and have lots of laughs, among so many more career building opportunities. I'm proud of myself for taking a chance back in 2019 and moving to Oklahoma where I didn't know anyone—it was worth it. I didn't understand then just how special the National Weather Center was, but now I know, and am thankful I get to be part of the community.

While OU provided the foundation to become a great scientist, I wouldn't be here without the support of my advisors. Matt, I want to thank you for providing a place for me in your research group as soon as I mentioned I wanted to work with y'all (and for writing a proposal on my dream research topic, I couldn't have asked for a more perfect project). I am also thankful you created a group for all of your students, and

provided a collaborative environment for us to learn in. I have learned so much in the past four years from both of you during our science chats, and those discussions always remind me why we do what we do. I think back to four years ago and I can see just how much I have grown as a scientist under y'all's guidance. You have also opened so many doors for me, and I am thankful for every opportunity you provided and all those you encouraged me to take. I am also thankful for the trust y'all have put in me, especially when I doubted myself—my confidence has grown because of it (to an acceptable level). Beyond science, I want to thank both of you always being so understanding and supportive when I had took time to put my family first. You have shown me so much empathy, so much kindness, and I am forever thankful I had that during some of the most difficult times of my life. I hope I can one day be the kind of mentor for someone as you both were for me—I want to be just like you y'all when I grow up!

To my committee members, Cameron, Stacey, David, and Joe, thanks for taking the time to serve on my committee and provide different perspectives on my work. Cameron, thank you for your support from my Master's to Ph.D. and being a part of it from start to end. Your praise always makes me feel proud. I will always brag about having the best committee.

I also want to thank all of those, besides my advisors, that helped me professionally along the way. Rachel, thanks so much for tackling all of this sounding data with me. I'm glad we didn't have to do it alone, and I am so thankful I had someone there to bounce ideas off of. Also, thanks for your overall support throughout my entire graduate school career, and always being there to listen. Tony, thank you for always entertaining me with discussion of SE severe storms as me, you, and Erik spent endless hours driving across the country during TORUS and PERiLS. Also, thank you for letting me join you for damage surveys—I am glad I had that experience and I learned

so much. Thanks to Matt, Mike, Rachel, Tony, Bobby, Isabelle, Morgan, and Andy for all the science chats during research group and grant meetings, especially the chats we had about 12 times regarding the same plot (you know the one). I learned so much over the years getting during those discussions, and always looked forward to meeting with the group. I hope we can all continue to do science together.

The past seven years were made fun (and possible) primarily because of the people I got to do it with. Sean, thank you for being there for me from my second day in Norman. To my first roommate here and birthday buddy, Mike, I am glad we went through this journey together, and my grades thank the giant whiteboard we put up in the kitchen. To Morgan and Francesca, I loved living with you two and all the good times we had in the Edgemere house. While our house taking a direct hit from a tornado wasn't in the plan, we saw just how quickly our people would come together for us. Thank you to everyone who helped us in that time—I hope we never have to pick tens of thousands of pieces of fiberglass from our yard again. Especially thank you to Mel, for organizing the cleanup. However, Mel, I need to thank you for so much more, for always answering my coding or LaTex questions, for always giving the best advice, and for never letting me doubt myself. Brian, thank you for setting up my Zotero, you saved me so much time in writing this Dissertation. Anna and Francesca, thank y'all for being the best friends throughout this entire journey. Also to Ben, Billy, Kelsey, Elisa, Hrag, Bryony, Cody, and all the friends along the way, thanks for your kindness and friendship. I love all of you dearly.

Max, when we met at AMS Phoenix back in January of 2019, I didn't know at the time I would be attending OU eight months later, but I knew I wanted to be your friend. Fast forward to now, and we are planning our wedding (however I wouldn't recommend doing this while trying to write a Dissertation). Max, thank you for being my biggest supporter, my constant encourager, and my place of comfort. You have

made this graduate school journey easier (believe it or not that *is* possible, thanks to you being him) and so much more enjoyable. Thank you for always listening when I have an idea, and for always given an honest perspective from a forecaster (the best forecaster, honestly). Thanks for always celebrating me, especially in this. I am so blessed that I get to do life with you, and now thrilled that everyone will have to call us "Mr. and Dr." from now on. I love you lots. To Debbie, Ken, Sam, and Katie-Jane, I never imagined I'd gain such a wonderful family—thanks Max! Thank y'all for your support over the past five years. The Ungars are truly the best at showing their love and support for one another. I love all of you.

To my Dad, thanks for always telling me I have the best resume, even if you haven't ever seen it. Thanks for never letting me think I am not capable, or not worthy of something (with humor of course). To MawMaw, I have to thank you for being scared of storms, as that is what sparked my interest in severe weather nearly 25 years ago. Franny, thank you for always watching weather documentaries with and always being curious about my passions. I love to think back on the constant joke Baby and I had saying "it ain't going to rain," even if it was—I guess I was destined to study the weather. To Mia and Jacob, thank you for (sometimes) thinking I am cool for what I do and bragging about your older sister—it means more than you know. To my family, all my aunts, uncles, and cousins (of which there are too many to name) thank you for always trusting in my hurricane forecasts (even though I am NOT a tropical expert), and always being excited to hear about what I do. Thanks for being there for me always, especially this year. I love y'all.

To my Mom, thank you for saying "that's silly, why would you not just go to school for meteorology" whenever I was in high school debating what I wanted to major in (everything but meteorology) and where I wanted to go to school. Thank you for making me do what I was passionate about, and reminding me that I could. Thank

you for always trying to remember all of the weather-related acronyms I'd tell you, and always trying to understand my work, even if I explained it in a way too technical way. I finally got the title, but I will let you and my dad calling me Dr. Pounds before it was true slide—I am glad I got to hear you call me that. I know you proud you were of me, how proud you'd be now, and how you'd love to tell anyone who would listen. I wouldn't be here today without you. I love and miss you always.

I've had more family and friends impacted by tornadoes in the SE than one would believe (can't forget the hurricanes either). I spend much of my time in the spring watching over every family and friend icon in RadarScope to ensure sure they're aware of what is going on and are safe. While this is a small thing I enjoy doing, it is how I can best show I am always thinking of them, and it brings me so much joy to be able to watch out for those I love the most. It makes sense that I spent the past four years studying SE tornado environments, and somehow got a Ph.D. out of it. All of this to say, I get to do what I love, and do it for the people I love, and I am forever grateful for that. I am so thankful for all of you who have been supportive of my passion ever since I was little girl obsessed with watching the Weather Channel. Thanks to those who encouraged me to make career out of it. I will always being watching out for you. I will always be your personal meteorologist.

Table of Contents

Acknowledgments iv

List of Tables xii

List of Figures xiii

Abstract xxii

1 Introduction 1
- 1.1 Data background 2
- 1.2 Research Background 5
  - 1.2.1 Storm classification 6
  - 1.2.2 Thermodynamic environmental characteristics 8
  - 1.2.3 Ground-relative kinematic environmental characteristics 10
  - 1.2.4 Storm-relative kinematic environmental characteristics 11
- 1.3 Research questions 15

2 Creating a Database of Southeast United States Observed Soundings 17
- 2.1 Introduction 17
- 2.2 Data sources and case selection 19
  - 2.2.1 Case selection and field campaigns 19
- 2.3 Sounding quality control 22
  - 2.3.1 Windsonde composites 25
  - 2.3.2 Interpolation 25
  - 2.3.3 Surface corrections 26
  - 2.3.4 Lapse rates 27
  - 2.3.5 Ascent rates 27
- 2.4 Mesocyclone identification and classification 30
  - 2.4.1 Storm mode 30
  - 2.4.2 Mesocyclone identification 35
  - 2.4.3 Tornadoes 36
- 2.5 Summary and potential dataset usages 39
  - 2.5.1 Summary 39
  - 2.5.2 Potential dataset usages 39

3 Composite Southeast United States Convective Environments from Field Campaign Sounding Observations . . . 42
3.1 Introduction . . . 42
3.2 Data . . . 46
3.2.1 Cases . . . 46
3.2.2 Soundings . . . 47
3.2.3 Radar-derived MRMS variables . . . 47
3.3 Methods . . . 48
3.3.1 Storm object identification . . . 48
3.3.2 Mesocyclone identification . . . 48
3.3.3 Storm mode classification . . . 49
3.3.4 Tornadoes associated with each mesocyclone . . . 50
3.3.5 Sounding composites . . . 50
3.3.6 Statistical testing . . . 51
3.4 Results . . . 52
3.4.1 RM environments . . . 58
3.4.2 QLCS environments . . . 65
3.4.3 RM+QLCS environments . . . 67
3.4.4 Storm motion impact on environments supporting both tornadic and nontornadic mesocyclones . . . 68
3.5 Environmental parameter dependence on storm motion . . . 69
3.5.1 RM storm motion . . . 69
3.5.2 QLCS storm motion . . . 71
3.6 Discussion . . . 72
3.7 Summary and conclusions . . . 74

4 Comparison of Model Sounding Profiles to Field-Project Soundings in the Southeast United States: Implications for Southeast U.S. Environmental Studies . . . 83
4.1 Introduction . . . 84
4.2 Data and methods . . . 89
4.2.1 SFCOA and HRRR data . . . 89
4.2.2 Interpolation . . . 90
4.2.3 Spatial and temporal criteria . . . 91
4.2.4 Composite profiles . . . 93
4.2.5 Statistical analysis . . . 94
4.3 Results . . . 95
4.3.1 Thermodynamic errors . . . 95
4.3.2 Ground-relative kinematic errors . . . 105
4.3.3 Storm-relative kinematic errors . . . 113
4.4 Conclusions and discussion . . . 124

5 Conclusions . . . 130

5.1 Conclusions 130
5.2 Forecasting implications 133
5.3 Future work 135

Reference List 138

List of Tables

2.1 Table of all cases used for dataset creation from VORTEX-SE (25 cases), meso18-19 (8 cases), and PERiLS (7 cases) field projects. The first column is the case number, the second column the time range of the first sounding associated with the case to the last, the third column is the project and IOP, the fourth columns describes the number of mesocyclones for the case, and the final column is the number soundings in the dataset for that case. 20

2.2 Table with details of each of the different formats used. The first column is the format number, the second column is the field project, year(s), and organization, and the third column is notes on the format type. Columns used include: time, altitude, latitude, longitude ("Alt", "Lat", "Lon"), temperature ("Temp"), dew point ("Dewpt"), relative humidity ("RH"), wind direction ("Dir"), wind speed ("Spd"), and wind components ("Ucmp", "Vcmp", "Wcmp"). An "X" indicates no variables fit that criteria; "*" indicates a note in the sixth column. 28

2.3 Table detailing the sounding system used by each team in each year of the three field campaigns (VORTEX-SE, Meso18-19, and PERiLS). The first column is each different radiosonde/windsonde type used. Each cell lists the organization that used the sonde type for each campaign/year. A "-" indicates a sonde was not used by any organization for that project/year. 29

2.4 Table detailing the storm mode classification scheme. The first column lists the major storm mode category, the second lists the subclassification, and the third provides a unique ID number. The fourth and fifth columns describe the major and minor classification criteria, respectively. The final column indicates whether the storm mode is classified as a RM or QLCS. 34

3.1 Table of all variables used, with their abbreviations and their definition. 53

List of Figures

2.1 Fig. 3 of Flournoy et al. (2026), showing a map of all sounding locations during the 2016–2023 field campaigns. Note from their caption: "For clarity, soundings launched within 15 km of each other are binned into the same circles." 23

2.2 Flowchart of storm mode based on Fig. 2 of Smith et al. (2012). 31

2.3 MRMS composite reflectivity at 02:00:00 UTC and the associated 02:00:00 UTC sounding from Huntsville, AL (indicated by the red star) on 1 April 2016. The red dotted ring surrounding the sounding represents the 100–km radius where storm objects are considered for the analysis. The black outline surrounding each storm is the objectively identified storm object and the black dot at the center is the center point of the object. The blue lines represent the tornadoes that occurred on the event day with a white circle marking their start and end points. 37

3.1 Composite hodographs of (a, d) RM, (b, e) QLCS, and (c, f) RM+QLCS for (a-c) tornadic and (d-f) nontornadic mesocyclones. The soundings included in the RM composite requires only RM modes present within the search radius and inflow of the sounding, the QLCS composite requires only QLCS modes present, and the RM+QLCS composite required at least one mesocyclone of a RM mode and QLCS mode to be present. The modes in RM consist of storm modes 4-1, 5-1, 4-2, 5-2, 2-2, 4-3, and 5-3 (see Fig. 2.2) and modes in QLCS consist of storm modes 1-1, 1-2, and 2-1 (see Fig. 2.2). The $n_{soundings}$ is displayed for both ground-relative (GR) and storm-relative (SR) composites while and n_{cases} remains the same for both. The thin lines on each individual plot are all individual SR hodographs included in the composite, and the thicker lines are the composite (mean) of all individual hodographs, where the color-filled line with a white line on top and outlined in grey is the GR composite hodograph and the color-filled line with a black outline is the SR composite hodograph. The number of hodographs making up each composite is found in grey text in the bottom left corner of each plot. The hodograph coloring follows the standard National Weather Service (NWS) colors, where 0–3-km is red, 3–6-km is lime green, 6–9-km is dark green, and 10-km and greater is purple, with additional resolution within the red 0–3-km layer due to its relevance for tornado-related processes and forecasting. 55

3.2 Composite skew-Ts of (a, d) RM, (b, e) QLCS, and (c, f) RM+QLCS for (a-c) tornadic and (d-f) nontornadic mesocyclones. The mode classifications are the same as in Fig.3.1. The thin red and green lines are each temperature and dew point profile, respectively, included in the composite. The thicker red and green lines with a black outline and a white line through the middle are the composite temperature and dew point profile, respectively. 56

3.3 Table showing all variables listed in Table 3.1 and their statistical significance for RM tornadic vs. RM nontornadic. Each box is color-coded and labeled for the significance value, where green is $\geq$ 75%, yellow is $\geq$ 90%, red is $\geq$ 95%, purple is $\geq$ 99%, and white with a "NS" means no statistical significance. The percentage in each box is the level of significance using n_{cases} (refer to 4.24.2.5 for more detail). If the percentage stating the level of significance is bold, that means there is statistical significance ($\geq$ 95%) based on $n_{soundings}$. Column titles in white contain values for the entire subset, and column titles in grey contain values just where the associated mesocyclone has an AzShear $\geq$ 0.01 s^{-1}. The "tornadic mean" and "nontornadic mean" is the mean value for each variable for tornadic and nontornadic, respectively. The "difference in means" column represents the tornadic mean minus the nontornadic mean with the percentage difference of the difference in means in parentheses. Therefore, positive values indicate that the tornadic value is larger, and negative values indicate that the nontornadic value is larger. The bold outlined column in the middle is the significance level for that variable from Coniglio and Parker (2020) for the right-moving supercells in the Great Plains. The box is grey with "NA" in it if that variable is not included in both this analysis and Coniglio and Parker (2020). The asterisk (*) next to the SRW and GRW are placed because Coniglio and Parker (2020) used the SR and GR wind speeds at that level in their study, whereas we used a layer-average, therefore it is not a one to one comparison. 58

3.4 Table showing all variables listed in Table 3.1 and their statistical significance as in Fig. 3.3 but for QLCS tornadic vs. QLCS nontornadic. . 59

3.5 Composite hodographs of (a, d) RM, (b, e) QLCS, and (c, f) RM+QLCS storm modes for (a-c) weaker LL AzShear $\geq$ 0.002 s^{-1} and $<$ 0.01 s^{-1} and (d-f) stronger LL AzShear $\geq$ 0.01 s^{-1}. The details of the hodograph composites are the same as in Fig. 3.1. 60

3.6 Composite skew-Ts of (a, d) RM, (b, e) QLCS, and (c, f) RM+QLCS storm modes for (a-c) weaker LL AzShear $\geq$ 0.002 s^{-1} and $<$ 0.01 s^{-1} and (d-f) stronger LL AzShear $\geq$ 0.01 s^{-1}. The details of the Skew-T composites are the same as in Fig. 3.2. 61

3.7 Table showing all variables listed in Table 3.1 and their statistical significance for RM with two different LL AzShear ranges, with those being "weaker" (AzShear ≥ 0.002 s^{-1} and < 0.01 s^{-1}) and "stronger" (AzShear ≥ 0.01 s^{-1}). The statistical significance color-coding and bolded values follow the same formulation as in Fig. 3.3. The "difference in means" columns represents the "weaker" bin minus the "stronger" bin, therefore, positive values indicate that the "weaker" bin has a larger value, and negative values indicate that the "stronger" bin has a larger value. 62

3.8 Table showing all variables listed in Table 3.1 and their statistical significance as in Fig. 3.7 but for QLCS. 79

3.9 Composite SR hodographs of (a) RM and (b) QLCS environments where both a tornadic and nontornadic mesocyclone are present in the inflow of the sounding. The RM and QLCS mode classifications are the same as in Fig. 3.1. The solid black line "all" is the composite SR hodograph using all mesocyclones present in the mixed tornadic and nontornadic environment. The blue hodograph is created using the nontornadic mesocyclones and the red hodograph is for the tornadic mesocyclones. The colored dots to represent the height levels are the same as in Fig.3.1 and shown in the legend, with all mesocyclones having a black outline, tornadic having a red outline, and nontornadic having a blue outline. The mean storm motion (SM) is plotted on the hodograph with a star and color coded as the hodographs are. The n_{cases} and $n_{soundings}$ (GR) will remain the same, as each sounding is required to have both a tornadic and nontornadic mesocyclone. The $n_{soundings}$ (SR) varies because there may be multiple tornadic and/or nontornadic mesocyclones associated with one sounding. The SR $n_{soundings}$ included in the tornadic composite is shown in red and the $n_{soundings}$ included in the nontornadic composite is shown in blue. 80

3.10 Kernel Density Estimation plots of tornadic (reds with no fill) and nontornadic (color-filled blues) observed storm motion deviation from the a,c,e) mean wind (GRW6km) and from b,d,f) Bunkers right storm motion for a,b) all RMs, c,d) non-linear RMs (modes 4-1, 4-2, 5-1, and 5-2 in Fig. 2.2) and e,f) linear RMs (modes 2-2, 4-3, and 5-3 in Fig. 2.2). The x-axis is the deviation in v (v′) and the y-axis is the deviation in u (u′), therefore, points within the upper (lower) quadrants have a faster (slower) observed storm motion than the mean wind or Bunkers, and points in the left (right) quadrants have a more leftward (rightward) observed storm motion than the mean wind or Bunkers. The values for $n_{soundings}$ and n_{cases} for tornadic (red) and nontornadic (blue) are in the top right quadrant of each subplot. In the bottom right quadrant is the mean value for u′ and v′ in red for tornadic and blue for nontornadic. The value in parentheses is the significance of u′ and v′ between the tornadic and nontornadic subsets using n_{cases}. 81

3.11 KDE plots of tornadic (reds with no fill) and nontornadic (color-filled blues) observed storm motion deviation from the a) mean wind (SH6km) and from b) Bunkers right storm motion for all QLCS modes (modes 1-1, 1-2, and 2-1, see Fig. 2.2). The other aspects of the plot are the same as the panels described in Fig. 3.10. 82

4.1 Schematic illustrating the grid point selection method for HRRR (purple squares, 3–km grid) and SFCOA (green triangles, 40–km grid) model profiles relative to two example OBS sounding locations (black stars). For each OBS sounding, profiles at the four surrounding model grid points are extracted at the hour before and after the OBS time. Dashed lines connect each sounding location to its four surrounding model grid points. 92

4.2 Composite ground-relative (GR) hodographs of (a) RM tornadic, (b) QLCS tornadic, (c) RM nontornadic, and (d) QLCS nontornadic mesocyclones. The soundings included in the RM composite requires only RM modes present within the search radius and inflow of the sounding and the QLCS composite requires only QLCS modes present. The modes in RM consist of storm modes 4-1, 5-1, 4-2, 5-2, 2-2, 4-3, and 5-3 and modes in QLCS consist of storm modes 1-1, 1-2, and 2-1 (see Fig. 2.2 and the associated text in Chapter 2 for more information on each storm mode). The number of hodographs making up each composite is found in gray text in the bottom left corner of each plot. The colored-coded circles indicate certain height levels, as shown in the legend. 99

4.3 Composite skew-Ts of (a) RM tornadic, (b) QLCS tornadic, (c) RM nontornadic, and (d) QLCS nontornadic mesocyclones. The soundings included in the RM and QLCS modes are as described in Fig. 4.2. Since there are no SR thermodynamic parameters, the $n_{soundings}$ and n_{cases} will match the GR values in Fig. 4.2. The grey outlined lines are the temperature (T) and dew point (T_d) for OBS. The SFCOA T is shown in maroon while HRRR T is shown in pink. The SFCOA T_d is shown in dark green while HRRR T_d is shown in lime green. 100

4.4 The SFCOA and HRRR mean errors (ME) and mean absolute errors (MAE) for a,c) RMs (left) and b,d) QLCSs (right) for a-b) temperature (°C) (top) and c-d) dewpoint (°C). The errors are obtained by subtracting either SFCOA (blue and red lines) or HRRR (cyan and pink lines) from OBS. The red/pink lines are for the tornadic subset and the blue/cyan lines are for the nontornadic subset. Positive MEs mean HRRR/SFCOA are overestimating, or OBS is smaller, indicative of a warm/fast bias. Negative MEs mean HRRR/SFCOA are underestimating, or OBS is larger, indicative of a cool/slow bias. 101

4.5 The percent difference in means between OBS and SFCOA/HRRR for various thermodynamic parameters for (a) RM and (b) QLCS storm modes. The thermodynamic parameters included are (from bottom to top): 3CAPE, 6CAPE, MLCAPE, MLCIN, MLLCL, LR100m, and LR3-6km. There are three subsets used to compare OBS vs. HRRR and OBS vs. SFCOA represented by different shaped symbols, including tornadic storms (triangles), nontornadic storms (squares) cases and both tornadic and nontornadic combined (circles). The fill color denotes statistical significance from Monte Carlo permutation testing, where significance at a confidence interval $\geq 75\%$ is green, $\geq 90\%$ is yellow, $\geq 95\%$ is red, $\geq 99\%$ is purple, and no significance has no fill (white). Black edge coloring on the symbol represents the OBS vs. SFCOA comparisons and gray edge coloring represents the OBS vs. HRRR comparisons. The numbers to the left of the symbol represent the means of the two subsets that are being compared. For all points, the "O =" represents OBS, and "H =" is used when comparing to the HRRR and "S =" is used when comparing to SFCOA. The text is displayed in bold if it is significant at $\geq 95\%$ or 99%. Positive percent difference values (right of 0) indicate the OBS mean is larger than HRRR/SFCOA and a negative percent difference (left of 0) means the HRRR/SFCOA mean is larger than the OBS mean. 103

4.6 The percent difference in means between the tornadic and the nontornadic subset for various thermodynamic parameters for (a) RM and (b) QLCS storm modes. The thermodynamic parameters included are (from bottom to top): 3CAPE, 6CAPE, MLCAPE, MLCIN, MLLCL, LR100m, and LR3-6km. The difference in means between tornadic and nontornadic is compared for all three data sets, with each being represented by different shaped symbols, OBS (starts), SFCOA (diamonds), and HRRR (pentagons). The fill color denotes statistical significance from Monte Carlo permutation testing, where significance at a confidence interval $\geq$ 75% is green, $\geq$ 90% is yellow, $\geq$95% is red, $\geq$ 99% is purple, and no significance has no fill (white). The numbers to the left of the symbol represent the means of the two subsets that are being compared (i.e., tornadic vs. nontornadic). For all points, the "T =" represents the tornadic mean and "N =" represents the nontornadic mean. The text is displayed in bold if it is significant at $\geq$ 95% or 99%. Positive percent difference values (right of 0) indicate the tornadic mean is larger than the nontornadic mean and a negative percent difference (left of 0) means the nontornadic mean is larger than the tornadic mean. 105

4.7 Same as Fig. 4.4, but for the errors in the ground-relative a-b) u component of the wind (ms^{-1}) and c-d) v component of the wind (ms^{-1}). . 109

4.8 The same as in Fig. 4.5, but for GRW. The GRW parameters included are (from bottom to top): GRW100m, GRW250m, GRW500m, GRW1km, GRW3km, GRW6km, GRW3km-6km, and GRW6km-10km. 110

4.9 The same as in Fig. 4.6, but for GRW. The GRW parameters included are (from bottom to top): GRW100m, GRW250m, GRW500m, GRW1km, GRW3km, GRW6km, GRW3km-6km, and GRW6km-10km. 111

4.10 The same as in Fig. 4.5, but for shear. The shear parameters included are (from bottom to top): SH100m, SH250m, SH500m, SH1km, SH3km, SH6km, SH3km-6km, SH6km-10km, and SHeff. 112

4.11 The same as in Fig. 4.6, but for shear. The shear parameters included are (from bottom to top): SH100m, SH250m, SH500m, SH1km, SH3km, SH6km, SH3km-6km, SH6km-10km, and SHeff. 117

4.12 Same as in Fig. 4.2, but for SR hodographs, using both observed storm motion and Bunkers storm motion. The $n_{soundings}$ is displayed for both ground-relative (GR) and storm-relative (SR) while and n_{cases} remains the same for both. While there is no GR hodograph plotted, this number tells us the number of unique hodographs in each composite. The SR $n_{soundings}$ minus the SR $n_{soundings}$ gives the number of hodographs that are used more than once, but for a different mesocyclone (with a different storm motion). The solid colored lines represent the composite mean SR hodographs using observed storm motion, and the colored hodographs with white dashes overlaid are the SR hodographs using Bunker storm motion. 118

4.13 The SFCOA and HRRR mean errors (ME) and mean absolute errors (MAE) for the RM (a–b) SR u-component (ustm) (ms^{-1}) and (d–e) SR v-component (vstm) (ms^{-1}) using a,d) observed storm motion and b,e) Bunkers estimated storm motion. The errors are obtained by subtracting either SFCOA (blue and red lines) or HRRR (cyan and pink lines) from the OBS sounding (using observed storm motion for all). The red/pink lines are for the tornadic subset and the blue/cyan lines are for the nontornadic subset. The errors using the observed storm motion (b,e) are then subtracted from the errors using Bunkers storm motion (a,d) to obtain the difference in errors (c,f) when using Bunkers rather than observed storm motion. Positive MEs mean HRRR/SFCOA are overestimating, or OBS is smaller, indicative of a fast bias. Negative MEs mean HRRR/SFCOA are underestimating, or OBS is larger, indicative of a slow bias. 119

4.14 The same as in Fig. 4.13, but for QLCS. 120

4.15 The same as in Fig. 4.5, but for SRW. The SRW parameters included are (from bottom to top): SRW100m, SRW250m, SRW500m, SRW1km, SRW3km, SRW6km, SRW3km-6km, and SRW6km-10km. 121

4.16 The same as in Fig. 4.6, but for SRW. The SRW parameters included are (from bottom to top): SRW100m, SRW250m, SRW500m, SRW1km, SRW3km, SRW6km, SRW3km-6km, and SRW6km-10km. The one addition here from the contents in Fig. 4.6 is an additional set of symbols representing the means using Bunkers storm motion since SRW is a storm-relative parameter. Black edge coloring on the symbol represents the tornadic vs. nontornadic comparisons when observed storm motion is used and gray edge coloring represents the tornadic vs. nontornadic comparisons when Bunkers storm motion is used. 122

4.17 The same as in Fig. 4.5, but for SRH. The SRH parameters included are (from bottom to top): SRH100m, SRH250m, SRH500m, SRH1km, SRH3km, SRHeff, and CRIT. 123

4.18 The same as in Fig. 4.6, but for SRH. The SRH parameters included are (from bottom to top): SRH100m, SRH250m, SRH500m, SRH1km, SRH3km, SRHeff, and CRIT. Both Bunkers storm motion and observed storm motion mean calculations are included as in Fig. 4.16. 129

Abstract

Proximity sounding studies related to convective storms primarily focus on the Great Plains region and supercells, despite the highest percentage of deadly tornadoes and non-supercellular tornadoes occurring in the Southeast (SE) United States. Using hundreds of observed soundings across 39 cases from recent SE-focused field projects, we create and analyze a proximity sounding dataset for tornadic and nontornadic environments for various storm modes. Environmental differences between right-moving supercell (RM) and quasi-linear convective system (QLCS) modes are evaluated through composite profiles and statistical testing of common forecast parameters for subsets of tornadic vs. nontornadic environments and subsets of stronger vs. weaker mesocyclone environments. We find tornadic environments for both RM and QLCS modes have significantly higher storm-relative wind (SRW) than nontornadic environments, but the largest differences in SRW are found above 1 km for RMs and below 1 km for QLCSs. However, SRW does not significantly differentiate mesocyclone strengths. Our findings of higher statistical significance in the storm-relative parameters and larger differences in the storm-relative vs. ground-relative hodographs emphasize the importance of storm motion on a storm's tornadic potential. We find tornadic RMs deviate significantly more to the right of the Bunkers RM motion estimate than nontornadic RMs. Values of many parameters that are on the low end of favorability for the Great Plains are the mean of the tornadic samples for the SE, further emphasizing the benefits of a SE convective environment climatology in helping to elucidate regional differences in environments conducive for tornadoes.

Soundings derived from mesoscale and convection-allowing numerical weather prediction models are a valuable tool for assessing convective environments. Due to model

assumptions, sounding profiles exhibit errors that can affect the computation of forecast parameters. In this study, soundings from the Storm Prediction Center Mesoscale Analysis System (SFCOA) and the High-Resolution Rapid Refresh (HRRR) model are compared to observed proximity soundings collected during SE field campaigns in the vicinity of RM mesocyclones and QLCS mesovortices. Prior Plains-centric work has indicated that SFCOA tends to underestimate low-level kinematic fields, whereas HRRR analyses more closely resemble observed soundings. Whether these findings are transferable to the SE remains uncertain and provides the primary motivation for this study. Relative to observations, the largest model errors are found in the low-level wind field. The HRRR generally overestimates inflow and the v-component component of the winds, while SFCOA underestimates these quantities. Despite these opposite-signed biases, both SFCOA and HRRR underestimate low-level vertical wind shear. The use of observed storm motions rather than estimated storm motions in conjunction with modeled soundings can impact the skill of storm-relative forecast parameters. An evaluation of parameter skill indicates that storm-relative wind fields are most skillful when using observed soundings and observed storm motion. In contrast, SFCOA exhibits the highest skill for ground-relative winds, bulk shear, and storm-relative helicity. These results have research implications for environmental studies that rely on SFCOA soundings and operational implications for severe weather forecasting.

Chapter 1

Introduction

Severe storm environments in the Southeast U.S. (SE) are particularly unique in comparison to other regions within the continental U.S. (CONUS), especially the Great Plains (GP). SE environments are characterized by higher moisture, lower instability, and higher shear compared to other regions. SE environments often span the high-shear, low convective available potential energy (CAPE) (HSLC) parameter space (i.e., ≤ 500 J kg^{-1} of surface-based CAPE (SBCAPE) and ≥ 18 ms^{-1} of 0–6 km shear; Schneider et al., 2006; Sherburn and Parker, 2014; Sherburn et al., 2016; Anderson-Frey et al., 2019; Brown and Nowotarski, 2020). Favorable severe environments are more frequent in the SE, resulting in higher frequency of tornadoes without much diurnal or seasonal constraints (Guyer and Dean, 2010; Kis and Straka, 2010; Sherburn and Parker, 2014; Sherburn et al., 2016; Anderson-Frey et al., 2016; Childs and Schumacher, 2018). For example, in 2004–2005, 54% of significant tornadoes occurred in HSLC environments, and 56% of that subset occurred in the cool season (November–March) (Schneider et al., 2006). The SE is also home to a particularly vulnerable population, due to large numbers of manufactured homes and high poverty levels (e.g., Ashley et al., 2008; Strader and Ashley, 2018; Sutter and Simmons, 2010). These physical and social factors contribute to the higher proportion of deadly tornadoes occurring in the SE (Ashley, 2007; Ashley et al., 2008; Coleman and Dixon, 2014; Strader et al., 2017; Anderson-Frey et al., 2019). Observational research efforts in the SE have been historically lacking, especially compared to efforts in the GP. However, in the past decade,

multiple SE-focused field-based campaigns have generated a wealth of observational data in the region. Using these observational data, we explore the forecast parameters that characterize SE environments.

1.1 Data background

Atmospheric soundings are forecasters' primary environmental evaluation tool, and understanding the skillfulness of sounding-derived parameters is critical to improving forecasting efforts. "Favorable" threshold values for severe potential come are based on findings from sounding-based climatologies. There is often much overlap between the range of parameter values for differing environmental subsets (e.g., tornadic vs. nontornadic), making parameters-based ingredient forecasting an imperfect science. On longer timescales, however, without surface, radar, or satellite observations as additional forecasting tools, ingredient-based forecasting via soundings is the primary environmental diagnosis tool.

Proximity soundings have been used to diagnose atmospheric conditions for nearly a century (e.g., Showalter, 1943; Fawbush and Miller, 1952; Beebe, 1958; Darkow, 1969; Maddox, 1976; Davies and Johns, 1993; Rasmussen and Blanchard, 1998; Rasmussen, 2003; Craven and Brooks, 2004; Thompson et al., 2003, 2012; Parker, 2014; Wade et al., 2018; Coniglio and Parker, 2020). Proximity has been defined in various ways (Potvin et al., 2010, see their Table 1 for the spatial and temporal criteria past literature has used to define a proximity sounding), and the proximity definition used can result in statistically different parameter distributions (Potvin et al., 2010), as environments contain small-scale heterogeneities (e.g., Markowski et al., 1998; Parker, 2014; Coffer et al., 2017; Wade et al., 2018; Flournoy et al., 2020; Markowski, 2020; Coniglio and Parker, 2020) that can be caused by a variety of mesoscale features and

inter-storm dynamics. These environmental heterogeneities are theorized to play a role in varying mesocyclone strength and tornado production (e.g., Richardson et al., 2007; Davenport and Parker, 2015; Davenport et al., 2019; Flournoy et al., 2020; Markowski, 2020). Potvin et al. (2010) statistically evaluated the impact proximity criteria has on severe weather climatologies, and they found the "Goldilocks zone" (i.e., spatiotemporal distance from the storm in which the environment is representative), is 40–80 km away at 0–2 h prior (to significant tornado occurrence), or 0–40 km away at 1–2 h prior. More recent works have used 0–40 km (or 10–40 km) to define the near-field, and 40–120 km to define the far-field environment (e.g., Coniglio and Parker, 2020). It is unclear if the goldilocks zone from Potvin et al. (2010) found would vary for linear systems or for a SE subset, instances where storm motions are much faster. Details on how we define proximity and any associated limitations can be found in the subsequent chapters.

Decades of studies have explored what environmental forecasting parameters, and what values of these parameters, are favorable for tornadoes using observed soundings (e.g., Fawbush and Miller, 1952; Beebe, 1958; Maddox, 1976; Davies-Jones, 1984; Johns and Doswell, 1992; Brooks et al., 1994; Rasmussen and Blanchard, 1998; Craven and Brooks, 2004; Parker, 2014; Wade et al., 2018; Coniglio and Parker, 2020). Large sounding datasets have been compiled and analyzed specifically for field campaigns, including but not limited to the Verification of the Origins of Rotation in Tornadoes Experiment (VORTEX; Rasmussen et al., 1994; Markowski et al., 1998), the second field phase of VORTEX (VORTEX2; Parker, 2014; Wade et al., 2018), Mesoscale Predictability Experiment (MPEX/MiniMPEX; Wade et al., 2018), and the Plains Elevated Convection at Night (PECAN; Hitchcock et al., 2019). The evaluation of environments through sounding characteristics has historically been focused GP-centric and primarily focused on supercellular environments (Parker, 2014; Coniglio and Parker, 2020; Wade et al.,

2018).

As vertical and horizontal resolution has increased in weather models, thus greater spatial and temporal resolution of model-derived soundings, model-based sounding climatologies have been developed (e.g., Thompson et al., 2003, 2007, 2012; Markowski et al., 2003; Houston et al., 2008; Nowotarski and Jensen, 2013; Anderson-Frey et al., 2016) to increase the sample size limited in observational climatologies. Model-based climatologies allow for higher spatiotemporal diagnosis of an ever-evolving atmosphere. The Rapid Refresh RAP; or Rapid Update Cycle (RUC) prior to 2012, but we will refer to it solely as "RAP" hereafter) (Benjamin et al., 2004b,a, 2016; Hu et al., 2017), the Storm Prediction Center (SPC) mesoscale surface objective analysis (SFCOA; Bothwell et al., 2022), and the High-Resolution Rapid Refresh (HRRR; Dowell et al., 2022) forecast model are three commonly used models for environmental climatologies and operational forecasting.

Both types of climatologies (i.e., observed and model-based) add insights to the wealth of environmental, parameter-based literature. However, there are discrepancies that exist between observed and model-based findings. The discrepancies exist for a variety of reasons, including, but not limited to, model parameterization schemes, inaccurate storm motion estimations, or biases in observed studies towards only the strongest storm in a given environment. The discrepancies are mostly confined to the relative importance that low-level kinematics has in distinguishing between tornadic and nontornadic environments (e.g., Coffer et al., 2019; Coniglio and Parker, 2020; Coniglio and Thompson, 2024; Coffer et al., 2025). Further information on these discrepancies, and discrepancies specific to the SE, can be found in Chapter 4.

1.2 Research Background

The four main ingredients necessary for severe storms to form are moisture, instability, lift, and wind shear, which can all be found in synoptically favorable regimes (Galway and Pearson, 1981; Sherburn et al., 2016). The ingredients are quantified through a range of forecast parameters calculated via atmospheric sounding profiles. Forecast parameters provide insights on how "favorable" an environment is for storm formation, storm maintenance, and potential severe hazards. SE environments differ greatly from the typical GP environments (e.g., Rogers et al., 2016; Anderson-Frey et al., 2016; Lin et al., 2023). Parameters deemed "favorable" for SE severe storms in previous literature are described in the following subsections. We explore favorability of severe storm environments (specifically to SE environments where there is existing literature) via various forecasting parameters, broken down by storm classifications we use throughout this Dissertation such as storm mode, mesocyclone strength, and tornadic potential.

Throughout, we focus on sounding-derived forecast parameters that characterize severe storm environments. However, there are many characteristics of the storm itself (e.g., radar structures, updraft speeds, and/or cold pool strength) that can reveal information about a storm's severe potential and be linked to certain environmental conditions. These storm characteristics can be diagnosed from other observing systems (e.g., mesonets, radar, LiDAR, etc.), but not from a single environmental sounding. While understanding how the environment can impact storm-scale features is important to reconcile uncertainties storm evolution and improve forecasts, our focus herein will take and ingredient-based, forecast parameter approach and focus on what we can infer from environmental soundings, without additional storm-scale information.

1.2.1 Storm classification

In the creation of any environmental climatology, storms must be classified by the characteristics the environmental climatology is designed to represent (e.g., supercell, strong rotation, or tornadic). For example, to create a climatology of environments supportive of supercell storms, storms of interest must be classified as supercells before extracting proximal environmental information. In this Dissertation, we classify storms by their storm mode, their mesocyclone strength, and their tornado production, all of which can provide understanding on storm's potential within a given environment.

Supercells (a term first used by Browning, 1964), or storms with a persistent, rotating updraft (i.e., mesocyclone) and a coexisting downdraft, often receive the most attention, as they are the most frequent producers of both tornadoes and large hail (e.g., Doswell III and Burgess, 1993; Smith et al., 2012). Specifically, supercells produce $\geq$ 95% of EF3+ tornadoes (Smith et al., 2012). However, quasi-linear convective systems (QLCSs), while often shorter-lived and more transient than supercell mesocyclones, can produce both tornadoes and straight-line winds via embedded mesovortices (e.g., Fujita, 1978; Forbes and Wakimoto, 1983; Przybylinski, 1995; Weisman and Trapp, 2003; Atkins et al., 2004; Trapp et al., 2005; Atkins and Laurent, 2009a,b; Schenkman et al., 2012; Lyza et al., 2017). QLCS are responsible for 18–25% of tornadoes in the U.S. (Trapp et al., 2005), and 30–50% in the SE (Ashley et al., 2019). QLCS tornado warnings, and tornado warnings in HSLC environments regardless of mode, have higher false alarm rates (FAR), lower probability of detection (POD), and shorter lead times (e.g., Dean and Schneider, 2008; Schneider and Dean, 2008; Dean and Schneider, 2012; Brotzge et al., 2013; Davis and Parker, 2014; Anderson-Frey et al., 2016). Specifically, Anderson-Frey et al. (2016) found the POD to be only 49% for QLCS tornadoes, in part because 24% of the QLCS tornadoes in their dataset were nocturnal

(e.g., Trapp et al., 2005; Kis and Straka, 2010; Ashley et al., 2019). The dynamics necessary for tornadogenesis via supercell mesocyclones and QLCS mesovortices vary, and, consequently, environmental conditions favorable for tornadogenesis can differ. In this Dissertation, the Smith et al. (2012) storm mode scheme is used to categorize storm mode, and the two main storm modes focused on herein will be "right-mover" (RM) (i.e., supercell) and QLCS.

Understanding potential environmental controls on mesocyclone strength can provide insight on supercell evolution (e.g., Rasmussen and Blanchard, 1998; Thompson et al., 2003) as well as tornado potential (Markowski and Richardson, 2014; Coffer and Parker, 2015, 2017; Coffer and Markowski, 2018). Mesocyclone strength may play a role in environmental evolution and favorability, as Faletti et al. (2026) found that stronger supercells amplify their kinematic environments "more strongly" than weaker supercells. Lyza et al. (2022a) found predictability in tornadic strength using maximum azimuth shear (AzShear) (i.e., a measure of mesocyclone strength) during the tornadic period of each storm. They did find sensitivity in skill to distance to nearest radar with AzShear, as with rotational velocity V_{rot}. Thompson et al. (2012) compared storms of varying mesocyclone strengths, but only for composite parameters, and found large supercell composite parameter (SCP; Thompson et al., 2003, 2004, 2007, 2012) and the significant tornado parameter (STP; Thompson et al., 2004) were favorable for stronger mesocyclones (see their Figs. 13–14). These composite parameters have both thermodynamic and kinematic elements, but Flournoy et al. (2020) found peak AzShear was more strongly correlated to kinematic parameters than thermodynamic parameters. These findings indicate that AzShear (i.e., mesocyclone strength) may be a valuable tool in warning operations (Lyza et al., 2022a). We explore both tornadic and nontornadic and strong vs. weak mesocyclone environments to understand if environments supporting strong mesocyclones are different than those supporting tornadic

storms.

The following three sections will detail the thermodynamic (section 1.2.2), ground-relative kinematic (section 1.2.3), and storm-relative kinematic (section 1.2.4) parameters and their threshold values or range of values that favor RM vs. QLCS storm mode, strong vs. weak mesocyclone, and tornadic vs. nontornadic environments. Further details on the criteria and specifications used to classify each storm are provided in 2.4.

1.2.2 Thermodynamic environmental characteristics

SE environments often have higher moisture contents due to the region's close proximity to the Gulf of Mexico. Higher moisture contents, especially in the low-levels, can led to a reduction in lifting condensation level (LCL) heights. Lower LCL heights are more favorable for tornadic storms and have skill in distinguishing between tornadic and nontornadic environments in both the SE and GP (Rasmussen and Blanchard, 1998; Thompson et al., 2003; Craven and Brooks, 2004; Wade et al., 2018; Coniglio and Parker, 2020). Lower mixed-layer (ML)LCL heights may be more supportive of tornadic environments due to more buoyant outflow (e.g., Markowski et al., 2002; Kumjian, 2011; French et al., 2015) and stronger low-level mesocyclones (i.e., stronger AzShear, Flournoy et al., 2024; Brown and Nowotarski, 2019). Low LCLs (< 1000 m) are often coupled with HSLC environments (Schneider et al., 2006), and are lower for QLCS tornadoes than RM tornadoes (Anderson-Frey et al., 2016).

Relatively "low" CAPE can support severe storms in the SE (Schneider et al., 2006; Sherburn and Parker, 2014; Anderson-Frey et al., 2016; Sherburn et al., 2016; King et al., 2017; Thompson et al., 2012), with even lower CAPE requirements in the cool season (Childs and Schumacher, 2018) and nocturnally (Kis and Straka, 2010; Sherburn and Parker, 2014; Ashley, 2007). Thompson et al. (2012) found 45% of

QLCS tornado events had CAPE $\leq$ 500 J kg^{-1}, but the number was only 15% for RMs (for the entire U.S., not the SE). Anderson-Frey et al. (2016) confirmed QLCS tornadoes have significantly lower values of MLCAPE than RM tornadoes. In a subset of just lower Mississippi Valley tornadoes QLCS tornadoes, Rogers et al. (2016) found a "slight positive relationship" between MLCAPE and tornado rating, where MLCAPE was $>$ 200 J kg^{-1} higher for EF1+ tornadoes compared to EF0 tornadoes, though was still not a sufficient discriminator between EF-scale rating. They also found CAPE to be 400 J kg^{-1} lower for their subset of EF1+ tornadoes compared to the rest of the CONUS. McCaul and Weisman (2001) showed that buoyancy is more likely to influence storm intensity in low CAPE environments. However, there has been no evidence that CAPE can be a significant discriminator between tornadic and nontornadic environments (Rasmussen and Blanchard, 1998; Craven and Brooks, 2004; Thompson et al., 2012) in the CONUS or the SE (Jackson and Brown, 2009, specifically for 0–3 km CAPE).

Convective inhibition (CIN) is often lower in the SE due the lack of an elevated mixed-layer (EML) advected in from the desert southwest. Large CIN can act to inhibit severe storms, as evidenced by the higher mixed-layer (ML)CIN for nontornadic QLCS cases compared to tornadic cases (Thompson et al., 2012). Brown et al. (2021) found HSLC (compared to HSHC) environments tended to destabilize (i.e., decreases in CIN and increases in CAPE) later in the evening, in contrast to the late evening increasing boundary layer stability in the GP. Lapse rates are weaker, especially in the mid-levels, in the SE compared to the GP (Guyer and Dean, 2010) primarily due to the lack of an EML. In creation of a HSLC-specific composite parameter, Sherburn and Parker (2014) and Sherburn et al. (2016) found the 0–3 km and 700–500 hPa lapse rate to be the most skillful forecasting parameter in distinguishing severe (tornado, wind, and hail) events from non-events in HSLC environments, likely due to the release of

potential instability. Brown et al. (2021) also found larger 0–1 km lapse rates had skill in distinguishing tornadic and nontornadic HSLC supercells. QLCS tornadic events also tend to have steeper lapse rates than nontornadic events (Pardun et al., 2025).

1.2.3 Ground-relative kinematic environmental characteristics

Wind shear, the change in wind speed and/or direction with height, is necessary to support storm organization, and thus storm rotation (Rotunno and Klemp, 1982). Without sufficient shear, the updraft, downdraft, and precipitation regions can overlap, which inhibits a sustained updraft and downdraft region, and thus storm maintenance (i.e., a long lived supercell) (Weisman and Klemp, 1982, 1984). It is recognized that at least 15–20 ms^{-1} of 0–6 km shear is necessary for severe convection (e.g., Rasmussen and Blanchard, 1998; Thompson et al., 2003; Craven and Brooks, 2004). Schneider et al. (2006) found 97% of significant tornadoes in 2004–2005 occurred with ≥ 15 ms^{-1} of 0–6 km shear. Specifically for QLCSs, Rogers et al. (2016) found shear magnitudes to be similar for Lower Mississippi Valley (i.e., the SE) tornadoes compared to tornadoes in all other regions.

The amount of deep-layer shear can distinguish between RMs and QLCSs, but not as well between their tornadic and nontornadic subsets (Thompson et al., 2012, see their Fig. 8). Pardun et al. (2025) found the separation between 0–6 km shear for tornadic and nontornadic mesovortices to be highest in the SE. Meanwhile, stronger low-level shear is also associated with longer-lived supercells (Davenport and Parker, 2015). Low-level shear is also best at discriminating between tornadic and nontornadic subsets and different tornado strength subsets, for both RM (Markowski et al., 2003; Thompson et al., 2012) and QLCS (Thompson et al., 2012). Specifically, for QLCSs, significant tornado (EF-2+) environments are characterized by stronger vertical shear (mean of 40 kts) compared to nontornadic QLCS environments (mean of 21 kts, Thompson et al.,

2012, see their Fig. 10). For RMs, Markowski et al. (2003) found low-level shear (i.e., $\leq$ 500 m) is nearly double for significantly tornadic cases vs. weakly tornadic or nontornadic cases (with little separation between these two subsets). Nocturnal, lower-CAPE, events in the SE have been shown to have larger shear (and storm-relative helicity; SRH) compared to daytime higher CAPE events (Sherburn et al., 2016; King et al., 2017; Brown et al., 2021).

Other measures of wind shear, such as ground-relative winds (GRWs) have been shown to be important for discriminating between tornadic and nontornadic supercell environments (Markowski et al., 2003; Nowotarski and Jensen, 2013; Coniglio and Parker, 2020; Saba et al., 2026). Recent work has emphasized the potential role that larger low-level GRWs may have on increasing turbulence in the boundary layer, and thus inducing coherent vorticity streaks that could promote tornadogenesis (Markowski, 2024; Gebauer et al., 2026).

1.2.4 Storm-relative kinematic environmental characteristics

When observed storm motions are unavailable, whether it be for forecaster's use pre-convection initiation (CI), or in large research studies where obtaining observed storm motions via manual efforts is not feasible, estimates must be used. The most common estimate of storm motion is the Bunkers estimated storm motion (Bunkers et al., 2000). Bunkers storm motion (hereafter referred to solely as "Bunkers") is a Galilean invariant method which uses the wind profile to predict supercell motion (for both RM and left-mover (LM) supercells, but our focus will be on RM supercells). Bunkers was developed using two key components responsible for storm motion: 1) advection of the storm by the mean wind and 2) rightward (or leftward for LM) propagation away from the mean wind towards the vertical shear. Storms often do not follow Bunkers exactly, especially in environments with mesoscale or storm-scale features that may

impact storm propagation (e.g., boundaries or cell mergers), and those with large SRH (Coniglio and Parker, 2020). It has been shown that strong supercells turn right (i.e., deviate to the right of the mean wind) (Newton and Katz, 1958; Rotunno and Klemp, 1982; Coniglio and Parker, 2020; Flournoy et al., 2021) due to pressure perturbations, resulting in an increase in tornadic potential (Flournoy et al., 2021) (and maximum hail size; Homeyer et al., 2023, 2025). The rightward turn, or the deviation from the mean wind, results in an increase in storm-relative winds (SRWs) (especially above 500 m), which in turn increases storm-relative helicity (SRH), both of which have been shown to increase tornado favorability (e.g., Davies-Jones, 1984; Darkow and McCann, 1977; Brooks et al., 1994; Kerr and Darkow, 1996; Thompson, 1998). QLCSs often propagate faster than the mean wind, which can lead to underestimation of SRH. Both elements of storm motion (i.e., speed and direction) contribute to increasing SRWs (Bunkers, 2018; Gutierrez and Kumjian, 2021; Lin and Kumjian, 2022; Bunkers et al., 2022; Homeyer et al., 2023, 2025).

The magnitude of the SRW (specifically a minimum of 10 ms^{-1} of 0–3 km) is important for prediction of storm type (i.e., supercell) (Droegemeier et al., 1993; Brandes et al., 1988; Nowotarski and Jensen, 2013; Peters et al., 2020) and mesocyclone strength (Droegemeier et al., 1993; Thompson et al., 2003; Peters et al., 2019, 2020). However, minimal to no skill has been found for SRW in distinguishing tornadic and nontornadic supercell environments (Thompson, 1998; Thompson et al., 2003; Markowski et al., 2003; Thompson et al., 2007; Nowotarski and Jensen, 2013; Coffer et al., 2019; Peters et al., 2023). Conversely, when using observed storm motions as opposed to estimated storm motions in the aforementioned studies, Coniglio and Parker (2020) found significance in the SRW's ability to distinguish tornadic and nontornadic environments. Recent studies have confirmed that the use of observed storm motions was the main contributor to the significant skill for SRW Coniglio and Parker (2020) found

(Coniglio and Jewell, 2022; Coniglio and Thompson, 2024; Coffer et al., 2025).

SRH (i.e., SREH) was first used as a forecast parameter by Davies-Jones et al. (1990), specifically SRH integrated through the 0–3 km layer. Succeeding the Davies-Jones et al. (1990) conference paper, the ability of SRH to provide information on mesocyclone rotational properties (Droegemeier et al., 1993) and to distinguish between tornadic and nontornadic environments was explored and confirmed (Rasmussen, 2003; Esterheld and Giuliano, 2008). Multiple sounding-based studies found SRH can skillfully distinguish tornadic and nontornadic environments (Kerr and Darkow, 1996; Rasmussen and Blanchard, 1998; Rasmussen, 2003; Thompson et al., 2003; Markowski et al., 2003; Parker, 2014; Coffer et al., 2019; Coniglio and Thompson, 2024). However, Edwards and Thompson (2000) and Rasmussen (2003) (by incorporating it in the composite energy helicity index; EHI) found 0–1 km SRH was more skillful than 0–3 km SRH. Thompson et al. (2003) found the lower quartile of 0–1 km SRH for significant tornado events to be 100 m^2s^{-2} (and is the threshold value used in STP), while Anderson-Frey et al. (2016) found it to be larger (see their Fig. 2), and larger in the SE compared to other regions (Anderson-Frey et al., 2016, see their Fig. 12).

Rasmussen (2003) suggested that even shallower layers (e.g., 0-500 m SRH) could provide more skill than 0–1 km SRH, which was confirmed by Esterheld and Giuliano (2008) using sounding observations (however, all observations were from Oklahoma). More recent studies also found 0–500 m SRH to be an important, skillful parameter for predicting tornadogenesis (Parker, 2014; Coffer and Parker, 2017; Coffer et al., 2017, 2019). In their composite tornadic and nontornadic environments from VORTEX2 soundings, Parker (2014) found significantly larger 0–500 m SRH in tornadic environments, attributing such to the environment rather than storm-induced modifications. In contrast, Coniglio and Parker (2020), using a larger dataset of GP-based field campaigns, found deeper-layer SRH (e.g., 0–3 km) to be more skillful in distinguish-

ing between tornadic and nontornadic environments. Coniglio and Jewell (2022) and Coniglio and Thompson (2024) found the increased significance Coniglio and Parker (2020) found in deeper-layer SRH was due to the use of observed storm motions (similar to their findings of skillfulness of SRW). Larger 0–3 km SRH has also been shown to be correlated to stronger mesocyclones (and lower MLLCL heights) (Flournoy et al., 2024).

Tornadic QLCSs have been shown to have higher SRH than nontornadic, but was not skillful in distinguishing between tornadic and nontornadic mesovortices (Pardun et al., 2025). In simulated QLCSs, Marion and Trapp (2021) found larger low-level hodographs, thus higher 0–500 m SRH to be associated with the most intense and persistent tornado-like vortices (TLVs). Murphy et al. (2022) found rapid increases in SRH with an approaching QLCS in north Louisiana on 12 April 2020. 0–1 km SRH increased > 200 m^2s^{-2} and 0-3 km SRH increased > 300 m^2s^{-2} between 1200 UTC (sounding observation) and 1400 UTC (KSHV VWP observation) prior to the first tornado occurrence. Murphy et al. (2022) was not able to determine if the large increase in SRH was environmental or was storm induced. The occurrence of the tornadoes in Murphy et al. (2022) occurred in the early morning hours, which is not uncommon in the SE. Larger SRH has been shown to increase the risk of nocturnal supercell tornadoes in the GP (Fischer and Davies, 2009).

Increasing SRH due to suspected storm-induced modifications has been noted in many GP based supercell studies (Brooks et al., 1994; Potvin et al., 2010; Parker, 2014; Coffer and Parker, 2017; Wade et al., 2018; Potvin et al., 2019; Coniglio and Parker, 2020; Flournoy et al., 2020; Britt et al., 2020; Laser et al., 2022; Faletti et al., 2026). It has also been noted that tornadic (Parker, 2014; Wade et al., 2018; Flournoy et al., 2020; Coniglio and Parker, 2020) and stronger (Faletti et al., 2026) supercells modify their kinematic environments (e.g., SRH) more than nontornadic and weaker super-

cells. Faletti et al. (2026) finds stronger supercells amplify SRH in their near-storm environments by 1) an increase in ground-relative winds, and 2) stronger rightward storm motion (as in Coniglio and Parker (2020)). Their findings agree with findings of Coniglio and Parker (2020), who found increased SRH due to increasing SRW.

1.3 Research questions

This work addresses questions about Southeast U.S. severe environments and explores how environments in the region differ from the commonly studied Great Plains using observations. To answer these questions, a dataset of observed soundings is created. Once the dataset is created, the following research questions are explored:

1. How do SE environments compare to the commonly studied GP?
2. How do environments supporting various storm modes compare? What differences in tornadic potential and rotational potential exist for various storm modes?
3. How do observed storm motions compare to estimated storm motions?

Since observations are not always available, model-derived soundings are also used to explore SE environments. A modeled sounding may not show the same differences between environments (e.g., tornadic vs. nontornadic) that are evident in observed soundings, and can also differ based on the storm motion used (e.g., observed vs. estimated). Comparison of the observed sounding dataset to modeled soundings are used to answer the following questions:

1. What biases are found in modeled profiles relative to observed profiles?
2. Do some forecasting parameters have more/less skill in distinguishing between tornadic and nontornadic environments when observed profiles are used vs. modeled?

3. Does observed vs. estimated storm motions impact the biases? Does it change the skill of storm-relative parameters?

The creation of the dataset is detailed in Chapter 2. Additional details of the dataset will be published in a Technical Report, which is currently in preparation. The sounding dataset is then used to create composites of varying SE environments depending on tornadic potential, storm mode, and mesocyclone strength—which is detailed in Chapter 3. Chapter 3 has been submitted for publication and is under review in *Monthly Weather Review*. The final three research questions are answered in Chapter 4 by comparing the observed composite soundings to modeled composite soundings. The comparison provides context for forecasters on biases present in commonly used models. Chapter 4 is in preparation and will be submitted for publication in the near future to *Monthly Weather Review*.

The research questions outlined above are specific to Chapters 3 and 4. The overarching theme explored is: *What makes Southeast U.S. environments unique, and what forecasting parameters show skill in distinguishing between different environmental subsets?* Specifically, the environmental subsets of greatest interest are: 1) RM vs. QLCS, 2) strong vs. weak mesocyclones, and 3) tornadic vs. nontornadic. If any forecast parameters are skillful in distinguishing between these subsets of environments, would they be of value to operational forecasters?

Chapter 2

Creating a Database of Southeast United States Observed Soundings

2.1 Introduction

The Southeast U.S. (SE) is one of the most vulnerable regions in the U.S. to severe weather hazards (Ashley, 2007; Anderson-Frey et al., 2019), for both physical and societal reasons (Strader and Ashley, 2018). HSLC environments often result in high nocturnal tornado risk (Simmons and Sutter, 2005; Ashley, 2007; Anderson-Frey et al., 2019). The SE proximity to the Gulf of Mexico leads to consistently higher moisture content—a necessary ingredient for severe storms. Tornadoes in the SE tend to occur year-round, with less seasonality than in other regions of the U.S. (Childs and Schumacher, 2018; Anderson-Frey et al., 2019). Socially, a large portion of the SE lives below the poverty line and there is a high concentration of mobile homes (Sutter and Simmons, 2010; Strader and Ashley, 2018), which are particularity dangerous structures to be in during a tornado (Brooks et al., 2002).

Despite the SE being the most vulnerable region and having the highest number of deadly tornadoes (Ashley, 2007; Anderson-Frey et al., 2019), field-based research efforts in the Southeast U.S. (SE) have been limited until the Verification of the Origins of Rotation in Tornadoes Experiment-Southeast (VORTEX-SE; Rasmussen, 2015, now

VORTEX-USA) program was created via Congressional mandate following the tragic April 27th, 2011 tornado outbreak. The lack of field efforts in the region is partially attributable to the difficulty in observing tornadoes in the SE. There are a number of factors that play into this, but primarily it is due to highly forested areas and particularly fast storm motions. The forested regions make it difficult to both get a clear visual of the storm (which is necessary for mobile operations) and clear view for instruments that need minimal obstructions between the instrument and storm (e.g., mobile radar and LiDARs). In the Great Plains, mobile observing teams are often able to follow and consistently sample the storm throughout its life cycle due to slower storm motions, meanwhile in the SE, there is often only one chance to sample a storm due to much faster motions.

Through the VORTEX-USA program, years of field efforts between 2016–2023 have resulted in a wealth of observed data from the SE. Such observations have existed for decades in the Great Plains, and have yielded the creation of large climatologies of severe wether environments (e.g., Brooks et al., 1994; Rasmussen and Blanchard, 1998; Craven and Brooks, 2004; Parker, 2014; Wade et al., 2018; Coniglio and Parker, 2020). These climatologies provide reference threshold values of various forecasting parameters that are considered "favorable" for rotating and potentially tornadic storms. Utilizing the observations collected over the past decade in the SE, similar climatologies can now be created for the SE. SE environments are understood to be unique in comparison to other regions (Sherburn and Parker, 2014; Sherburn et al., 2016; Wade and Parker, 2021; Lin et al., 2023), and comparing regional differences between Great Plains and SE environments is not possible until large, observed datasets are collected in the SE. The goal in this Chapter is to create an observed dataset capable of quantifying the differences in forecasting parameters threshold values (e.g., amount of CAPE or shear) that characterize SE environments.

The ideal observation platform to be used for such efforts are atmospheric soundings for a variety of reasons. Field-observed soundings in conjunction with the National Weather Service (NWS) provide twice daily observations. These supplement the thousands of soundings that were collected in the field by several institutions across the SE from 2016–2023. Soundings allow for quantification and evaluation of any sounding-derived forecasting parameter desired. Thousands of sounding observations collected during the various VORTEX-SE funded field-campaigns are retrieved and compiled into a large database. The details of the sounding database can be found in the technical report describing the dataset (see Flournoy et al., 2026), but some necessary details are provided throughout. The remainder of this chapter will detail the creation of a tangential dataset—the mesocyclones, and the characteristics thereof, associated with each sounding. We opt to focus on soundings with a mesocyclone in the vicinity for the purpose of evaluating near-storm environments.

2.2 Data sources and case selection

2.2.1 Case selection and field campaigns

A total of 39 cases were selected for this dataset and the subsequent analysis (see Table 2.1 for details on each case). All cases were drawn from the collection of intensive operating periods (IOPs) from recent SE-based field campaigns, which are expanded on in the following subsections. Inclusion of a case was dependent on severity and tornadic potential of storms within the vicinity of the available observations. The main objectives in building the dataset are to 1) explore the evolution of tornadic environments and 2) evaluate the differences between tornadic and nontornadic environments in the SE for various storm modes. Given the objectives, cases with tornadic storms

Table 2.1: Table of all cases used for dataset creation from VORTEX-SE (25 cases), meso18-19 (8 cases), and PERiLS (7 cases) field projects. The first column is the case number, the second column the time range of the first sounding associated with the case to the last, the third column is the project and IOP, the fourth columns describes the number of mesocyclones for the case, and the final column is the number soundings in the dataset for that case.

Case No.	Time Range (UTC)	Project and IOP	No. Mesocyclones	No. Soundings
1	17:24:09 31 Mar 2016–02:04:00 01 Apr 2016	VORTEX-SE 2016 IOP 3	134	54
2	17:34:00 29 Apr 2016–00:00:00 30 Apr 2016	VORTEX-SE 2016 IOP 4b	7	16
3	14:26:00 30 Apr 2016–23:02:43 30 Apr 2016	VORTEX-SE 2016 IOP 4c	35	39
4	11:01:51 25 Mar 2017–20:03:00 25 Mar 2017	VORTEX-SE 2017 IOP 1a	17	34
5	11:04:29 27 Mar 2017–03:04:00 28 Mar 2017	VORTEX-SE 2017 IOP 1b	365	87
6	10:55:00 05 Apr 2017–23:30:00 05 Apr 2017	VORTEX-SE 2017 IOP 3b	94	102
7	23:00:56 26 Apr 2017–06:03:00 27 Apr 2017	VORTEX-SE 2017 IOP 4a	5	22
8	11:01:07 30 Apr 2017–03:05:00 01 May 2017	VORTEX-SE 2017 IOP 4c	31	78
9	11:01:16 19 Mar 2018–02:01:32 20 Mar 2018	VORTEX-SE 2018 IOP 1	59	40
10	11:05:51 28 Mar 2018–17:02:43 29 Mar 2018	VORTEX-SE 2018 IOP 2a	9	26
11	17:07:24 03 Apr 2018–11:08:19 04 Apr 2018	VORTEX-SE 2018 IOP 3	23	33
12	11:02:51 06 Apr 2018–11:40:46 07 Apr 2018	VORTEX-SE 2018 IOP 4	24	45
13	11:04:25 13 Apr 2018–17:15:00 14 Apr 2018	VORTEX-SE 2018 IOP 5	27	48
14	23:01:12 03 Nov 2018–17:24:46 06 Nov 2018	meso18-19 IOP 1	38	105
15	11:16:33 01 Dec 2018–11:10:13 02 Dec 2018	meso18-19 IOP 2	29	104
16	10:59:31 06 Feb 2019–18:22:13 07 Feb 2019	meso18-19 IOP 3	3	108
17	05:00:40 23 Feb 2019–06:06:46 24 Feb 2019	meso18-19 IOP 5	47	109
18	10:58:00 03 Mar 2019–23:04:52 03 Mar 2019	meso18-19 IOP 6	2	36
19	10:55:03 09 Mar 2019–11:44:49 10 Mar 2019	meso18-19 IOP 7	57	105
20	22:52:41 12 Apr 2019–15:33:35 14 Apr 2019	meso18-19 IOP 8	58	135
21	04:57:00 18 Apr 2019–11:34:50 19 Apr 2019	meso18-19 IOP 9	32	89
22	11:02:47 16 Dec 2019–11:33:41 17 Dec 2019	VORTEX-SE 2020 IOP 1	26	38
23	11:02:05 29 Dec 2019–01:13:45 30 Dec 2019	VORTEX-SE 2020 IOP 2	6	18
24	23:02:38 10 Jan 2020–20:12:50 11 Jan 2020	VORTEX-SE 2020 IOP 3	15	47
25	11:00:53 05 Feb 2020–16:29:06 06 Feb 2020	VORTEX-SE 2020 IOP 4	55	54
26	11:01:40 12 Feb 2020–11:26:23 12 Feb 2020	VORTEX-SE 2020 IOP 5	29	40
27	06:00:26 03 Mar 2020–17:09:27 04 Mar 2020	VORTEX-SE 2020 IOP 6	23	42
28	11:00:37 24 Mar 2020–23:42:04 24 Mar 2020	VORTEX-SE 2020 IOP 7	5	23
29	11:00:52 28 Mar 2020–11:38:55 29 Mar 2020	VORTEX-SE 2020 IOP 8	5	43
30	11:00:38 08 Apr 2020–11:28:53 09 Apr 2020	VORTEX-SE 2020 IOP 9	3	37
31	11:01:01 12 Apr 2020–05:01:50 12 Apr 2020	VORTEX-SE 2020 IOP 10	25	48
32	11:05:00 23 Apr 2020–23:21:31 23 Apr 2020	VORTEX-SE 2020 IOP 11	1	26
33	11:01:07 22 Mar 2022–23:44:16 22 Mar 2022	PERiLS 2022 IOP 1	133	87
34	11:01:30 30 Mar 2022–02:08:16 31 Mar 2022	PERiLS 2022 IOP 2	149	98
35	05:01:06 05 Apr 2022–23:06:16 05 Apr 2022	PERiLS 2022 IOP 3	83	61
36	11:02:29 13 Apr 2022–23:25:39 13 Apr 2022	PERiLS 2022 IOP 4	55	70
37	11:00:54 16 Feb 2023–01:13:08 17 Feb 2023	PERiLS 2023 IOP 1	75	99
38	16:56:32 24 Mar 2023–05:57:51 25 Mar 2023	PERiLS 2023 IOP 3	85	98
39	14:59:40 31 Mar 2023–11:03:37 01 Apr 2023	PERiLS 2023 IOP 4	116	153

(or at least tornado-warned storms) were prioritized. In total, 39 of the 52 IOPs during the 2016–2023 field campaigns were further evaluated.

2.2.1.1 VORTEX-SE

VORTEX-SE is a research program with a field component focused on understanding tornadic environments and characteristics in the SE (Rasmussen, 2015). Research efforts were focused around Huntsville, AL, but not all intensive operating periods (IOPs) were confined to the north Alabama domain. Multiple organizations assisted in data collection and most observational units were mobile, including sounding platforms. An additional season of VORTEX-SE efforts was completed in 2019-2020. These efforts were led by the University of Alabama at Huntsville (UAH) teams with a focus on north Alabama. Twenty five of the 39 events in the dataset are from the VORTEX-SE campaign.

2.2.1.2 meso18-19

Meso18-19 was a sub-project of VORTEX-SE, with similar objectives, but a different operations plan. Meso18-19 took place between 1 November 2018 and 30 April 2019 to capture both cool and warm season events. Participating teams (i.e., the National Severe Storms Laboratory (NSSL), Mississippi State University (MSU), Texas A&M University (TAMU), UAH, University of Louisiana at Monroe (ULM), and the University of South Alabama (USA)) and NWS weather forecast offices (WFOs) within the domain (i.e., SGF, FWD, CRP, SHV, LCH, LZK, LIX, JAN, OHX, BMX, TAE, and FFC) launched soundings at multiple fixed sites over a 48–h window, with the severe event taking place near the middle of the window. NWS WFO Memphis (MEG) and Mobile, AL (MOB) did not launch routine soundings, but the MSU and UAH team performed sounding launches from these sites, respectively, during operations.

Soundings were launched every 6 h, at 0000, 0600, 1200, and 1800 UTC from all sites.

2.2.1.3 PERiLS

The Propagation, Evolution, and Rotation in Linear Storms (PERiLS; Kosiba et al., 2024) operations took place in the Spring of 2022 and 2023, with the goal of observing tornado-producing QLCSs or other non-classical tornado-producing storms, though some supercells were observed during several IOPs. The project's goal was to sample the pre-QLCS environment, QLCS evolution, and the interaction with the local environment (Kosiba et al., 2024). Multiple mobile-sounding platforms were active, including windsondes launched in rapid succession of advancing convection.

2.3 Sounding quality control

There are a total of 2,497 soundings included in the sounding database—see Fig. 2.1 (Flournoy et al. 2026, Fig. 3) for a map of all sounding launch locations. There were additional soundings associated with each case, but they were either spatially or temporally outside of the relevant convective environment (e.g., soundings taken multiple states away or multiple hours before convection initiation) and therefore not considered. More information and statistics on the number and geographic characteristics of the dataset are available in Flournoy et al. (2026). All 2,497 soundings are subject to quality control (QC), but all soundings do not have convection in the vicinity, and therefore are not used the in mesocyclone dataset detailed herein and the subsequent analysis in Chapters 3 and 4. However, all soundings are QC'ed are available for others' use.

The teams involved in data collection used various sondes and receivers, meaning there are different biases depending on hardware and software used (described in Table

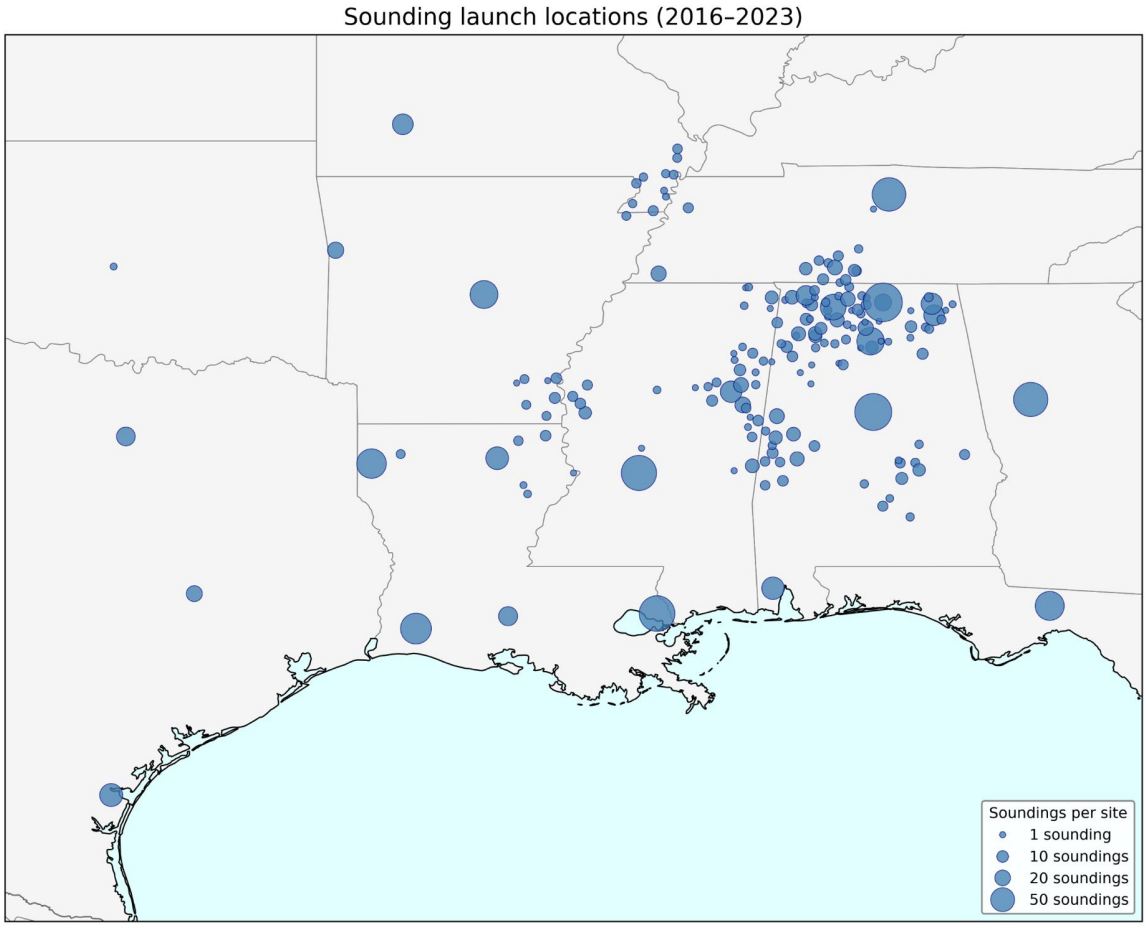


Figure 2.1: Fig. 3 of Flournoy et al. (2026), showing a map of all sounding locations during the 2016–2023 field campaigns. Note from their caption: "For clarity, soundings launched within 15 km of each other are binned into the same circles."

2.2). While these biases are important to acknowledge, there is a lack of peer-reviewed literature comparing and quantifying these biases (e.g., LeBel et al., 2024). The literature of inter-comparisons that does exist is limited (e.g., Bessardon et al., 2019; Diedrichsen et al., 2025). Due to the large sample size used in our analysis, the biases are likely dampened enough to not bias the findings. However, further inter-comparison would be a fruitful avenue for future work.

In order to compare and composite soundings, they must all be interpolated to a common grid. Since each team post-processed their data in-house, various sounding

formats were used (i.e., different variables, units, and available metadata, as detailed in Table 2.3[1]). The conversions and calculations necessary to create a common format for each sounding were time-intensive and the varying formats introduced unique challenges to the QC methods. Primarily, the lack of necessary metadata created challenges that ultimately resulted in some data not being usable. For example, for metadata lacking the altitude at launch site, difficulties converting to AGL arose. If the exact sounding launch time was not provided, which is necessary whenever comparing to time relative to a storm or tornado occurrence, the sounding could be not used. Other issues resulted from the lack of necessary variables in some formats (especially the raw SHARPpy output). For example, if updraft w (or ascent rate) information was not provided, soundings that entered the updraft could not be objectively removed (more details provided below). Additional challenges due to the lack of available variables or data resolution in certain formats are further detailed in the following subsections. Motivated by the formatting challenges we encountered, we strongly encourage future field-campaigns to commit to a universal sounding format and post-prossessing methods for their publicly available data—ideally the Earth Observing Laboratory (EOL) format used for all teams in VORTEX-SE 2016 (and by some teams in VORTEX-SE 2017).

The details of the QC are expanded on below. The thresholds chosen for what is considered "good" and "bad" data (e.g., the w threshold where data is contaminated by an updraft or the lapse rate values considered nonphysical) are based on peer-reviewed literature, however, the QC algorithm was written with maximum flexibility and user-choice. Depending on a user's objectives, users could obtain the raw data and modify the QC script to their research needs and produce a QC'ed dataset on a common grid of choice.

[1]There is no format #6 (as that was a format that was originally used but removed from the final dataset

2.3.1 Windsonde composites

During the PERiLS field campaign, numerous windsondes were rapidly launched (around 2 minutes between launches) from the same location ahead of an approaching storm. The primary objective for the windsondes was to collect in-storm observations, but they are also at times useful for characterizing the background environment when they do not encounter convection or before they enter storm-modified air. The windsondes were composited to obtain one profile (or multiple, depending on the number of similarities of profiles from a launch site) at a mean time at each launch site rather than having multiple profiles representing nearly the same environment at multiple closely-spaced times. The compositing was done subjectively via manual inspection of each consecutive profile. The number of profiles in each composite varied, but typically the profiles in each composite occurred within a 30-minute or less window. An additional composite from one launch site was created if there were notable environmental changes between windsondes or the temporal range exceeded 30 minutes. The composite profiles were then incorporated into our sounding database and the QC methods were applied.

2.3.2 Interpolation

To account for the data resolution variance depending on sonde type, all soundings were interpolated to a common vertical grid with the first level at 10 m (within the Dissertation, when "surface" or "0 " is used it is referring to the first level at 10 m AGL), the second level at 50 m, and every 50 m thereafter until the sounding termination point. However, due to the inaccuracies of and lack of relevance of winds above 10 km, kinematic parameters were only interpolated up to 10 km. Prior to interpolation to a common grid, all soundings were converted to m AGL using the altitude at the

launch location. For select NWS soundings (i.e., formats #8 and #11) where only geopotential height was provided, height data was converted from geopotential height to height MSL and then to m AGL. Interpolation was conducted by applying a Gaussian function to all data points within 100 m of each level with data points required both above and below the target interpolation level. Data was required on both sides of the interpolation level to ensure data from higher levels were not biasing lower-level data. The interpolation was conducted on individual variables, meaning that missing wind data had no impact on whether the thermodynamic data was interpolated and vice versa.

2.3.3 Surface corrections

Near-surface (< 10–m) data in soundings can contain errors due to when and where the sonde is turned on relative to launch time (Coniglio and Parker, 2020). Errors are almost always related to proximity to a heat source (e.g., blacktop in a parking lot), resulting in a very shallow superadiabatic layer. Co-located surface observations from mobile mesonets or nearby stations can be used to mitigate these errors; however, this method is not feasible for this dataset since most sounding sites did not have a co-located mobile mesonet or a fixed surface station nearby (Wade et al., 2018). Some past studies (Craven and Brooks, 2004; Potvin et al., 2010) did not manually adjust the surface observations on the soundings as the differences were believed to be insignificant when dampened out in the statistical analysis with such a large sample. Since our dataset is smaller than Craven and Brooks (2004) and Potvin et al. (2010), we opted to correct the soundings deemed to have erroneous, non-physical surface observations by removing all temperature data below 20 m where the lapse rate exceeded -15°C km^{-1}, indicative of superadiabatic lapse rates likely to be unrepresentative of the surrounding environment.

2.3.4 Lapse rates

Additional temperature lapse rate checks were performed for the entirety of the profile with a rolling 50 m lapse rate calculation to ensure unrealistic lapse rates were removed while preserving as much data as possible. For example, as the sonde emerges from cloud layers, the sensor can still be saturated and report unrepresentative cooling due to evaporation. At all points where relative humidity dropped below 90% from a previously saturated state, the lapse rate to the immediate level above was calculated to ensure it did not exceed -9 °C km^{-1}. If this threshold was exceeded, all temperature data was removed from the top of the cloud layer to the level where the lapse rate was within more representative environmental bounds. Additionally, both temperature and dew point observations were removed if the dew point exceeded the temperature at a level.

2.3.5 Ascent rates

Occasionally soundings, in particular windsondes, encountered storm-scale updrafts. If w was provided or could be calculated with provided variables (see Table 2.2), a 5-point average was calculated to determine if a point exceeded a 15 m s^{-1} ascent rate. If the average was equal to or exceeded the 15 m s^{-1} threshold, all data recorded after this point was removed. Furthermore, all data collected while the sonde encountered a downdraft (negative ascent rates or increasing pressure) were removed.

Table 2.2: Table with details of each of the different formats used. The first column is the format number, the second column is the field project, year(s), and organization, and the third column is notes on the format type. Columns used include: time, altitude, latitude, longitude ("Alt", "Lat", "Lon"), temperature ("Temp"), dew point ("Dewpt"), relative humidity ("RH"), wind direction ("Dir"), wind speed ("Spd"), and wind components ("Ucmp", "Vcmp", "Wcmp"). An "X" indicates no variables fit that criteria; "*" indicates a note in the sixth column.

No.	Field campaign, year(s): organization format was used by	Format Notes	Standard variables calculated	Standard variables not able to be calculated	Notes
1	VORTEX-SE, 2016: NOAA ATDD, UAH, MSU, ULM, NWS, Purdue, TTU (all teams); VORTEX-SE, 2017: NOAA ATDD, MSU, ULM, NWS, Purdue, TTU, CSU	EOL Sounding Composite (ESC) format	Wcmp*	X	Wcmp is included, but where there are data gaps the time is reported incorrectly so Wcmp must be recalculated
2	VORTEX-SE, 2017: UAH; Meso18-19, 2018–2019: UAH		Ucmp, Vcmp, Wcmp	X	
3	VORTEX-SE, 2019–2020: NWS		X	Time, Wcmp	
4	Meso18-19, 2018–2019: NSSL		Wcmp*	X	Wcmp is included, but where there are data gaps the time is reported incorrectly so Wcmp must be recalculated
5	Meso18-19, 2018–2019: TAMU, ATDD, USA, ULM and PERiLS, 2022–2023: FARM	SHARPpy format	Ucmp, Vcmp, RH	Time, Lat, Lon, Wcmp	
7	PERiLS, 2022–2023: NSSL windsondes		Ucmp, Vcmp, Wcmp	X	
8	PERiLS, 2022–2023: NWS		Ucmp, Vcmp, RH	Time, Wcmp	
9	PERiLS, 2022–2023: composite windsondes for PSU, NSSL, SBU		*	*	Composite windsonde variable calculations depend on variables available from the sondes included in the composites
10	PERiLS, 2022–2023: PSU windsondes		Ucmp, Vcmp, Dewpt, Wcmp	X	
11	VORTEX-SE, 2020: NWS (specifically 01/11/2020)	1s data obtained from Univ. of Wyoming sounding archive	Ucmp, Vcmp, Wcmp	X	
12	PERiLS, 2022–2023: ULM	Format #2 with different units	Ucmp, Vcmp, Wcmp	X	
13	PERiLS, 2022–2023: NSSL	Format #2 with extra column	Wcmp*	X	Wcmp is included, but where there are data gaps the time is reported incorrectly so Wcmp must be recalculated

Table 2.3: Table detailing the sounding system used by each team in each year of the three field campaigns (VORTEX-SE, Meso18-19, and PERiLS). The first column is each different radiosonde/windsonde type used. Each cell lists the organization that used the sonde type for each campaign/year. A "-" indicates a sonde was not used by any organization for that project/year.

Sounding System	VORTEX-SE (2016)	VORTEX-SE (2017)	VORTEX-SE (2018)	Meso18-19 (2018–19)	VORTEX-SE (2020)	PERiLS (2022)	PERiLS (2023)
GRAW DFM-17	–	–	–	–	–	NWS (BMX, LCH, LZK, OHX, SHV, SGF)	NWS (BMX, LCH, LZK, OHX, SHV, SGF)
GRAW DFM-09	NOAA ATDD	NOAA ATDD	–	NOAA ATDD	–	FARM	FARM
LM Sippican LMS-6	NWS (BMX, FFC, FWD, JAN, LZK, OHX, SHV, TAE)	NWS (BMX, FFC, FWD, JAN, LZK, OHX, SHV, TAE)	NWS (BMX, FFC, FWD, JAN, LZK, OHX, SHV, TAE)	NWS (BMX, FFC, FWD, JAN, LZK, OHX, SHV, TAE)	NWS (BMX, FFC, FWD, JAN, LZK, OHX, SHV, TAE)	–	–
Vaisala RS41-NG	–	–	–	–	–	NWS (JAN, LIX, TAE)	NWS (JAN, LIX, TAE)
Vaisala RS92-NGP	NWS (LCH, LIX, SGF)	NWS (LCH, LIX, SGF)	NWS (LCH, LIX, SGF)	NWS (LCH, LIX, SGF)	NWS (LCH, LIX, SGF)	–	–
Vaisala RS92-SGPD	TTU	TTU	–	–	–	–	–
Vaisala RS41-SGP	–	CSU	–	NSSL	–	NSSL	NSSL
WindSond S1H	–	UAH	UAH	UAH	UAH	UAH	–
WindSond S1H2	MSU	MSU	–	–	–	NSSL	NSSL
Windsond S1H3-S	–	Purdue	–	–	–	–	–
Windsond S1H3-R	–	–	–	–	–	SBU	SBU, PSU
iMet-1-ABxn	ULM, MSU, Purdue	ULM, MSU, Purdue, UAH	ULM, UAH	UAH	–	–	–
iMet 3050-A	–	–	–	USA	–	–	–
iMet-4	–	–	–	ULM, TAMU	UAH	UAH	–
iMet-4C	–	–	–	TAMU	–	–	–
iMet-4A	–	–	–	MSU	–	–	–
iMet-4-AB	–	–	–	–	–	ULM	ULM

2.4 Mesocyclone identification and classification

After all soundings were cataloged and QC'ed, any mesocyclones present within proximity to the sounding were documented. The methods used for mesocyclone identification are expanded below. As mentioned previously, the main goals in creating the dataset is to explore tornadic vs. nontornadic environments and how they evolve in the SE for various storm modes. Given the objectives, each identified mesocyclone was classified by storm mode and the mesocylone's associated tornadoes were documented (if applicable). The data and methods used to classify and categorize each mesocyclone are further detailed in the following subsections.

2.4.1 Storm mode

Trapp et al. (2005) evaluated tornado production for three storm modes (cell, QLCS, and other). Grams et al. (2012) also used three categories of storm modes (discrete cell, QLCS, and cluster), differing from Trapp et al. (2005) only in the creation of the "cluster" category rather than "other" which was dominated by tornadic rainbands in Trapp et al. (2005). Gallus et al. (2008) added subclassifications to their three major classifications (i.e., cellular, nonlinear, and linear) resulting in nine storm modes (Duda and Gallus, 2010). Storm mode classification was further expanded by Smith et al. (2012) to include five "major storm mode classes," or "major classifications". Each storm object is assigned a major classification and a subclassification. The major classifications are: 1. QLCS, 2. linear hybrid[2], 3. supercell (LM)[3], 4. supercell (RM),

[2]In Smith et al. (2012), the two linear hybrid subclassification modes are placed into either: 1) major classification "QLCS" with either a "line" or "bow echo" subclassification or 2) major classification "supercell (RM)" with subclassification "cell in line". We opted to keep "linear hybrid" as its own major classification to see if there were any relevant environmental differences.

[3]We broke LM and RM supercells into two distinct major classifications, differing from Smith et al. (2012) where LM and RM are subclassifications of the "supercell" major classification, which results in six major classifications rather than five. However, "Supercell (LM)" was excluded from the

5. supercell (marginal), and 6. disorganized. Each classification has two or three "subclassifications" resulting in a total of 16 different storm modes (see Fig. 2.2 for all subclassifications).

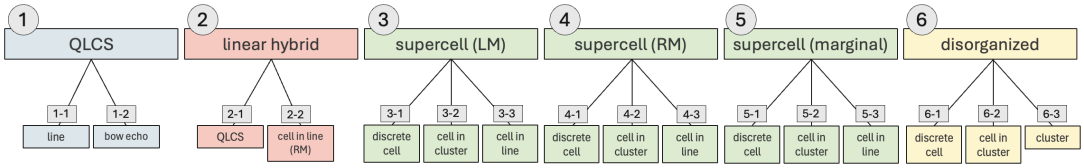


Figure 2.2: Flowchart of storm mode based on Fig. 2 of Smith et al. (2012).

Each mesocyclone (see the following subsection) within a storm object is assigned a mode using the criteria detailed in 2.2. The storm mode is determined based on the storm characteristics at the time of sounding launch (or nearest radar volume to sounding launch). The storms are interrogated using Gibson Ridge Analyst 2.0 (GR2Analyst) software with Archived Level II WSR-88D data obtained from Amazon Web Services (AWS). Each storm mode is assigned an identifier, using a format #-#, where the first # is the major classification and the second # is the subclassification (see Fig. 2.2 for the identifiers for each of the 16 modes). For example, 4-1 represents a RM (4) that is a discrete cell (1). The criteria used to define each storm mode are detailed in Table 2.4.

While 16 different modes is a large number, and probably not feasible for forecasters to identify during warning operations, the large number of modes does have research benefits. The Smith et al. (2012) classification scheme gives researchers flexibility to use all 16 modes, focusing on just the subclassifications (e.g., compare "cell-in-line" to "discrete cells") or major classifications (e.g., compare "supercell (RM)" to "supercell (marginal)"). Additionally, other modes can be consolidated to create larger overarching classifications. For example, within the analysis in Chapters 3 and 4, modes

analysis since there were no LM in the dataset.

4-1, 5-1, 4-2, 5-2, 2-2, 4-3, and 5-3 (see Fig. 2.2) are combined to create a larger RM classification and modes 1-1, 1-2, and 2-1 (see Fig. 2.2) to create a larger "QLCS" classification (see the last column of Table 2.4). Overall, using the Smith et al. (2012) storm mode classifications allows for a greater range of future research questions to be explored because of the detail, but also allows for condensation into simplified overarching mode classifications (e.g., RM vs. QLCS).

The further the storm is from a radar site, the more difficult the classification becomes. As detailed descriptions as possible were used when defining storm mode to limit the subjectivity of the manual storm mode identification process (Table 2.4). However, these methods are inherently subjective and will result in some bias. Smith et al. (2012) commented on the challenges of mode classification and how the methodology can greatly impact the results. For example, due to the addition of contiguous reflectivity criteria, tornadoes were classified as discrete, line, or cluster RM supercells in their study compared to the same tornadoes being classified as QLCS in Kis and Straka (2010). Other studies have defined storm mode using the dominant mode over the storm's lifetime (Gallus et al., 2008) or at the time of a specific severe report (Smith et al., 2012). We determine mode classification for each mesocyclone by that of the parent storm at sounding launch time, but storm mode can rapidly change, and that can not be accounted for using these methods.

We acknowledge the inherent biases associated with storm mode classification due to the subjective nature of the methods. However, in current forecasting operations, storm mode identification is done subjectively by individual forecasters. While this will vary from forecaster to forecaster, providing clear definitions of each mode is the best way to be able to consistently reproduce similar datasets and also apply these findings to operations. However, the development of an objective storm mode classification (alike those of Potvin et al., 2010) could lead to increased reproducibility of studies such as

this one and lead to improvement of our understanding of what possible behaviors and range of outcomes we can infer from a storm's mode.

Table 2.4: Table detailing the storm mode classification scheme. The first column lists the major storm mode category, the second lists the subclassification, and the third provides a unique ID number. The fourth and fifth columns describe the major and minor classification criteria, respectively. The final column indicates whether the storm mode is classified as a RM or QLCS.

Major classification	Subclassification	ID #	Major Classification Criteria	Sublassification Criteria	RM or QLCS
QLCS	line	1-1	Peak rotational velocity $\geq$ 10 m/s, rotation $\geq$ 1/4 the depth of the storm, rotational duration of at least 15 minutes	–	QLCS
QLCS	bow echo	1-2	Contiguous reflectivity at or above threshold ($\geq$ 35 dBZ) for horizontal distance of at least 100 km. Length to width ratio must be $\geq$ 3:1.	Does not need to meet the length requirement of QLCS (bowing segment of line)	QLCS
Linear Hybrid	QLCS	2-1	Mix of QLCS and line RM characteristics. Mode is assigned when mode is not clear when considering all volumetric radar data (Smith et al., 2012)	Depth of mesocyclone is considered (shallower)	QLCS
Linear Hybrid	cell in line (RM)	2-2	Mix of QLCS and line RM characteristics. Mode is assigned when mode is not clear when considering all volumetric radar data (Smith et al., 2012)	Depth of mesocyclone is considered (deeper)	RM
Supercell (LM)	discrete cell	3-1	Peak rotational velocity $\geq$ 10 m/s, rotation $\geq$ 1/4 the depth of the storm, rotational duration of at least 15 minutes	No weaker echo connecting the cell ("isolated cell" in Gallus et al. 2008)	–
Supercell (LM)	cell in cluster	3-2	Peak rotational velocity $\geq$ 10 m/s, rotation $\geq$ 1/4 the depth of the storm, rotational duration of at least 15 minutes	Cell connected by weaker radar echoes ("cell cluster" in Gallus et al. 2008)	–
Supercell (LM)	cell in line	3-3	Peak rotational velocity $\geq$ 10 m/s, rotation $\geq$ 1/4 the depth of the storm, rotational duration of at least 15 minutes	Individual cells arranged in linear fashion ("broken-line" in Gallus et al. 2008)	–
Supercell (RM)	discrete cell	4-1	Peak rotational velocity $\geq$ 10 m/s, rotation $\geq$ 1/4 the depth of the storm, rotational duration of at least 15 minutes	No weaker echo connecting the cell ("isolated cell" in Gallus et al. 2008)	RM
Supercell (RM)	cell in cluster	4-2	Peak rotational velocity $\geq$ 10 m/s, rotation $\geq$ 1/4 the depth of the storm, rotational duration of at least 15 minutes	Cell connected by weaker radar echoes ("cell cluster" in Gallus et al. 2008)	RM
Supercell (RM)	cell in line	4-3	Peak rotational velocity $\geq$ 10 m/s, rotation $\geq$ 1/4 the depth of the storm, rotational duration of at least 15 minutes	Individual cells arranged in linear fashion ("broken-line" in Gallus et al. 2008)	RM
Supercell (Marginal)	discrete cell	5-1	Weak rotation, just below the threshold for supercell (RM). Rotation for no more than 2 volume scans.	No weaker echo connecting the cell ("isolated cell" in Gallus et al. 2008)	RM
Supercell (Marginal)	cell in cluster	5-2	Weak rotation, just below the threshold for supercell (RM). Rotation for no more than 2 volume scans.	Cell connected by weaker radar echoes ("cell cluster" in Gallus et al. 2008)	RM
Supercell (Marginal)	cell in line	5-3	Weak rotation, just below the threshold for supercell (RM). Rotation for no more than 2 volume scans.	Individual cells arranged in linear fashion ("broken-line" in Gallus et al. 2008)	RM
Disorganized	discrete cell	6-1	Does not display any of the other criteria	No weaker echo connecting the cell ("isolated cell" in Gallus et al. 2008)	–
Disorganized	cell in cluster	6-2	Does not display any of the other criteria	Cell connected by weaker radar echoes ("cell cluster" in Gallus et al. 2008)	–
Disorganized	cluster	6-3	Does not display any of the other criteria	Strongest radar echoes are organized in a connected but non-linear fashion (Gallus et al., 2008)	–

2.4.2 Mesocyclone identification

Each storm object (identified via the methods of Wade et al. (2018), see Section 3.3.1 for more information) was investigated to determine if a mesocyclone or mesovortex[4] was present in radar observations (i.e., rotational couplet was identifiable) within 100 km of the sounding at the sounding launch time (see Fig. 2.3 for an example). Most of the time the mesocyclones were sampled between 2–5 km above radar level, although in some instances (e.g., HSLC environments) mesocyclones were identified closer to the ground. The latitude, longitude, and distance and azimuth from the sounding of all mesocyclone(s) present within an object were recorded. More than one mesocyclone can be present within an object, especially in objects that do not fall within the "discrete cell" sub-category.

Since all mesocyclones (i.e., a storm with a rotational couplet) were identified in the manual phase, regardless of the mesocyclone strength (i.e., rotational velocity), another step was necessary to remove extremely weak mesocyclones that are not of interest. Rotational velocity (V_{rot}) was not chosen due to its dependence on range form the radar. Rather, we opted to use Multi-Radar Multi-Sensor (MRMS; Smith et al., 2016) azimuthal shear (AzShear) to have a more objective, consistent measure of mesocyclone strength. Both 0–2–km AzShear (hereafter "low-level AzShear"), and 2–5–km AzShear (hereafter "mid-level AzShear") from MRMS are used (Mahalik et al., 2019). The low- and mid-level AzShear for each mesocyclone was obtained by searching 10 km around the manually identified mesocyclone, following the methods of Flournoy et al. (2022). A range of 10 km was used to account for any updraft tilt and slight differences in time from sounding launch to the closest available AzShear analysis time. Both a smaller and larger range was tested, but did not largely impact results. A minimum low-level

[4]For simplicity's sake, we use "mesocyclone" when referring generally to cyclones or vortices across storm modes, but when specifically discussing QLCSs, "mesovortex" will be used.

AzShear value of 0.002 s^{-1} was used to define a mesocyclone (slight modifications to this threshold do not alter the results).

Since our study only considers a mesocyclone at sounding launch, the methods to obtain storm motion differ from other studies that use mean storm motions over longer periods (Markowski et al., 2003; Thompson et al., 2003; Coniglio and Parker, 2020). Coniglio and Parker (2020) averaged the storm motions found from a five-point weighted average of instantaneous storm motions for three volume scans after sounding launch time. They found their methods were better able to identify deviant motions preceding tornadoes, where averaging storm motion over longer periods did not (e.g., Coniglio and Parker, 2020; Bunkers et al., 2022). Due to the importance Coniglio and Parker (2020) found in storm-relative winds distinguishing between tornadic and nontornadic environments, having a near-instantaneous storm motion is important to not dampen the impact storm motion has on the storm-relative winds. The observed average storm motion of each mesocyclone over a roughly 20 minute period was determined manually using GR2Analyst using the storm motion from approximately 10 minutes before to 10 minutes after time of mesocyclone identification, or between two volume scans before and two volume scans after the sounding time.

2.4.3 Tornadoes

The OneTor dataset (SPC, 2024) was used to identify the tornadoes associated with each mesocyclone [5]. OneTor is generated by the Storm Prediction Center (SPC) and combines all tornado segments from the National Center for Environmental Information (NCEI) *Storm Data* publication to document full tornado tracks and path

[5]There are two corrections to the OneTor dataset for tornadoes associated with soundings within the dataset. The start time for the Blount County tornado on 01 Apr 2016 in the OneTor database and in Storm Data is incorrect—the start time should be 01:42:00 rather than 02:42:00 UTC. The start time for the Blount County tornado on 23 Feb 2019 in the OneTor database and in Storm Data is incorrect—the start time should be 22:37:00 rather than 21:37:00 UTC.

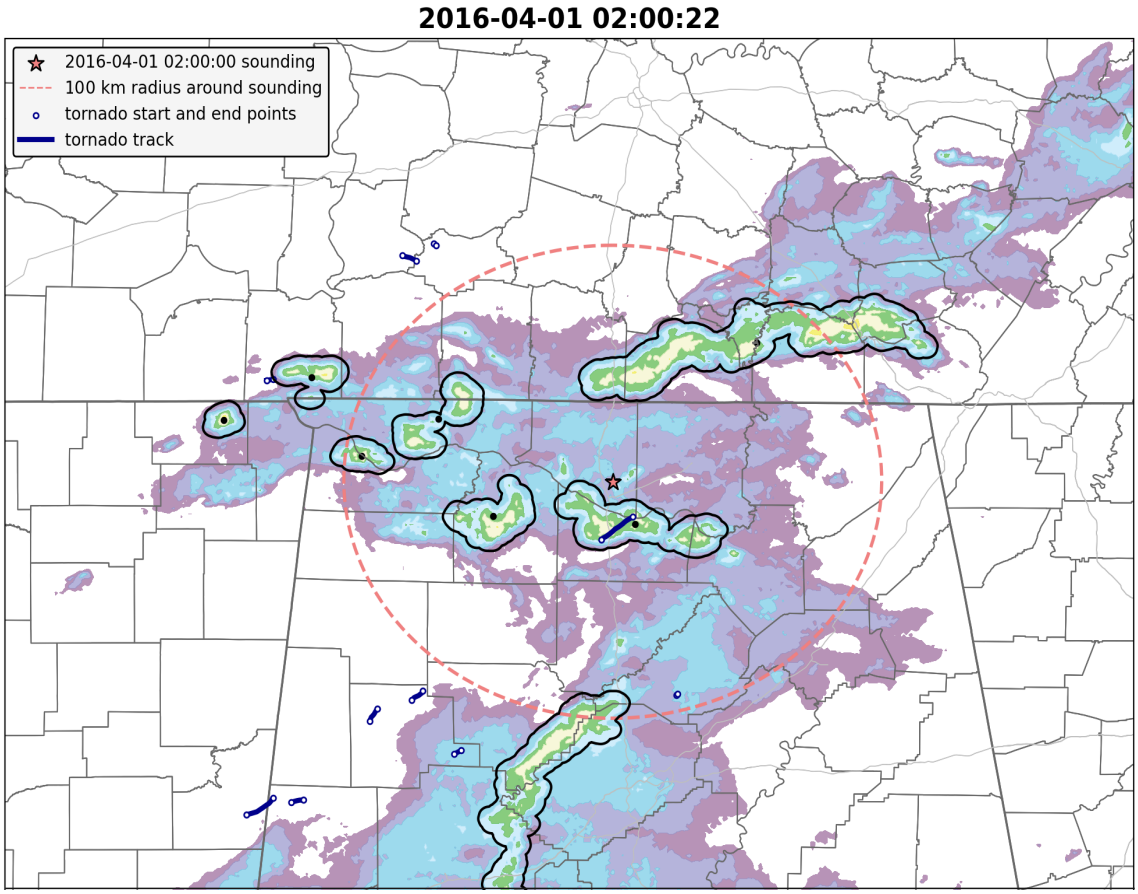


Figure 2.3: MRMS composite reflectivity at 02:00:00 UTC and the associated 02:00:00 UTC sounding from Huntsville, AL (indicated by the red star) on 1 April 2016. The red dotted ring surrounding the sounding represents the 100–km radius where storm objects are considered for the analysis. The black outline surrounding each storm is the objectively identified storm object and the black dot at the center is the center point of the object. The blue lines represent the tornadoes that occurred on the event day with a white circle marking their start and end points.

characteristics. Quality control is performed by the SPC post segment combination. To ensure no tornadoes were missed or miss-classified, each tornado was cross-checked with information available in the Damage Assessment Toolkit (DAT). Track information was extracted from the Damage Assessment Toolkit (DAT) where applicable. Not all tornado tracks are included in the DAT, so the start and end points from OneTor are used to estimate the tornado track for those tornadoes.

Multiple studies have set spatiotemporal thresholds to define a "tornadic" sounding (Potvin et al., 2010; Parker, 2014; Wade et al., 2018; Coniglio and Parker, 2020), though these studies focus on supercell storms rather than QLCS or mixed-mode storms. These studies also all use observed soundings from the Great Plains, and do not include observations from the SE, where storm motions are faster. Faster storm motions mean a storm comes in contact with environment ahead of the storm faster than a slower-moving storm. For this study, we characterized a mesocyclone as tornadic if it produced a tornado between 40 min prior and 90 min after the sounding launch time (similar to Coniglio and Parker, 2020). If the associated sounding occurred after a tornado, the time between tornado and sounding was determined using the tornado end time [6]. Mesocyclones that were not associated with a tornado during this time-frame were deemed nontornadic. There are cases where both tornadic and nontornadic mesocyclone are associated with one sounding. In those cases, the sounding is classified as tornadic (for more information on cases with both tornadic and nontornadic mesocyclones, see Section 3.5 and Fig. 3.9). Further subclassification into "pre-tornadic" and "post-tornadic" was considered, but robust results were not able to be gathered from this sub-setting due to a smaller, insufficient sample size. Time relative to sounding is included in the dataset, allowing subsetting by time relative to tornado in future works if desired.

[6]Tornado end time (and duration) is not a standard variable in OneTor, but is available often via the DAT or NCEI. End time information was pulled from these sources and added to OneTor for all associated tornadoes

2.5 Summary and potential dataset usages

2.5.1 Summary

Atmospheric soundings collected for 39 cases during recent SE-based field campaigns, including VORTEX-SE, Meso18-19, and PERiLS, are compiled into a large sounding database. There are 2,497 soundings that fall within relevant spatial and temporal ranges to the convection of interest for each case. The details of the entire sounding database can be found in the Flournoy et al. (2026) technical report. For this dataset, we only consider soundings that have an objectively identified storm object containing a mesocyclone within a 100 km radius of the sounding at the sounding launch time. Each storm object is investigated manually in GR2 to identify and assign a storm mode to any associated mesocyclone(s) using the methods of Smith et al. (2012). Any tornado(es) associated with a mesocyclone are identified and their time of occurrence is logged relative to sounding launch time.

2.5.2 Potential dataset usages

The dataset detailed in this Dissertation was created with the goal of producing a climatology of severe convective environments in the SE. The main objective is to create composite atmospheric profiles based on a variety of storm and environmental characteristics such as storm mode and strength. This will further the research community's understanding of SE environments and infer the physical processes relating environments to storm behavior. The climatology will also be useful as a reference for real-time forecasting. The resulting composites and associated analysis are detailed in Chapter 3. One of the main motivations for creation of this dataset, outside of creating reference hodographs, is to make an observed SE-based sounding database more

accessible to other researchers to encourage more SE-based studies.

There are a large number of case studies completed using some of 39 cases included in the dataset (e.g., Markowski et al., 2019; Tanamachi et al., 2019; Lyza et al., 2020; Hill et al., 2021; McDonald and Weiss, 2021; Trier et al., 2021; Lyza et al., 2022b; Hosek et al., 2023; LaFleur et al., 2023; Ostaszewski et al., 2025, among many others). However, observational datasets such as this one allow for observation-based longitudinal studies, which are lacking in the SE. There are such works in progress using the dataset. First, Miller et al. (2026, in preparation), is using all soundings in the dataset that are associated with tornadoes to explore environments supporting different tornado characteristics (e.g., tornado path length, tornado duration, and tornado strength). This work is one example of how SE tornado environments can be explored with this dataset. As part of their research efforts, mesocyclone and tornado tracks are added to the information already available in the dataset. The compilation of this data opens many avenues of exploration for researchers. For example, questions about HSLC environments in need of observational evidence would benefit from the content in this dataset.

A dataset for observational-based studies in the SE was the original intent for this work, however, we envision many other usages for these sounding observations in research efforts. All observational platforms contain limitations, therefore, comparison to the sounding dataset could serve as a necessary validation dataset for other instruments. Coupling one type of observation (i.e., soundings) with others available for the 39 cases (e.g., radar, StickNets, LiDAR) can support additional analysis techniques. For example, data assimilation, especially post-event analysis such as EnKF analysis greatly benefit from various observational datasets (Faletti et al., 2026) such as observed soundings. If not assimilated, this dataset of observed soundings could be used as a validation or comparison source for such analyses.

Additionally, Saba et al. (2026, in preparation) is using the composites generated from the dataset (shown in Chapter 3) to simulate supercells in SE environments via Cloud Model 1 (CM1). Supercells have not been initialized and simulated in an idealized model using an observed SE environmental profile—primarily due to the difficulty of idealized simulations in low-CAPE environments. This study opens up the potential to further model SE environments based on various subsets of soundings depending on the research question.

While the dataset is used in this Dissertation to evaluate near-storm environments, there are thousands of soundings representative of environments further from convection, post-convective environments, and environmental characteristics of various research interests. More SE-based studies are necessary to fill the knowledge gap that exists between the SE and the commonly studied Great Plains. We hope the dataset will reduce the necessary workload for researchers who wish to use a large number of observed soundings, resulting in more time for analysis and research output. Additionally, we envision the methods used here being applied in the future across more soundings (for various field-projects in various regions), which could then be combined with this dataset to generate an a larger, more widely applicable dataset.

Chapter 3

Composite Southeast United States Convective Environments from Field Campaign Sounding Observations

3.1 Introduction

The Southeast United States (hereafter, SE) has more deadly tornadoes than any other region (Ashley, 2007; Anderson-Frey et al., 2019), including the Great Plains (hereafter, GP)—where observational tornado research has historically been focused. This emphasizes the need to further our understanding and forecasting abilities of tornadoes in the SE. Many factors play into the differing tornado statistics in the SE, both social and physical, including, but not limited to, a particularly vulnerable population (Ashley et al., 2008; Strader and Ashley, 2018; Sutter and Simmons, 2010) and the prevalence of HSLC environments that pose difficult forecast challenges including a higher nocturnal tornado risk (Anderson-Frey et al., 2019). There have been limited large climatological studies on SE environments (Davis and Parker, 2014; Sherburn and Parker, 2014; Sherburn et al., 2016; Anderson-Frey et al., 2019), but with the recent

field campaign focus shifted to the SE spurred in part by the NOAA Verification of the Origins of Rotation in Tornadoes Experiment-SE (VORTEX-SE) project (now known as VORTEX-USA), there now exists a wealth of high-resolution observational data in the SE to help address this problem.

An additional complicating factor in the SE is the prevalence of QLCS events. Over 30–35% of tornadoes and 50–85% of wind reports (highest in winter) in SE states are associated with the QLCS storm mode (Ashley et al., 2019). Storm mode can inform a forecaster of a storm's potential to produce severe hazards and that hazard's severity (e.g., hail size, maximum wind gust, or tornado intensity). Supercells are the most common producers of severe hail (Nelson and Knight, 1987; Thompson et al., 2003; Duda and Gallus, 2010; Grams et al., 2012; Smith et al., 2012; Dawson et al., 2014; Blair et al., 2017; Murphy et al., 2023) and tornadoes (Doswell III and Burgess, 1993; Moller et al., 1994). Strong vertical shear allows for storm organization and promotes supercellular storm modes (Fawbush and Miller, 1953; Browning, 1962), specifically, at least 15–20 m s^{-1} (approximately 30–40 kts) of 0–6 km shear (Markowski et al., 1998; Rasmussen and Blanchard, 1998; Thompson et al., 2003). Linear systems that are composed of a collection of storms in a cellular or "slabular" manner along a common outflow most commonly produce tornadoes and severe winds. Studies estimate that 18–25% of annual tornadoes in the U.S. (and more in HSLC SE events, Anderson-Frey et al., 2019) are associated with QLCSs (Trapp et al., 2005; Smith et al., 2012; Ashley et al., 2019). The range of QLCS tornado intensities is generally lower compared to supercell tornadoes (Trapp et al., 2005; Smith et al., 2012; Murphy et al., 2023) with the distribution centered more strongly on weaker intensities for QLCSs. Given the relatively equally distributed percentages of tornadoes that occur with QLCSs vs. supercells in the SE, this dataset provides a novel observational insight into their respective environments.

Large datasets have been compiled and analyzed for various field campaigns in the GP (Rasmussen et al., 1994; Parker, 2014; Markowski et al., 1998; Wade et al., 2018; Hitchcock et al., 2019; Coniglio and Parker, 2020). Many observed sounding climatologies have been created to identify skillful forecast parameters in tornadic environments across the U.S. (Fawbush and Miller, 1952; Beebe, 1958; Darkow, 1969; Maddox, 1976; Darkow and McCann, 1977; Schaefer and Livingston, 1988; Johns and Doswell, 1992; Brooks et al., 1994; Rasmussen and Blanchard, 1998; Thompson et al., 2003; Rasmussen, 2003; Craven and Brooks, 2004; Parker, 2014; Wade et al., 2018; Coniglio and Parker, 2020). While many robust storm-environment relationships have been found, these studies sometimes reveal variations on a given forecast parameter's skill due to factors such as seasonality, regionality, or variability within the dataset, thus motivating a similar large-scale examination of observed environments in the SE. This study aims to fill a gap in the literature, as there has not been, to the authors' knowledge, a large climatology of SE severe/tornadic environments from observed SE-focused field campaign soundings. In addition to tornado-focused analyses, we also use radar-derived observations of mesocyclone strength (via azimuthal shear, discussed more in the next section) to quantify any relationships between the environment and strength of storm-scale rotation (e.g., Warren et al., 2021) regardless of tornadic activity.

One commonality of past environmental climatologies (among many commonalities, which will be expanded on later in relation to our findings) is the importance of storm-relative helicity (SRH) (Rasmussen, 2003; Thompson et al., 2007; Markowski and Richardson, 2014; Coffer et al., 2017, 2019; Peters et al., 2023) for tornadic potential. Anderson-Frey et al. (2019) showed the importance of SRH may be higher in the SE (see their Fig. 2b). Despite the strong correlation between SRH and tornado potential, there is uncertainty in the most skillful layer for computing SRH. Many have

found the highest skill using near-ground layers (e.g., 0–0.5 or 0–1 km SRH) for tornado prediction (Markowski et al., 1998; Rasmussen and Blanchard, 1998; Markowski et al., 2003; Rasmussen, 2003; Thompson et al., 2003; Craven and Brooks, 2004). However, in a field-based observational study Coniglio and Parker (2020) found that deep-layer SRH is more skillful when using observed storm motion vs. estimated Bunkers right storm motion (Bunkers et al., 2000), as also identified in Coffer et al. (2025). Coniglio and Parker (2020) and Coffer et al. (2025)'s findings emphasize the gap that exists between a parameter's skill related to tornado predictability when using estimated storm motions from environmental wind information vs. observed storm motion. To ensure the most accurate measure of storm-motion-dependent variables (e.g., STP, SRH, etc.) commonly used in tornado forecasting, we use observed storm motion herein. We explore the variations in observed storm motion vs. Bunkers storm motion in the SE to compare to those in the Great Plains.

With the generation of an observed SE convective environment climatology for various storm modes via observed soundings, we explore how: 1) SE environments compare to those in the commonly studied GP, 2) environments supporting different storm modes compare and the differences in tornadic and rotational potential for a given storm mode, and 3) Bunkers storm motion deviates from observed storm motions. The overarching goal of this study is to identify forecast parameters that could aid forecasters in distinguishing between tornadic and nontornadic environments in the SE.

3.2 Data

3.2.1 Cases

A total of 39 cases were used to create a database of soundings compiled from multiple SE field projects, including the Verification of the Origins of Rotation in Tornadoes Experiment-Southeast (VORTEX-SE; Rasmussen, 2015) campaign (2016-2020), Meso18-19 (2018-2019) (EOL, 2019), and the Propagation, Evolution, and Rotation in Linear Storms (PERiLS; Kosiba et al., 2024) (2022-2023) projects. Tornadic cases were prioritized, but cases with tornadic potential (i.e., mesocyclones that had rotation in environments supportive of severe storms) were included (Table 2.1). The VORTEX-SE field component was focused on understanding SE environments with efforts generally focused around Huntsville, AL and featured several sounding platforms from multiple institutions. Meso18-19 was a sub-project of VORTEX-SE, with similar objectives, but a different operations plan in which the National Severe Storms Laboratory (NSSL), four Universities, and several National Weather Service (NWS) offices across most of the SE launched soundings at multiple fixed sites over a 48-h window, every 6-h, at 0000, 0600, 1200, and 1800 UTC. PERiLS operated over multiple southern states including LA, AR, AL, MS, TN, and MO, including the Mississippi and Arkansas Delta, the "Black Belt" region of MS and AL, and the Tennessee Valley regions. PERiLS included a goal to observe tornado-producing QLCSs and other non-classical tornado-producing storms, though supercells were also observed during several intensive operating periods (IOPs).

3.2.2 Soundings

Most field project sounding data for this study were obtained from the National Center for Atmospheric Research (NCAR) Earth Observing Laboratory (EOL) repository, which was subject to quality control (QC) procedures generally outlined in Ciesielski et al. (2012). NWS sounding data were used to supplement the soundings from the field campaigns in our dataset when they met the proximity criteria (described later). Multiple institutions were involved in data collection using different systems and formats (details in Tables 3.1 and 2.2), which complicates the implementation of quality control (QC) methods that were performed on top of those done by EOL. Each sounding was QC'd to remove minor inconsistencies or errors in the data and interpolated to a common grid. These additional QC methods are detailed in the Appendix.

3.2.3 Radar-derived MRMS variables

Multi-Radar Multi-Sensor (MRMS; Smith et al., 2016) products are used to objectively identify storms. MRMS products incorporate data from the Weather Surveillance Radar-1988 Doppler (WSR-88D) network, satellites, and other observing platforms to create gridded radar and radar-derived products. MRMS products used here include composite reflectivity, 0-2-km azimuthal shear (AzShear) (hereafter "low-level AzShear"), and 2-5-km AzShear (hereafter "mid-level AzShear") (Mahalik et al., 2019). Reflectivity is calculated on a 0.01° latitude and longitude grid (roughly 1 km grid) at 2-minute intervals, while AzShear products are calculated on a higher resolution 0.005° latitude and longitude grid (roughly 0.5 km grid) at 5-minute intervals. The MRMS data is used for mesocyclone tracking and object identification methods (described in the following section).

3.3 Methods

3.3.1 Storm object identification

A modified version of the Wade et al. (2023b) storm object identification algorithm was used to identify all storms within 100 km of each observed sounding at the MRMS analysis time closest to the sounding launch time[1] and create the storm object(s). The storm object method uses thresholds of reflectivity to mask regions unassociated with a storm and then generates and merges polygons based on given distance and reflectivity thresholds to obtain storm object polygons. This method was preferred over methods that used a dBZ threshold to identify a storm (Smith et al., 2012) given its ability to quickly and objectively identify all candidate storms.

3.3.2 Mesocyclone identification

Each storm object was investigated to determine if a mesocyclone or mesovortex[2] was present (i.e., rotational couplet was identifiable) within 100 km of the sounding at the sounding launch time using the Gibson Ridge Analyst 2.0 (GR2Analyst) software with Archived Level II WSR-88D data obtained from Amazon Web Services (AWS). Most of the time the mesocyclones were sampled between 2–5 km above radar level, although in some instances mesocyclones were identified closer to the ground (e.g., HSLC environments). The latitude, longitude, and distance and azimuth from the sounding of all mesocyclone(s)[3] present within an object were recorded.

Low- and mid-level AzShear for each mesocyclone was obtained by searching 10 km

[1]Since MRMS reflectivity data is available every 2 minutes, there is no greater than a 1-minute time difference between the MRMS analysis time and sounding launch time.

[2]For simplicity's sake, we use "mesocyclone" when referring generally to cyclones or vortices across storm modes, but when specifically discussing QLCSs, "mesovortex" will be used.

[3]More than one mesocyclone can be present within an object, especially in objects that do not fall within the "discrete cell" sub-category.

around the identified mesocyclone, following the methods of Flournoy et al. (2022). A range of 10 km was used to account for any updraft tilt and slight differences in time from sounding launch to the closest available AzShear analysis time. A minimum low-level AzShear value of 0.002 s^{-1} was used to define a mesocyclone (slight modifications to this threshold do not alter the results).

The motion of each mesocyclone was determined manually using GR2Analyst and was used as the observed storm motion. The storm motions between two volume scans before and two volume scans after the sounding time when the mesocyclone was identified (approximately 10 minutes before and after) are used to calculate an average motion over roughly 20 min. Motions computed over smaller time periods (e.g., Markowski et al., 2003; Thompson et al., 2003; Coniglio and Parker, 2020) are more able to identify increasingly deviant motions preceding or associated with tornadoes (e.g., Coniglio and Parker, 2020; Bunkers et al., 2022).

3.3.3 Storm mode classification

Once mesocyclones were identified, a storm mode for each mesocyclone was assigned using the methods of Smith et al. (2012). Recognizing that storm modes are often complex, researchers have sought to refine storm mode-hazard relationships beyond a simple supercell or QLCS classification (e.g. Trapp et al., 2005; Gallus et al., 2008; Duda and Gallus, 2010; Grams et al., 2012). The flowchart shown in Fig. 2.2 illustrates the 16 possible storm modes from Smith et al. (adapted from 2012, their Fig. 2). While we used 16 different storm modes herein guided by past work, our analysis condenses those storm modes into larger, overarching categories that may be more useful for real-time diagnosis in an operational setting.

This classification method attempts to discretize the full spectrum of storm modes and has limitations. In addition to the inherent subjectivity, distance from the closest

radar site and rapidly evolving storm structures complicate mode identification. While some studies identify dominant mode over the entire lifetime (Gallus et al., 2008) or at the time of a specific severe report (Smith et al., 2012), we followed Smith et al. (2012) and classified one mode at the sounding launch time.

3.3.4 Tornadoes associated with each mesocyclone

The SPC OneTor dataset (SPC, 2024) was used to identify tornadoes associated with each mesocyclone. A mesocyclone was characterized as tornadic if it produced a tornado between 40 min prior and 90 min after the sounding launch time (similar to Coniglio and Parker, 2020). If the associated sounding occurred after a tornado, the time between tornado and sounding was determined using the tornado end time. Mesocyclones that were not associated with a tornado during this timeframe were deemed nontornadic.

3.3.5 Sounding composites

Sounding composites were generated based on varying criteria (as shown in the following two sections). Hodographs are shown in both the ground-relative (GR) reference frame and the storm-relative (SR) and storm-rotated (hereafter, referred to as "SR" hodographs) reference frame. The SR hodographs were created following Coniglio and Parker (2020), where the wind profile is rotated such that observed storm motion lies along the positive x axis, and then shifted such that observed storm motion falls at the origin. For a sounding to be considered proximity and included in the composites, it must have occurred between 40° (left of) and -135° (right of) the storm motion (centered at 0°), which represents in inflow sector (similar to Coniglio and Parker, 2020, see their Fig. 6). Composites were created using the SHARPpy python package (Blumberg

et al., 2017a). Incomplete profiles are included in the hodograph and skew-T composites, but are not used to calculate certain thermodynamic and kinematic parameters if the levels needed for the calculations are missing, resulting in a varying number of profiles contributing to composite hodographs, composite skew-Ts, and other parameter calculations.

A sounding was included in the SR hodograph composite more than once if one sounding is associated with multiple mesocyclones meeting the criteria of that composite (e.g., two mesocyclones that fall under the same mode classification or/and are both either tornadic or nontornadic). This was allowed since the SR hodograph would differ due to different storm motions for each associated mesocyclone, despite being the same sounding. A sounding that was used more than once for the SR composite was only allowed to be included in the composite once for the GR hodographs and skew-T composites since there would be no differences in hodograph shape or profile for each of the mesocyclones. We tested allowing only the mesocyclone closest to the sounding, if there were multiple mesocyclones associated with one sounding, to contribute to the composite. The hodograph shape remained the same using this method with minor differences in means, but with a reduced sample size. Since the conclusions presented did not change, we opted to use all mesocyclones in proximity to the sounding to keep proximity criteria consistent and ensure a sufficient sample size.

3.3.6 Statistical testing

The statistical significance of the difference in means between two subsets at four different significance levels (75%, 90%, 95%, and 99%) were determined using a two-tailed Monte Carlo test with 10000 iterations. The variables used for statistical testing are described in Table 3.1. Two different sample sizes for significance testing were used in order to address possible uncertainties in the effective sample sizes. These sample

sizes include 1) the number of unique soundings included in each subset ($n_{soundings}$), and 2) the number of unique cases (out of 39) included in each subset (n_{cases}). The latter reduces the degrees of freedom to assess significance if one (aggressively) assumes that no soundings taken during the same event are statistically independent. In most comparisons, the resulting statistical significances are similar (e.g., both are $> 95\%$ and "significant" or $< 95\%$ and "insignificant"). Important instances where this is not the case are highlighted appropriately. If there is more than one mesocyclone associated with a single sounding, as in the SR composites, each SR parameter (e.g., SRW or SRH) derived from the same sounding was counted. This results in $n_{soundings}$ being larger for SR parameters than GR parameters.

3.4 Results

We condense storm mode into two overarching subsets of "RM" and "QLCS" (see caption of Fig. 3.1 for each mode included in the two subsets) to examine differences in tornadic and nontornadic environments in the SE via composite profiles (Figs. 3.1 and 3.2) and statistical analysis (Fig. 3.3 and 3.4) for the two mode subsets. RM and QLCS allow only RM or only QLCS modes, respectively, to be present in the inflow of the sounding to be characterized as RM or QLCS. A third subset called "RM+QLCS" includes all soundings where both a mesocyclone(s) of a RM mode and QLCS mode is present in the inflow. The creation of RM+QLCS allows for comparison of environments that support both RM and QLCS modes, which is a common occurrence in the SE. The RM+QLCS subset also removes any potential bias from the RM and QLCS subsets (e.g., if QLCS dynamics influence the evolution of a RM mesocyclone).

To be included in the tornadic bin in the following analysis, all mesocyclones associated with the sounding (e.g., in the inflow and within the 100 km search radius)

Table 3.1: Table of all variables used, with their abbreviations and their definition.

Abbreviation	Definition
SH####	Bulk wind difference (BWD) (ms^{-1}), a vertical wind shear proxy, between 0–100 m (SH100m), 0–250 m (SH250m), 0–500 m (SH500m), 0–1 km (SH1km), 0–3 km (SH3km), 0–6 km (SH6km), 3–6 km (SH3-6km), 6–10 km (SH6-10km), and effective layer (SHeff)
SRH####	Storm relative helicity (SRH) (m^2s^{-2}) between 0–100 m (SRH100m), 0–250 m (SRH250m), 0–500 m (SRH500m), 0–1 km (SRH1km), 0–3 km (SRH3km), and effective layer (SRHeff)
CRIT	Acute angle (^{o}) between the storm-relative wind at the surface and the shear vector over the lowest 500 m
SRW####	Storm relative wind (SRW) (kts) between 0–100 m (SRW100m), 0–250 m (SRW250m), 0–500 m (SRW500m), 0–1 km (SRW1km), 0–3 km (SRW3km), 0–6 km (SRW6km), 3–6 km (SRW3-6km), and 6–10 km (SRW6-10km)
GRW####	Ground relative wind (GRW) (kts) between 0–100 m (GRW100m), 0–250 m (GRW250m), 0–500 m (GRW500m), 0–1 km (GRW1km), 0–3 km (GRW3km), 0–6 km (GRW6km), 3–6 km (GRW3-6km), and 6–10 km (GRW6-10km)
MLCAPE	Convective available potential energy (CAPE) (Jkg^{-1}) using a lowest 100 hPa mixed-layer (ML)
#CAPE	Convective available potential energy (Jkg^{-1}) in the 0–3 km (3CAPE) and 0–6 km (6CAPE) layers
DCAPE	Downdraft convective available potential energy (Jkg^{-1})
MLCIN	Convective inhibition (CIN) (Jkg^{-1}) using a lowest 100 hPa mixed-layer parcel
MLLCL	Lifted condensation level (LCL) (m) using a lowest 100 hPa mixed-layer parcel
LR####	Lapse rate ($^\circ C\ km^{-1}$) between 0–100 m (LR100m), 0–250 m (LR250m), 0–500 m (LR500m), 0–1 km (LR1km), 0–3 km (LR3km), and 3–6 km (LR36km)
LLMIX	Low-level (0–1 km) mean mixing ratio ($g\ kg^{-1}$)
PWAT	Precipitable water (inches)
FZL	Height (m) of the freezing level
WBZ	Height (m) of the wet bulb zero (WBZ) level
STP	Significant Tornado Parameter (STP) (unitless) from Thompson et al. (2012) using the effective inflow layer
SCP	Supercell composite parameter (SCP) (unitless) from Thompson et al. (2004) using the effective inflow layer
SHERB	Severe hazards in environments with reduced buoyancy parameter (unitless) from Sherburn and Parker (2014)

must be either tornadic or there must be at least one tornadic mesocyclone present if there are multiple mesocyclones. If there are multiple mesocyclones associated with a sounding, and at least one mesocyclone is nontornadic, the nontornadic mesocyclone

is not included in this composite. To be considered nontornadic, the mesocyclone, or all mesocyclones if there are more than one, associated with the sounding must be nontornadic.

We also include statistical analysis of tornadic and nontornadic environments when only considering strong mesocyclones (AzShear ≥ 0.01 s^{-1}). This is due to a bias noted in the Coniglio and Parker (2020) study of GP field soundings, specifically that the nontornadic sample is biased toward the stronger end of the nontornadic spectrum. This is because operations are typically only conducted in environments supportive of tornadoes, whereas nontornadic storms also often occur in environments known to have very little tornado potential. The same bias is probably in our SE dataset, but is likely mitigated somewhat by including some more marginal events (due to extended forecast/decision-making processes) and including all mesocyclones near the soundings rather than just a single, strong target storm.

Finally, we include comparison of environments of varying mesocyclone strength (i.e., AzShear) via the same analysis methods (see Figs. 3.5 and 3.6 for composites and Figs. 3.7 and 3.8 for statistical analysis). The environmental features seen when binned by mid-level AzShear yielded similar results (not shown) as when binned by low-level AzShear. For this reason, and because many of the mesocyclones included in this dataset are shallow due to the often low-topped nature of SE convection, we focus on low-level AzShear. Three AzShear bins are used: "weaker" where AzShear ≥ 0.002 s^{-1} and < 0.01 s^{-1} and "stronger" where AzShear ≥ 0.01 s^{-1}. As previously mentioned, there often is more than one mesocyclone associated with a sounding. To avoid a sounding contributing to more than one composite, a sounding is only used for the mesocyclone with the strongest AzShear value if there is more than one mesocyclone.

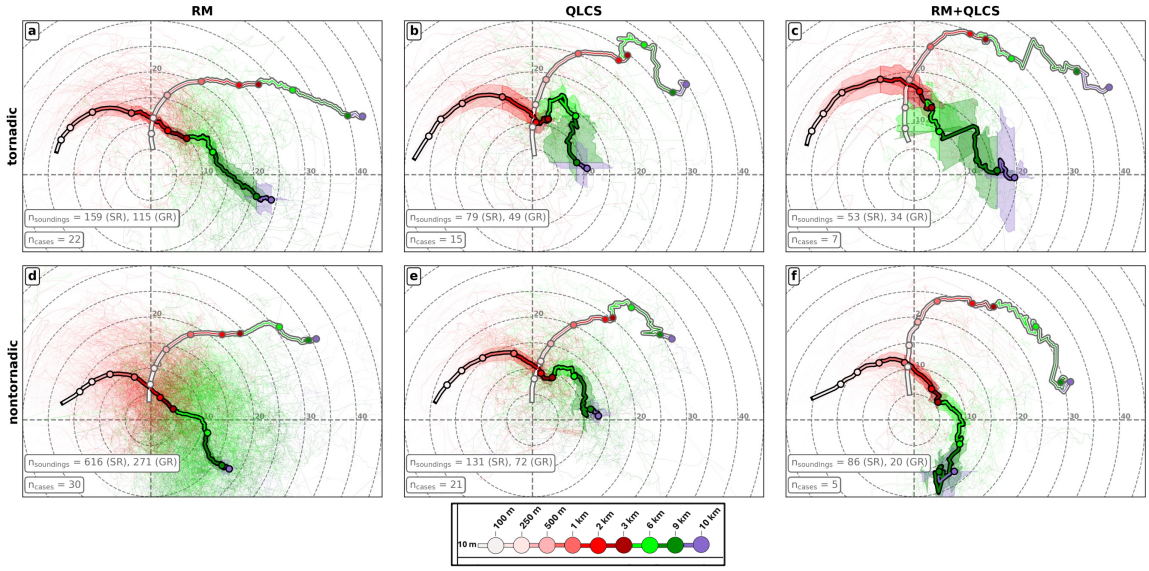


Figure 3.1: Composite hodographs of (a, d) RM, (b, e) QLCS, and (c, f) RM+QLCS for (a-c) tornadic and (d-f) nontornadic mesocyclones. The soundings included in the RM composite requires only RM modes present within the search radius and inflow of the sounding, the QLCS composite requires only QLCS modes present, and the RM+QLCS composite required at least one mesocyclone of a RM mode and QLCS mode to be present. The modes in RM consist of storm modes 4-1, 5-1, 4-2, 5-2, 2-2, 4-3, and 5-3 (see Fig. 2.2) and modes in QLCS consist of storm modes 1-1, 1-2, and 2-1 (see Fig. 2.2). The $n_{soundings}$ is displayed for both ground-relative (GR) and storm-relative (SR) composites while and n_{cases} remains the same for both. The thin lines on each individual plot are all individual SR hodographs included in the composite, and the thicker lines are the composite (mean) of all individual hodographs, where the color-filled line with a white line on top and outlined in grey is the GR composite hodograph and the color-filled line with a black outline is the SR composite hodograph. The number of hodographs making up each composite is found in grey text in the bottom left corner of each plot. The hodograph coloring follows the standard National Weather Service (NWS) colors, where 0–3-km is red, 3–6-km is lime green, 6–9-km is dark green, and 10-km and greater is purple, with additional resolution within the red 0–3-km layer due to its relevance for tornado-related processes and forecasting.

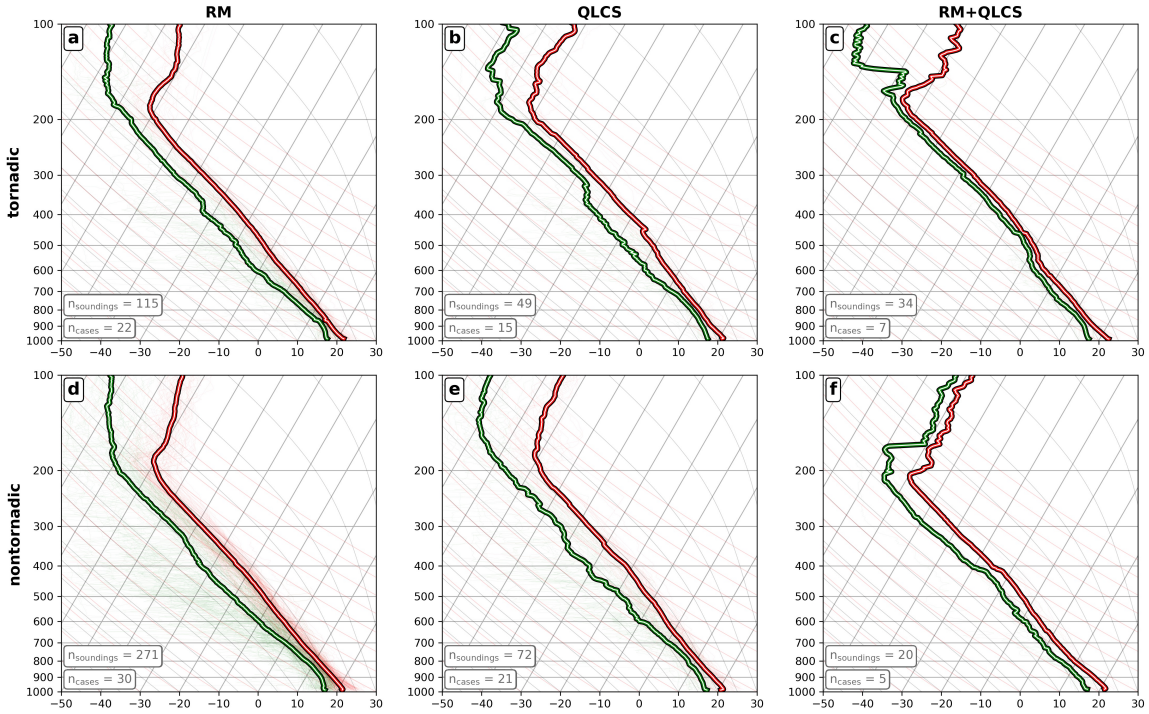


Figure 3.2: Composite skew-Ts of (a, d) RM, (b, e) QLCS, and (c, f) RM+QLCS for (a-c) tornadic and (d-f) nontornadic mesocyclones. The mode classifications are the same as in Fig.3.1. The thin red and green lines are each temperature and dew point profile, respectively, included in the composite. The thicker red and green lines with a black outline and a white line through the middle are the composite temperature and dew point profile, respectively.

RM tornadic vs. RM nontornadic	statistical significance	statistical significance (AzShear ≥ 0.01)	statistical significance in Coniglio and Parker (2020)	tornadic mean	tornadic mean (AzShear ≥ 0.01)	non-tornadic mean	non-tornadic mean (AzShear ≥ 0.01)	difference in means (% difference)	difference in means (% difference) (AzShear ≥ 0.01)
SH100m	NS	NS	> 75%	3.79	4.01	3.37	3.65	0.42 (12.6%)	0.36 (9.8%)
SH250m	NS	NS	> 75%	7.66	8.04	6.81	7.44	0.85 (12.5%)	0.60 (8.0%)
SH500m	**NS**	NS	> 75%	12.72	13.41	11.32	12.34	1.40 (12.4%)	1.07 (8.7%)
SH1km	**>75%**	**>75%**	> 95%	19.15	20.10	16.48	17.17	2.66 (16.2%)	2.94 (17.1%)
SH3km	**>75%**	**>75%**	NA	26.15	26.91	23.17	24.15	2.97 (12.8%)	2.76 (11.5%)
SH6km	NS	NS	> 95%	31.68	31.59	30.48	30.73	1.20 (3.9%)	0.87 (2.8%)
SH3-6km	NS	NS	NA	9.90	10.06	11.33	11.40	-1.42 (-12.6%)	-1.34 (-11.7%)
SH6-10km	NS	NS	NA	15.90	14.94	13.36	13.96	2.54 (19.0%)	0.98 (7.0%)
SHeff	NS	NS	> 75%	19.28	19.76	17.31	17.46	1.97 (11.4%)	2.31 (13.2%)
SRH100m	NS	**NS**	> 90%	39.74	45.66	35.62	32.48	4.12 (11.6%)	13.17 (40.6%)
SRH250m	NS	**NS**	> 90%	93.39	102.98	79.81	75.69	13.57 (17.0%)	27.29 (36.1%)
SRH500m	**>75%**	**>75%**	> 95%	191.06	208.05	133.22	133.38	57.84 (43.4%)	74.67 (56.0%)
SRH1km	**>95%**	**>95%**	> 99%	328.42	356.81	189.67	192.24	138.74 (73.1%)	164.57 (85.6%)
SRH3km	**>99%**	**>99%**	> 99%	472.72	520.41	241.51	259.71	231.21 (95.7%)	260.70 (100.4%)
SRHeff	**>99%**	**>99%**	> 99%	373.30	410.24	173.66	183.66	199.64 (115.0%)	226.58 (123.4%)
CRIT	**>95%**	**>95%**	NA	66.38	67.15	48.08	50.93	18.30 (38.1%)	16.22 (31.9%)
SRW100m	**>95%**	**>99%**	> 95%*	19.46	19.76	15.79	14.87	3.68 (23.3%)	4.89 (32.9%)
SRW250m	**>95%**	**>99%**	> 95%*	19.43	19.76	15.18	14.32	4.25 (28.0%)	5.44 (38.0%)
SRW500m	**>99%**	**>99%**	> 95%*	19.11	19.50	14.20	13.49	4.91 (34.5%)	6.01 (44.6%)
SRW1km	**>99%**	**>99%**	> 95%*	17.68	18.30	12.51	12.16	5.17 (41.3%)	6.14 (50.5%)
SRW3km	**>99%**	**>99%**	> 95%*	11.98	12.44	8.06	8.31	3.92 (48.6%)	4.12 (49.6%)
SRW6km	**>99%**	**>95%**	NA	10.94	11.44	7.31	7.53	3.63 (49.7%)	3.91 (51.9%)
SRW3km-6km	**>90%**	**>75%**	NA	14.38	14.25	11.77	12.02	2.61 (22.2%)	2.23 (18.5%)
SRW6km-10km	**>75%**	**>75%**	NA	20.68	21.62	17.54	18.01	3.14 (17.9%)	3.60 (20.0%)
GRW100m	**>75%**	**>75%**	> 75%*	8.62	8.58	7.27	7.42	1.35 (18.5%)	1.16 (15.7%)
GRW250m	**>90%**	**>75%**	> 75%*	10.90	10.99	9.08	9.35	1.82 (20.0%)	1.64 (17.5%)
GRW500m	**>90%**	**>75%**	> 90%*	13.66	13.95	11.39	11.83	2.27 (20.0%)	2.12 (17.9%)
GRW1km	**>95%**	**>90%**	> 99%*	17.36	17.93	14.40	14.93	2.96 (20.6%)	3.00 (20.1%)
GRW3km	**>90%**	**>95%**	> 99%*	22.47	23.25	19.16	19.48	3.31 (17.3%)	3.76 (19.3%)
GRW6km	**>90%**	**>90%**	NA	25.82	26.43	22.78	23.04	3.04 (13.4%)	3.38 (14.7%)
GRW3km-6km	**>75%**	**>75%**	NA	31.94	32.20	29.13	29.43	2.81 (9.6%)	2.77 (9.4%)
GRW6km-10km	**>90%**	**>90%**	NA	39.07	40.14	33.79	33.89	5.28 (15.6%)	6.25 (18.4%)
MLCAPE	NS	NS	NA	723.10	717.44	645.27	673.16	77.83 (12.1%)	44.28 (6.6%)
3CAPE	NS	NS	> 75%	55.86	55.49	56.54	65.29	-0.68 (-1.2%)	-9.79 (-15.0%)
6CAPE	NS	NS	NA	381.75	377.79	373.04	396.19	8.71 (2.3%)	-18.40 (-4.6%)
DCAPE	NS	NS	NA	485.22	454.04	502.99	517.10	-17.78 (-3.5%)	-63.06 (-12.2%)
MLCIN	NS	NS	> 90%	-30.30	-31.90	-41.24	-40.01	10.94 (-26.5%)	8.10 (-20.3%)
MLLCL	**>75%**	**>75%**	> 99%	814.27	825.55	933.15	988.64	-118.88 (-12.7%)	-163.09 (-16.5%)
LR100m	NS	NS	NS	7.02	6.83	5.35	4.78	1.67 (31.2%)	2.05 (42.9%)
LR250m	**>75%**	**>75%**	NS	7.43	7.29	5.56	5.18	1.87 (33.6%)	2.11 (40.8%)
LR500m	**>75%**	**>75%**	NS	6.93	6.78	5.58	5.29	1.34 (24.1%)	1.50 (28.3%)
LR1km	NS	NS	NS	6.34	6.32	5.98	5.93	0.36 (6.0%)	0.39 (6.6%)
LR3km	NS	NS	> 95%	6.48	6.47	6.51	6.65	-0.02 (-0.4%)	-0.18 (-2.7%)
LR3-6km	NS	NS	NA	6.43	6.42	6.33	6.33	0.10 (1.6%)	0.08 (1.3%)
LLMIX	**NS**	**NS**	> 99%	12.04	11.94	11.63	11.42	0.41 (3.5%)	0.52 (4.5%)
PWAT	NS	NS	NA	1.28	1.26	1.36	1.27	-0.07 (-5.3%)	-0.01 (-0.7%)
FZL	NS	NS	NA	3513.73	3477.15	3518.70	3436.55	-4.97 (-0.1%)	40.60 (1.2%)
WBZ	NS	NS	NA	3158.99	3136.86	3186.55	3101.63	-27.56 (-0.9%)	35.23 (1.1%)
STP	**>99%**	**>95%**	> 99%	1.80	1.89	0.66	0.78	1.14 (173.7%)	1.11 (142.8%)
SCP	**>99%**	**>95%**	NA	7.49	8.06	2.99	3.78	4.51 (150.7%)	4.28 (113.0%)
SHERB	**>90%**	**>75%**	NA	1.46	1.51	1.21	1.26	0.25 (20.6%)	0.25 (19.6%)

Figure 3.3: Table showing all variables listed in Table 3.1 and their statistical significance for RM tornadic vs. RM nontornadic. Each box is color-coded and labeled for the significance value, where green is $\geq$ 75%, yellow is $\geq$ 90%, red is $\geq$ 95%, purple is $\geq$ 99%, and white with a "NS" means no statistical significance. The percentage in each box is the level of significance using n_{cases} (refer to 4.24.2.5 for more detail). If the percentage stating the level of significance is bold, that means there is statistical significance ($\geq$ 95%) based on $n_{soundings}$. Column titles in white contain values for the entire subset, and column titles in grey contain values just where the associated mesocyclone has an AzShear ≥ 0.01 s^{-1}. The "tornadic mean" and "nontornadic mean" is the mean value for each variable for tornadic and nontornadic, respectively. The "difference in means" column represents the tornadic mean minus the nontornadic mean with the percentage difference of the difference in means in parentheses. Therefore, positive values indicate that the tornadic value is larger, and negative values indicate that the nontornadic value is larger. The bold outlined column in the middle is the significance level for that variable from Coniglio and Parker (2020) for the right-moving supercells in the Great Plains. The box is grey with "NA" in it if that variable is not included in both this analysis and Coniglio and Parker (2020). The asterisk (*) next to the SRW and GRW are placed because Coniglio and Parker (2020) used the SR and GR wind speeds at that level in their study, whereas we used a layer-average, therefore it is not a one to one comparison.

3.4.1 RM environments

The composite RM tornadic GR hodograph (Fig. 3.1a) shows the largest differences from the nontornadic (Fig. 3.1d) above 1 km. All measures of GRW show weak significance, but GRW1km is significantly larger (and GRW3km for cases with AzShear ≥ 0.01 s^{-1}) for tornadic (17.36 ms^{-1}) than nontornadic (14.40 ms^{-1}) RM environments (Fig. 3.3). Others (e.g., Markowski et al., 2003; Nowotarski and Jensen, 2013; Coniglio and Parker, 2020; Saba, 2024) have found that larger low-level GRW is a characteristic of tornadic environments, similar to our findings. GRW did not show as much significance when distinguishing between stronger and weaker mesocyclone environments (Fig. 3.7).

The shear vector is longer for tornadic (Fig. 3.1a) than nontornadic (Fig. 3.1d) in the upper-levels (above 6 km), but there are not significant differences in shear

QLCS tornadic vs. QLCS nontornadic	statistical significance	statistical significance (AzShear ≥ 0.01)	tornadic mean	tornadic mean (AzShear ≥ 0.01)	non-tornadic mean	non-tornadic mean (AzShear ≥ 0.01)	difference in means (% difference)	difference in means (% difference) (AzShear ≥ 0.01)
SH100m	NS	NS	4.34	4.72	3.66	4.26	0.68 (18.7%)	0.45 (10.6%)
SH250m	NS	NS	9.12	9.17	7.67	8.89	1.45 (18.9%)	0.28 (3.1%)
SH500m	>75%	NS	14.27	14.99	11.96	13.80	2.31 (19.3%)	1.19 (8.6%)
SH1km	>75%	>75%	21.29	22.40	17.55	19.21	3.74 (21.3%)	3.19 (16.6%)
SH3km	NS	NS	26.81	27.03	23.95	24.98	2.85 (11.9%)	2.05 (8.2%)
SH6km	NS	NS	30.33	31.05	28.12	28.54	2.21 (7.9%)	2.51 (8.8%)
SH3-6km	NS	NS	8.96	8.89	8.90	9.01	0.06 (0.7%)	-0.12 (-1.3%)
SH6-10km	NS	NS	13.51	13.60	12.48	12.48	1.03 (8.2%)	1.12 (9.0%)
SHeff	NS	NS	18.42	19.47	16.49	18.05	1.93 (11.7%)	1.41 (7.8%)
SRH100m	NS	NS	71.33	75.50	56.42	61.06	14.91 (26.4%)	14.43 (23.6%)
SRH250m	NS	NS	154.99	146.56	126.24	139.66	28.75 (22.8%)	6.89 (4.9%)
SRH500m	NS	NS	246.62	236.46	205.36	223.48	41.26 (20.1%)	12.98 (5.8%)
SRH1km	NS	NS	399.12	382.04	310.53	360.18	88.59 (28.5%)	21.86 (6.1%)
SRH3km	NS	NS	532.50	499.76	423.83	480.84	108.67 (25.6%)	18.92 (3.9%)
SRHeff	>75%	>75%	449.90	459.46	315.02	330.85	134.88 (42.8%)	128.61 (38.9%)
CRIT	NS	NS	64.98	61.70	55.70	60.28	9.28 (16.7%)	1.41 (2.3%)
SRW100m	>95%	>95%	22.56	22.44	18.89	18.99	3.67 (19.4%)	3.44 (18.1%)
SRW250m	>95%	>95%	22.27	21.92	18.20	18.48	4.07 (22.4%)	3.44 (18.6%)
SRW500m	>95%	>90%	21.78	21.28	17.33	17.77	4.45 (25.7%)	3.51 (19.7%)
SRW1km	>95%	>90%	20.59	20.16	16.01	16.47	4.58 (28.6%)	3.69 (22.4%)
SRW3km	>75%	NS	15.08	14.64	12.35	12.96	2.73 (22.1%)	1.67 (12.9%)
SRW6km	>75%	NS	14.03	13.75	11.34	12.43	2.68 (23.7%)	1.32 (10.6%)
SRW3km-6km	>75%	NS	15.57	15.40	12.65	13.64	2.92 (23.0%)	1.76 (12.9%)
SRW6km-10km	NS	NS	14.81	14.78	13.76	16.08	1.05 (7.7%)	-1.29 (-8.0%)
GRW100m	NS	NS	8.71	8.17	7.63	7.56	1.08 (14.1%)	0.61 (8.0%)
GRW250m	NS	NS	11.17	10.62	9.69	10.03	1.47 (15.2%)	0.59 (5.9%)
GRW500m	>75%	NS	14.34	13.94	12.30	13.03	2.04 (16.6%)	0.91 (7.0%)
GRW1km	>75%	NS	18.70	18.68	15.93	16.95	2.77 (17.4%)	1.73 (10.2%)
GRW3km	>75%	NS	24.45	24.20	21.40	22.29	3.05 (14.2%)	1.91 (8.6%)
GRW6km	>95%	>90%	27.87	27.90	24.13	24.49	3.74 (15.5%)	3.41 (13.9%)
GRW3km-6km	>95%	>90%	33.17	33.23	28.46	29.12	4.71 (16.5%)	4.11 (14.1%)
GRW6km-10km	NS	NS	34.45	34.20	31.59	33.39	2.86 (9.0%)	0.81 (2.4%)
MLCAPE	NS	NS	326.69	309.69	430.03	541.21	-103.34 (-24.0%)	-231.53 (-42.8%)
3CAPE	NS	NS	35.95	32.68	45.44	47.52	-9.49 (-20.9%)	-14.84 (-31.2%)
6CAPE	NS	NS	255.88	235.09	237.18	249.86	18.71 (7.9%)	-14.77 (-5.9%)
DCAPE	NS	NS	392.26	359.84	452.92	453.71	-60.65 (-13.4%)	-93.87 (-20.7%)
MLCIN	NS	NS	-35.99	-40.81	-44.13	-37.11	8.14 (-18.5%)	-3.70 (10.0%)
MLLCL	NS	NS	836.67	820.86	941.95	853.34	-105.27 (-11.2%)	-32.49 (-3.8%)
LR100m	NS	NS	6.44	6.13	4.11	2.43	2.33 (56.6%)	3.70 (152.2%)
LR250m	NS	NS	6.34	5.99	5.07	3.45	1.27 (25.0%)	2.54 (73.7%)
LR500m	NS	>75%	6.65	6.31	5.65	4.14	1.01 (17.8%)	2.17 (52.5%)
LR1km	NS	>75%	6.74	6.50	6.17	5.23	0.57 (9.3%)	1.26 (24.2%)
LR3km	NS	NS	6.29	6.21	6.42	6.24	-0.12 (-1.9%)	-0.03 (-0.4%)
LR3-6km	NS	NS	6.08	6.18	6.18	6.16	-0.10 (-1.6%)	0.02 (0.4%)
LLMIX	NS	NS	11.88	11.76	11.51	12.03	0.37 (3.2%)	-0.27 (-2.2%)
PWAT	NS	NS	1.31	1.29	1.32	1.39	-0.02 (-1.4%)	-0.10 (-6.9%)
FZL	NS	NS	3623.34	3572.80	3538.27	3624.09	85.07 (2.4%)	-51.29 (-1.4%)
WBZ	NS	NS	3296.92	3301.56	3219.32	3298.18	77.60 (2.4%)	3.37 (0.1%)
STP	NS	NS	1.20	1.23	1.04	1.18	0.15 (14.7%)	0.06 (5.0%)
SCP	NS	NS	6.03	7.54	4.98	6.04	1.05 (21.1%)	1.50 (24.8%)
SHERB	>75%	>75%	1.30	1.33	1.15	1.15	0.16 (13.8%)	0.18 (15.9%)

Figure 3.4: Table showing all variables listed in Table 3.1 and their statistical significance as in Fig. 3.3 but for QLCS tornadic vs. QLCS nontornadic.

at those levels, or any level (Fig. 3.3). There is greater statistical importance in shear below 3 km for different AzShear strengths. For example, SH500m is larger (23.3%) for stronger mesocyclones (12.7 ms^{-1}) than weaker mesocyclones (10.3 ms^{-1}),

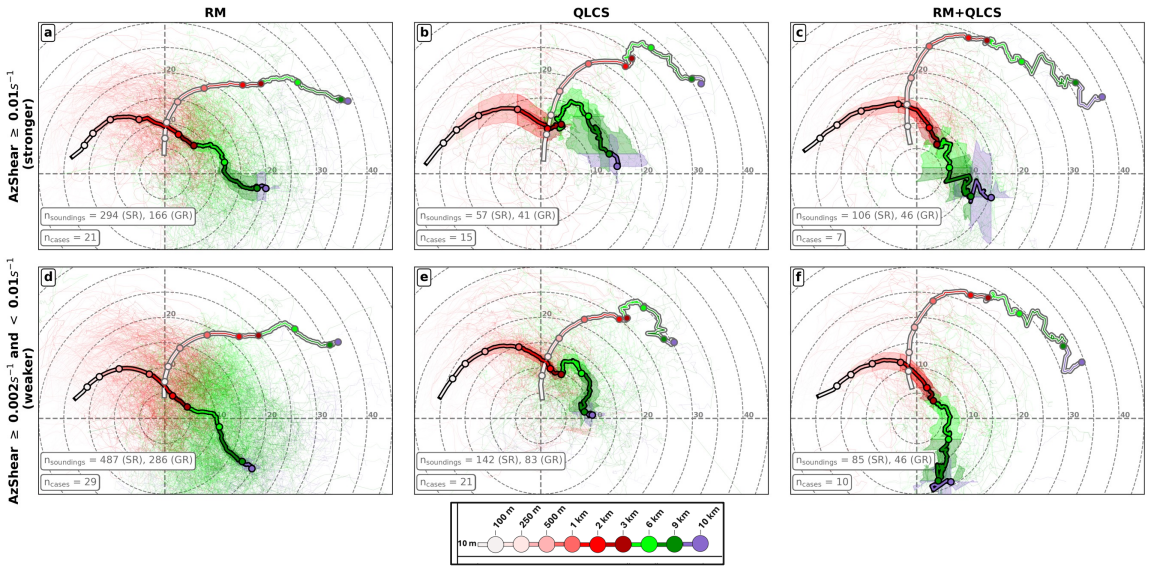


Figure 3.5: Composite hodographs of (a, d) RM, (b, e) QLCS, and (c, f) RM+QLCS storm modes for (a-c) weaker LL AzShear ≥ 0.002 s^{-1} and < 0.01 s^{-1} and (d-f) stronger LL AzShear ≥ 0.01 s^{-1}. The details of the hodograph composites are the same as in Fig. 3.1.

with statistical significance at $\geq 90\%$ (Fig. 3.7). Lower level shear such as SH100m, SH250m, and SH500m do show greater % difference in the means between different mesocyclone strengths than for tornadic vs. nontornadic mesocyclones. Despite shear having a more consistent relationship to mesocyclone strength (i.e., rotational potential) than tornado potential, it is likely resultant of shear values not being supportive of rotational potential. Overall, however, these cases all show relatively strong shear without large statistical differences, likely because field project operations typically occur when there is strong shear that would support tornadic environments. The differences that do emerge between differing AzShear bins are more subtle compared to the well-documented differences that separate tornadic (e.g., strong SRH and low LCL heights) from nontornadic RMs.

The SR hodograph shows greater differences than the GR hodograph for tornadic (Fig. 3.1a) and nontornadic (Fig. 3.1d) RMs, mostly due to significantly larger SRW

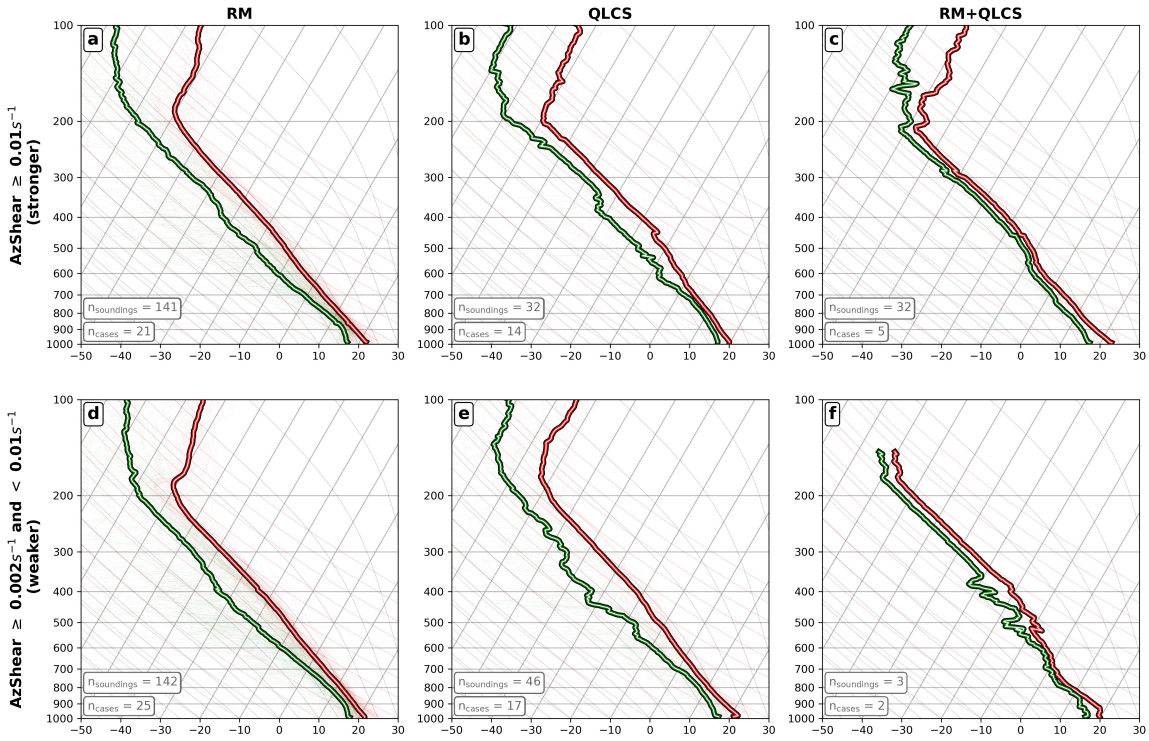


Figure 3.6: Composite skew-Ts of (a, d) RM, (b, e) QLCS, and (c, f) RM+QLCS storm modes for (a-c) weaker LL AzShear ≥ 0.002 s^{-1} and < 0.01 s^{-1} and (d-f) stronger LL AzShear ≥ 0.01 s^{-1}. The details of the Skew-T composites are the same as in Fig. 3.2.

for tornadic RMs (Fig. 3.3). SRW statistically differentiates RM tornadic and nontornadic environments for the SE field project soundings, as it does for GP field project soundings (Coniglio and Parker, 2020, see comparison to their findings in Fig. 3.3). SRW is significantly larger for all RM tornadic mesocyclones as well as for just strong RM tornadic mesocyclones (i.e., those with AzShear ≥ 0.01 s^{-1}). The percentage difference increases for successively deeper SRW layers where the tornadic mean SRW6km (10.9 ms^{-1}) is 49.7% higher than the nontornadic mean (7.3 ms^{-1}). There is increasing SRW with increasing mesocyclone strength (Fig. 3.5a,d) but differences are minor and lack statistical significance (there is weak significance between mesocyclone strength for SRW6km and SRW6km–10km, see Fig. 3.7). These findings suggest SRW has a stronger relation to tornadic potential versus rotational potential.

RM AzShear	statistical significance	AzShear ≥ 0.002 and < 0.01 mean (weaker AzShear)	AzShear ≥ 0.01 mean (stronger AzShear)	difference in means (% difference) (weaker - stronger)
SH100m	**NS**	3.09	3.77	0.68 (22.1%)
SH250m	**>75%**	6.18	7.66	1.47 (23.8%)
SH500m	**>90%**	10.31	12.71	2.40 (23.3%)
SH1km	**>75%**	15.76	18.31	2.55 (16.2%)
SH3km	**>75%**	22.31	25.21	2.90 (13.0%)
SH6km	NS	30.28	31.10	0.82 (2.7%)
SH3-6km	NS	11.09	10.80	-0.29 (-2.6%)
SH6-10km	NS	13.14	14.59	1.45 (11.0%)
SHeff	NS	17.14	18.31	1.17 (6.8%)
SRH100m	NS	39.92	44.63	4.70 (11.8%)
SRH250m	NS	84.83	100.18	15.34 (18.1%)
SRH500m	**>75%**	136.96	183.71	46.75 (34.1%)
SRH1km	**>75%**	205.62	286.34	80.72 (39.3%)
SRH3km	**>75%**	263.88	383.78	119.90 (45.4%)
SRHeff	**>75%**	197.33	284.80	87.47 (44.3%)
CRIT	**>75%**	49.15	58.88	9.73 (19.8%)
SRW100m	NS	17.10	17.87	0.77 (4.5%)
SRW250m	NS	16.54	17.57	1.03 (6.2%)
SRW500m	**NS**	15.45	16.85	1.40 (9.1%)
SRW1km	**NS**	13.36	15.24	1.88 (14.1%)
SRW3km	**NS**	8.43	10.08	1.64 (19.5%)
SRW6km	**>75%**	7.41	9.34	1.93 (26.0%)
SRW3km-6km	**NS**	11.73	13.37	1.64 (14.0%)
SRW6km-10km	**>75%**	16.60	19.40	2.80 (16.8%)
GRW100m	NS	7.39	7.85	0.46 (6.3%)
GRW250m	**NS**	9.09	9.98	0.89 (9.8%)
GRW500m	**>75%**	11.20	12.63	1.44 (12.8%)
GRW1km	**>75%**	14.09	16.05	1.96 (13.9%)
GRW3km	**NS**	19.04	20.82	1.78 (9.4%)
GRW6km	**NS**	22.63	24.23	1.60 (7.1%)
GRW3km-6km	NS	28.98	30.48	1.50 (5.2%)
GRW6km-10km	NS	33.66	35.91	2.24 (6.7%)
MLCAPE	NS	623.41	692.45	69.04 (11.1%)
3CAPE	**NS**	47.14	61.69	14.55 (30.9%)
6CAPE	NS	349.23	393.96	44.74 (12.8%)
DCAPE	NS	507.61	491.15	-16.46 (-3.2%)
MLCIN	NS	-41.19	-36.20	4.99 (-12.1%)
MLLCL	NS	864.06	914.91	50.84 (5.9%)
LR100m	NS	6.04	5.83	-0.22 (-3.6%)
LR250m	NS	6.20	6.16	-0.04 (-0.7%)
LR500m	NS	6.07	5.97	-0.10 (-1.6%)
LR1km	NS	6.07	6.10	0.03 (0.4%)
LR3km	NS	6.35	6.58	0.23 (3.6%)
LR3-6km	NS	6.34	6.37	0.03 (0.4%)
LLMIX	NS	11.95	11.66	-0.29 (-2.5%)
PWAT	**>75%**	1.45	1.27	-0.18 (-12.3%)
FZL	**>75%**	3636.73	3454.61	-182.12 (-5.0%)
WBZ	**>75%**	3292.42	3116.16	-176.26 (-5.4%)
STP	NS	0.81	1.17	0.36 (43.9%)
SCP	**>75%**	3.43	5.39	1.97 (57.4%)
SHERB	**>75%**	1.16	1.35	0.19 (15.4%)

Figure 3.7: Table showing all variables listed in Table 3.1 and their statistical significance for RM with two different LL AzShear ranges, with those being "weaker" (AzShear ≥ 0.002 s^{-1} and < 0.01 s^{-1}) and "stronger" (AzShear ≥ 0.01 s^{-1}). The statistical significance color-coding and bolded values follow the same formulation as in Fig. 3.3. The "difference in means" columns represents the "weaker" bin minus the "stronger" bin, therefore, positive values indicate that the "weaker" bin has a larger value, and negative values indicate that the "stronger" bin has a larger value.

SRH1km, SRH3km, and SRHeff (for all mesocyclones and those with AzShear $\geq$ 0.01 s^{-1}) are significantly larger for tornadic RMs compared to nontornadic (Fig. 3.3). Shallow, near-ground measures of SRH including SRH100m, SRH250m, and SRH500m are larger for tornadic than nontornadic RMs, but not significantly larger—differing from the GP (Coniglio and Parker, 2020). SRHeff does the best in differentiating environments, with the percent difference in means for tornadic (373 m^2s^{-2}) and nontornadic (173 m^2s^{-2}) being 115% (Fig. 3.3). The SRH1km RM tornadic mean of 328 m^2s^{-2} (357 m^2s^{-2} for mesocyclones with AzShear $\geq$ 0.01 s^{-1}) is very similar to Anderson-Frey et al. (2019)'s findings of SRH1km of 334 m^2s^{-2} for all SE tornado events and 355 m^2s^{-2} for HSLC SE tornado events, indicating that the samples obtained by the field projects do not stray much from the larger distribution of low-level shear for tornadic SE events.

Tornadic RMs have a CRIT closer than nontornadic RMs to 90°, with a mean of 66° and 48° for the two populations, respectively (Fig. 3.3). The tornadic CRIT closer to 90° indicates a larger streamwise vorticity component than crosswise component below 500 m (Esterheld and Giuliano, 2008). CRIT increases with AzShear, but not significantly (Fig. 3.7). Wade et al. (2018) and Parker (2014) found CRIT to be largely different for tornadic and nontornadic storms (although the studies showed disparate results on which category had CRIT closer to 90°). Coniglio and Parker (2020) pointed out that the distance and azimuth of the sounding from the storm could impact the CRIT due to spatial variability in the inflow sector, and is part of the reason Wade et al. (2018) and Parker (2014) find differences in CRIT. However, as in Coniglio and Parker (2020), we do not find large differences in the distributions of distance and azimuth between the tornadic and nontornadic subsets, ruling that out as a reason for the CRIT differences.

All measures of CAPE are slightly larger for the nontornadic subset than the tor-

nadic subset (Figs. 3.3 and 3.2a,d). This differs from the GP where larger CAPE tends to coincide with tornadic environments, but the differences in our study are not significant so we do not comment on this further. We did not compare between tornado intensity because of an insufficient sample size, but Anderson-Frey et al. (2019) found much larger CAPE for (E)F4+ tornadoes, but very little differences in MLCAPE for (E)F0-(E)F3 tornadoes compared to nontornadic cases. These findings differ from others who have found increasing MLCAPE with increasing severity (Rasmussen and Blanchard, 1998; Thompson et al., 2003). However, MLLCL heights are lower ($\geq$ 75% significance level) for tornadic RM (and tornadic RM with AzShear ≥ 0.01 s^{-1}), as in the Great Plains (Coniglio and Parker, 2020) and in past literature (Rasmussen and Blanchard, 1998; Thompson et al., 2003).

LR250m and LR500m both have weakly significantly steeper lapse rates for the tornadic subset than the nontornadic (Fig. 3.3). Lapse rates over deeper layers (e.g., LR1km, LR3km, LR3–6km) have little difference in means between tornadic and nontornadic subsets. There is little to no difference in lapse rates with different AzShear bins. Coffer et al. (2019) and Coniglio and Parker (2020) found LR3km was smaller for tornadic supercells, and Coniglio and Parker (2020) mentioned the smaller lapse rates for GP tornadic supercells might not hold for the SE. Steeper mean nontornadic lapse rates are only seen for LR3km, and the difference is negligible (.02 °C km^{-1}). Therefore, their finding does not hold true in the SE. Lapse rates overall are approximately 1 °C km^{-1} lower in the SE than the GP, which is probably linked to overall greater moisture content and/or more large-scale ascent associated with a greater occurrence of kinematic cool-season systems.

Finally, for RMs with AzShear ≥ 0.01 s^{-1}, the mean SCP is 3.4 for nontornadic and 5.4 for tornadic (150.7% increase), similar to the findings of Thompson (2023). STP is higher for RM tornadic (1.17) than nontornadic (0.81), but it is worth noting how

much smaller these values are in the SE compared to those Coniglio and Parker (2020) found for the GP, where tornadic was 4.6 and nontornadic was 1.8. SHERB (Sherburn and Parker, 2014), designed for HSLC environments, similarly has larger values for tornadic RMs as STP and SCP do, but with a smaller percent difference in the means. All the mentioned composite values show weak significant differences between tornadic and nontornadic RMs.

3.4.2 QLCS environments

There are far fewer parameters of significance that distinguish QLCS tornadic and nontornadic environments compared to RM environments (Fig. 3.4). The SR hodographs show more variation than the GR counterparts, with significantly larger low-level SRW (SRW100m, SRW350m, SRW500m, and SRW1km) for tornadic QLCS environments (Fig. 3.1b and Fig. 3.4). The percent difference in means between tornadic and nontornadic environments is largest for SRW1km, which is 28.6% higher (SRW100m) for tornadic QLCS environments (Fig. 3.4). For mesovortices with AzShear ≥ 0.01 s^{-1}, only the lowest levels of SRW (SRW100m and SRW250m) show significance between tornadic and nontornadic (Fig. 3.4). SRW6km and SRW6km–10km is significantly larger for stronger mesocyclones than weaker mesocyclones (Fig. 3.8). This implies that low-level SRW could be more important for tornadic potential and upper level may be more important for rotational potential. SRH, at all levels, shows greater significance between weaker vs. stronger AzShear than tornadic vs. nontornadic for QLCS environments. Again, this links SRH importance to be closer tied to rotational potential vs. tornadic potential. However, there are many more significant parameters when comparing weak and strong AzShear for QLCS mesovortices (Fig. 3.8), which could be due to a smaller sample size compared to other statistical analysis. Therefore, we do suggest further testing of our findings relating to rotational

potential for QLCS mesovortices.

The SRH1km mean for tornadic QLCS environments is 399 m^2s^{-2}, which is higher than the 341–372 m^2s^{-2} (depending on CAPE) that Anderson-Frey et al. (2019) found. This discrepancy is likely due to their use of estimated storm motion (to be explored later), but could also be due to our dataset being on the higher end of low-level shear present in SE environments. These findings are based solely on the motion of the mesocyclone, not the system (i.e., the QLCS) as a whole or the motion of reflectivity cores embedded in the system, so the increased SRW could be a result of the deviant motion of localized surges in the line. However, we recognize the motion of the mesocyclone rather than the associated line segment likely does not give us the whole picture. Further work would be needed to explore how in a line-relative, or system-relative framework, the flow towards the mesocyclone varies for tornadic and nontornadic mesocyclones.

The SRW difference in means between tornadic and nontornadic environments is less for QLCS mesovortices with AzShear ≥ 0.01 s^{-1} than all QLCS mesovortices, but not drastically less (e.g., SRW1km 22.4% vs. 28.6%, respectively) (Fig. 3.4). However, the difference in means for SRH is much lower for mesovortices with AzShear ≥ 0.01 s^{-1} compared to all mesovortices, especially above 1 km (e.g., SRH1km vs. 6.1% vs. 28.5%, respectively) (Fig. 3.4). Simply put, the difference in values of deeper-layer SRH between tornadic and nontornadic QLCS mesovortices is minimal when only considering strong mesovortices, but large differences in SRW values between tornadic and nontornadic mesovortices is still present when only considering strong mesovortices. This means that SRW appears to have a stronger relationship to QLCS tornadic potential, and SRH (especially above 1 km) has a stronger relationship to rotational potential.

All layers of GRW above 500 m show weak significance between between weaker and

stronger mesocyclones (Fig. 3.8), where all percent differences are $\geq 9.9\%$ higher for stronger AzShear mesocyclones. GRW6km and GRW3–6km are significantly larger for tornadic and nontornadic environments (Fig. 3.8). Shear parameters only show significance for stronger mesovortices vs. weaker (Fig. 3.8), not for tornadic vs. nontornadic (Fig. 3.4) (there is weak significance for tornadic to have larger shear for SH500m and SH1km). This points towards upper-level shear being important for mesocyclone strength in QLCS as it seemingly was for RM.

While not significant, buoyancy measures (MLCAPE and 3CAPE) are larger for nontornadic environments (Figs. 3.2e and 3.4) than tornadic (Figs. 3.2b and 3.4) environments, which is consistent with the findings of Thompson et al. (2012, see their Fig. 5 and Table 3). The differences are much less between stronger and weaker mesocyclones (Fig. 3.8). Similarly, low-level lapse rates (LR100m, LR250m, LR500m, LR1km) are insignificantly steeper for tornadic environments, but above 3 km (LR3km and LR3-6km) are insignificantly steeper for nontornadic environments (Fig. 3.4). It therefore seems like steeper lapse are not necessarily characteristic of tornadic QLCS environments in the SE, and a range of low-level thermodynamic profiles can still support tornadic mesovortices.

3.4.3 RM+QLCS environments

While statistics were not computed for RM+QLCS environments due to a limited sample size (especially for n_{cases}), there are some interesting features in the RM+QLCS tornadic vs. nontornadic mesocyclones (Fig. 3.1c,f and 3.2c,f) and RM+QLCS stronger vs. weaker AzShear mesocyclones (Fig. 3.5c,f and 3.6c,f). The tornadic RM+QLCS composite hodograph has larger low-level shear and curvature and appears closer in shape to the QLCS tornadic hodograph than the RM. The nontornadic (Fig. 3.1f), as well as the weaker AzShear composite hodograph (Fig. 3.5f) have the 3–10 km shear

vector pointing almost directly perpendicular to the storm motion, which is characteristically different from any other composite hodograph in the analysis. While we can not draw definite conclusions from the RM+QLCS composites, they do represent environments where QLCS dynamics may be impacting the evolution and hazard potential of RMs.

3.4.4 Storm motion impact on environments supporting both tornadic and nontornadic mesocyclones

We find storm-relative parameters often show the most significant differences between tornadic and nontornadic mesocyclones leading us to hypothesize that differing storm motions are the main differentiator between a tornadic and a nontornadic mesocyclone in a similar environment (i.e., a tornadic environment since there is a tornadic mesocyclone). To further explore this hypothesis, we composite all soundings that are in the inflow sector of at least one of both a tornadic and a nontornadic mesocyclone for RM (Fig. 3.9a) and QLCS (Fig. 3.9b). Composite SR hodographs are generated for all mesocyclones (black hodographs in Fig. 3.9), tornadic mesocyclones (red hodographs in Fig. 3.9), and nontornadic mesocyclones (blue hodographs in Fig. 3.9), drawn from the same number of GR soundings. We evaluate any resulting storm-relative differences between the three composite hodographs. There are negligible differences in mean storm motion and minimal differences in the RM hodograph shape with the only visually apparent difference being between 3–6 km. For QLCS, the tornadic storms do have a larger storm motion and thus larger low-level SRW, however, these differences are relatively minor. There are no statistically significant differences between tornadic and nontornadic mesocyclones in the same tornadic environment resulting from differences in storm motion for RM or QLCS. This finding tells us that the significant differences

in SRW and other storm-relative parameters between tornadic and nontornadic environments are not there when comparing tornadic vs. nontornadic mesocyclones both in similar tornadic environments. Therefore, these storm-relative parameters may not dictate tornadogenesis.

3.5 Environmental parameter dependence on storm motion

3.5.1 RM storm motion

Despite the lack of difference in mean storm motion between tornadic and nontornadic mesocyclones in similar environments, the use of observed storm motions do impact storm-relative parameters. We hypothesize that some differences in our findings from prior literature are due to our use of observed storm motion, motivating quantification of the differences between the Bunkers right-moving estimated storm motion (hereafter, "Bunkers") and observed storm motions. The differences between the mean wind (i.e., GRW6km) and observed storm motion (Fig. 3.10a,c,e) as well as between Bunkers and observed storm motion (Fig. 3.10b,d,f) for tornadic and nontornadic RMs are shown in Fig. 3.10. This subsection focuses on RMs ("all RM") (Fig. 3.10a-b), but RMs are subset by those that have linear characteristics ("linear RM") (Fig. 3.10c-d) and those that do not have linear characteristics ("non-linear RM") (Fig. 3.10e-f). See the caption of Fig. 3.10 for modes included in each subset. Fig. 3.10 is plotted in storm-motion-relative space, where u' and v' indicate observed motion perpendicular and parallel to the reference motion (either the mean wind or Bunkers), respectively.

Observed storm motions are to the right of and slower than the mean wind for both tornadic and nontornadic mesocyclones in all three groups: RMs (Fig. 3.10a),

non-linear RMs (Fig. 3.10b), and linear RMs (Fig. 3.10c). This mean-wind-relative deviance is expected given updraft interactions with the generally westerly shear profiles (populating the upper right quadrant of the hodograph) (e.g., Davies-Jones, 1984) and our focus on mature portions of the storm lifecycles as opposed to earlier periods (e.g., Flournoy et al., 2021).

We find observation motions are slower (i.e., v' is negative) for both tornadic and nontornadic samples, differing from Coniglio and Parker (2020) and Coffer et al. (2025) who found faster observed motions compared to Bunkers. The tornadic sample deviates more right of Bunkers (i.e., u' is larger) than the nontornadic sample in the three subsets (Fig. 3.10b,d,f). The non-linear (linear) RM mean u' is -0.12 ms^{-1} (11.12 ms^{-1}) for tornadic and -6.80 ms^{-1} (1.78 ms^{-1}) for nontornadic (Fig. 3.10e,f), implying linear RM generally deviate more right of Bunkers than non-linear RMs. For non-linear RMs (Fig. 3.10e), noting that nontornadic storms are typically left of Bunkers and tornadic storms are right of Bunkers in the GP (Bunkers, 2018; Coniglio and Parker, 2020; Flournoy et al., 2021; Coffer et al., 2025) could be useful for forecasting in the SE. The timing of the initial rightward turn of RMs in relation to tornado occurrence (i.e., pre- or post-tornado) is an important consideration, as Flournoy et al. (2021) found tornadic supercells deviated more to the right of Bunkers than nontornadic after the initial right turn. We were not able to quantify if deviance was greater in pre- or post-tornadic phases due to insufficient sample sizes. Deviance can also be dependent on the timescale over which storm motion is calculated (Coniglio and Parker, 2020) and is worth further exploration in the SE, but would require additional storm motion calculations than used herein, which is beyond the scope of this study.

3.5.2 QLCS storm motion

Our findings of larger storm-relative winds for tornadic QLCSs differ widely from those in the literature (Thompson et al., 2012; Anderson-Frey et al., 2019), likely due to our use of observed storm motion rather than Bunkers. When there is high SRH and strong clockwise low-level hodograph curvature, Bunkers largely underestimates SRH because of the importance of linear forcing and storm propagation in those supercell cases (Bunkers, 2018)—one of the many reasons Bunkers is not used for QLCS mesocyclone motion. We compared to Bunkers here though for consistency with the RM analysis and for context of our results with previous literature.

QLCS tornadic mesovortices deviate to the right of ($\geq$ 75% confidence interval) and have slower speeds than the mean wind compared to nontornadic ones (Fig. 3.11a). QLCS tornadic mesovortices also deviate more to the right of Bunkers (Fig. 3.11b) than nontornadic mesovortices. The difference in u′ from the mean wind is much larger for QLCSs (Fig. 3.11a) than RMs for both the tornadic and nontornadic subsets. The bearing-relative deviance from Bunkers is positive for both tornadic (u′ of 10.88 ms^{-1}) and nontornadic (u′ of 5.79 ms^{-1}), unlike for non-linear RM where only tornadic storms deviated right of Bunkers (Fig. 3.10e). The larger u′ for QLCSs is likely due to the mean wind being less representative of the advection on the mesovortex motion due to their shallow nature (similar to what Flournoy et al. (2021) found for the initial phase in supercells). There is large spread in v′ for both the deviance from the mean wind (Fig. 3.11a) in the tornadic and nontornadic subsets and from Bunkers (Fig. 3.11b) in the tornadic subset. Due to the large spread, it is difficult to draw further conclusions about differences between tornadic and nontornadic mesovortex speeds.

3.6 Discussion

Understanding the physical process(es) that lead to increased SRW for tornadic mesocyclones is important if SRW could aid forecasting efforts (e.g., monitoring deviant motions of modeled or ongoing storms). Coniglio and Parker (2020) attributes the stronger SRW for RM tornadic storms in the GP to larger GRW and larger deviant storm motions. In our dataset, larger deviant storm motions seem to play a larger role rather than GRW (though the role of GRWs cannot be discounted). Therefore, the key to understanding why larger SRW exists for SE tornadic environments is likely tied to understanding what causes more deviant storm motions in the first place. Coniglio and Parker (2020) states that strong SRW (due to increased deviant motion) could be increasing tornado potential by contributing to a stronger, wider updraft (Peters et al., 2020) and/or hydrometeor size sorting (Brooks et al., 1994; Kumjian and Ryzhkov, 2012) that leads to less undercutting of the mesocyclone by cold air or a more favorable inflow-outflow balance that helps vertically align the low- and mid-level mesocyclones. That leads us to ask: what is the cause of larger storm relative winds? Is it something we can forecast? Which factors mentioned by Coniglio and Parker (2020) could the increased SRW be contributing to factors that increases tornado probability?

Trapp et al. (2017) found increased near-surface vertical vorticity (and stronger mesocyclones) associated with increasing updraft width in various sheared environments. While large SRW is one of the main contributors to increased updraft width, many works succeeding Trapp et al. (2017) have found no link between near-surface vertical vorticity and increased updraft width (Coffer and Markowski, 2018; Fischer and Dahl, 2020; Goldacker and Parker, 2021). Sessa and Trapp (2023) also found mesocyclone width and mesocyclone intensity did not discriminate between tornadic and nontornadic storms. Brown and Nowotarski (2019) found the intensification of

near-ground rotation (i.e., increased tornado potential) is a function of mesocyclone alignment rather than mesocyclone strength. Alignment is a function of the low-level wind profile, which then influences the magnitude of SRW opposing the gust front (Brown and Nowotarski, 2019).

The "Z_{DR} arc" (i.e., increased Z_{DR} values along the forward-flank reflectivity gradient) (Kumjian and Ryzhkov, 2008) and "K_{DP} foot" (i.e., increased K_{DP} values collocated with the precipitation core) (Romine et al., 2008) are often separated due to hydrometeor size sorting (Kumjian and Ryzhkov, 2009; Dawson et al., 2014; Loeffler and Kumjian, 2018). Crowe et al. (2012) found larger separation for tornadic storms over nontornadic (Crowe et al., 2012) in the SE, and Loeffler and Kumjian (2020) found the distance and direction of the separation is correlated to the SRW in the sorting layer (i.e., layer where SRW are strong enough to advect hydrometeors). Very strong mid-level SRW (i.e., what is seen commonly in SE tornadic environments) decreases the amount of rain downstream of the updraft in the forward flank, which leads to less intense outflow and a slow to develop low-level mesocyclone (less susceptible to undercutting; Brooks et al., 1994).

Cold pool intensity is also controlled the evaporation of rain (Mallinson and Lasher-Trapp, 2019), which decreases in environments with low LCL heights (Brown and Nowotarski, 2019), which in turn lead to less negatively buoyant outflow which is more favorable for ingestion into the updraft via low-level dynamic accelerations. Too strong a cold pool can cause displacement of the near-surface rotation away from the strongest dynamic lifting (Markowski and Richardson, 2014) due to a tilted updraft (Guarriello et al., 2018), further emphasizing the importance of alignment. It is possible the SRW and their control on hydrometeors have a large impact on the development and strength cold pools in the SE compared to other cold-pool generation processes (e.g., melting of hail; Snook and Xue, 2008). Meaning, the SRW impact on mesocyclone

alignment could greatly influence tornado potential. This is only a hypothesis and warrants further exploration on what processes in the SE are most controlling of cold pools, and ultimately updraft alignment, as this might hold clues to tornadic potential. For example, if SRW is larger in the sorting layer, or the sorting layer is deeper in the SE (which would be possible due to strong SRW at all layers) compared to the GP, that would be another indicator that SRW might have more control on cold pool development in the SE. Given our findings of increased SRW in all layers for tornadic storms, this finding supports our emphasis on the importance of size sorting in the SE.

3.7 Summary and conclusions

The overarching motivation for this work was to explore the climatology of SE convective environments, which has not received nearly as much attention as environments in the Great Plains. The goal was to develop a climatology that is useful as a baseline for understanding the tornadic potential of convection within an environment typical of the SE compared to other parts of the U.S. To address this goal, we created a database of quality-controlled radiosonde observations (soundings) over 39 cases from the VORTEX-SE, Meso18-19, and PERiLS field campaigns to evaluate environments of different storm modes, strengths, and tornado production in the Southeast US. Mesocyclones (including mesovortices) within 100 km of each sounding were identified and assigned a storm mode based on Smith et al. (2012). Mesocyclone motion, any associated tornadoes, the distance and azimuth from the sounding, and mesocyclone MRMS AzShear were recorded. Soundings were then composited based on a variety of information such as storm mode and tornadic potential and compared to find consistent differences in their environments. The largest differences in environments between modes were found when combining all linear modes and right mover modes into two

generalized storm mode categories we referred to as "QLCSs" and "RMs". Within these two modes, environmental differences for tornadic potential and varying mesocyclone strength were explored. Since storm-relative variables showed significance and often Bunkers is used in forecasting, we explored the differences between the two storm motions. Our key findings are summarized as follows:

- *The environmental differences across the six storm mode major classifications were far less evident than the differences found among tornadic vs. nontornadic storms,* which means tornadic potential could have greater predictability via environmental characteristics leading up to an event than storm mode. Therefore, a forecaster's confidence in tornadic potential should not be hindered by confidence in storm mode.

- *There is greater separation between tornadic and nontornadic environments in the GP than the SE.* Many variables considered on the low end of favorable for the GP are actually the mean of the tornadic sample for the SE (e.g., STP, SCP, lapse rates, etc.). Most studies creating parameter-based climatologies are biased to the GP, and using those values in forecasting could lead to an biased estimation of tornadic potential in SE environments.

- *Few stark thermodynamic differences exist between RM and QLCS tornadic vs. nontornadic environments in the SE.* Differences in thermodynamic parameters show insignificant or only weakly significant differences between tornadic and nontornadic mesocyclones. The kinematic parameters are much more statistically meaningful for both RM and QLCS in differentiating both tornadic vs. nontornadic and stronger vs. weaker mesocyclones.

- *The most significant kinematic difference between tornadic and nontornadic RM and QLCS environments is the larger SRW for tornadic environments.* SRW is

still significantly larger for tornadic mesocyclones than nontornadic when only comparing strong, mature mesocyclones (e.g., those with AzShear ≥ 0.01 s^{-1}). This emphasizes the importance of observed storm motion in identifying storm-relative parameters for forecasting. However, for tornadic environment where both a tornadic and nontornadic mesocyclone(s) is present, we found no significant differences between the mean storm motion of the tornadic mesocyclone and nontornadic mesocyclone. *This finding indicates that there is more to tornadogenesis potential than storm-relative parameters, as the significant differences found between tornadic environments and nontornadic environments is not found when comparing tornadic and nontornadic mesocyclones both present in similar tornadic environments.*

- Deeper-layer GRW was also a significant differentiator of tornadic and nontornadic RM environments as in Coniglio and Parker (2020) and Saba (2024). However, the parameters showing the largest (however, only weakly significant) kinematic differences in environments supporting varying mesocyclone strengths for RMs (in addition to SRW) were SRH above 500 m, GRW500m, GRW1km, and various shear parameters (SH250m, SH500m, SH1km, SH3km). *These results led us to consider the impacts storm-motion (and storm-motion dependent variables) have on tornado potential, and the impact other variables (e.g., GRW or shear) have on potential mesocyclone strength.*

- *Tornadic RMs deviate significantly right of Bunkers compared to the nontornadic storms, which typically deviate left of Bunkers.* There is still uncertainty in the use of deviance from Bunkers for predictability because tornadic classification in our dataset ranges from 40 minutes pre-tornadogenesis to 90 minutes post-tornado. This uncertainty could be addressed through additional subsetting

(e.g., time before or after tornado). While conclusions were not drawn from this analysis due to a limited sample size, the "pre-tornadic" period (40 to 10 minutes prior to tornadogenesis) does not greatly differentiate from the entire RM tornadic subset in 1) deviance from Bunkers and 2) hodograph shape. Thus, the signal seen in the entire tornadic subset is likely also present in the pre-tornadic period and could be useful for tornado prediction.

- Coniglio and Jewell (2022) and Coffer et al. (2025) found that when using observed storm motions instead of motions estimated from the background wind field, the magnitude of differences in SRW between tornadic and nontornadic samples increases. This yields increased importance of deeper-layer SRH. Our findings support this, as across many subsets, deeper-layer SRH (e.g., 0–1 km in depth and above) showed significance where shallower layers did not. *Therefore, similar to how our understanding in the GP has evolved, it seems that deeper layers of SRH exhibit more skill in discriminating RM tornadic vs. nontornadic environments in the SE than shallower layers of SRH.*

The significance of storm-relative variables in distinguishing tornadic and nontornadic environments explain how small-scale storm and environmental evolution can impact the outcome(s) of different storms in similar environments. Our study shows a snapshot in time, and does not explore the environmental evolution (e.g., rapid destabilization) that often occurs prior to severe convection in the SE (King et al., 2017; Lin et al., 2023). It would be worthwhile for future work to explore how the most significant variables found herein (e.g., SRW) evolve preceding tornadogenesis and how the evolution changes with varying deviance from Bunkers storm motion. With a larger mesocyclone dataset than we have herein, it would be of interest to bin mesocyclones by AzShear (or rotational velocity) strength and within each AzShear bin subset by

tornadic and nontornadic mesocyclones (and subset by pre- and post-tornadic mesocyclones) to further explore if the storm-relative variables are still most significant in differentiating tornadic potential for different ranges of mesocyclone strengths. An analysis of this kind could give us information on how much tornadic potential can be predicted via storm-relative variables for a given mesocyclone strength (or if mesocyclone strength is relevant for tornado predictability). Objective methods for storm mode classification (like those of Potvin et al. (2010)) could help increase dataset size, and lead to larger, more complete climatologies across different regions, environments, seasons—all of which could lead to improvement of our understanding of what possible behaviors and range of outcomes we can infer from a storm's mode and mesocyclone strength.

QLCS AzShear	statistical significance	AzShear ≥ 0.002 and < 0.01 mean (weaker AzShear)	AzShear ≥ 0.01 mean (stronger AzShear)	difference in means (% difference) (weaker - stronger)
SH100m	**>75%**	2.96	4.50	1.53 (51.8%)
SH250m	**>90%**	6.42	9.31	2.90 (45.2%)
SH500m	**>95%**	9.91	14.62	4.71 (47.6%)
SH1km	**>99%**	15.56	21.15	5.59 (35.9%)
SH3km	**>75%**	22.74	26.42	3.68 (16.2%)
SH6km	NS	27.05	30.11	3.06 (11.3%)
SH3-6km	NS	8.48	9.25	0.76 (9.0%)
SH6-10km	NS	12.97	12.60	-0.36 (-2.8%)
SHeff	**>75%**	14.50	18.84	4.34 (29.9%)
SRH100m	**>75%**	40.55	69.47	28.92 (71.3%)
SRH250m	**>90%**	90.06	149.31	59.25 (65.8%)
SRH500m	**>90%**	144.25	238.74	94.48 (65.5%)
SRH1km	**>95%**	216.19	390.22	174.03 (80.5%)
SRH3km	**>75%**	328.81	531.34	202.53 (61.6%)
SRHeff	**>90%**	217.47	389.78	172.31 (79.2%)
CRIT	**>75%**	51.16	61.83	10.67 (20.9%)
SRW100m	NS	18.76	20.28	1.51 (8.1%)
SRW250m	**>75%**	17.96	19.86	1.90 (10.6%)
SRW500m	**>75%**	16.94	19.44	2.50 (14.8%)
SRW1km	**>90%**	15.39	18.46	3.07 (20.0%)
SRW3km	**>90%**	10.72	13.96	3.24 (30.3%)
SRW6km	**>95%**	8.87	13.04	4.17 (47.1%)
SRW3km-6km	**>95%**	11.07	14.75	3.68 (33.3%)
SRW6km-10km	**>90%**	10.24	16.39	6.15 (60.1%)
GRW100m	NS	8.08	8.06	-0.02 (-0.3%)
GRW250m	NS	9.80	10.57	0.77 (7.8%)
GRW500m	**>75%**	11.97	13.78	1.81 (15.2%)
GRW1km	**>90%**	15.17	18.15	2.97 (19.6%)
GRW3km	**>75%**	20.68	23.68	3.00 (14.5%)
GRW6km	**>75%**	23.88	26.25	2.37 (9.9%)
GRW3km-6km	**>75%**	28.19	31.27	3.08 (10.9%)
GRW6km-10km	>75%	29.47	34.52	5.05 (17.1%)
MLCAPE	NS	338.46	453.50	115.03 (34.0%)
3CAPE	NS	42.90	41.49	-1.41 (-3.3%)
6CAPE	NS	243.63	242.97	-0.66 (-0.3%)
DCAPE	NS	459.02	408.96	-50.06 (-10.9%)
MLCIN	NS	-44.67	-38.59	6.08 (-13.6%)
MLLCL	**>90%**	1007.19	832.50	-174.69 (-17.3%)
LR100m	NS	6.17	4.32	-1.85 (-30.0%)
LR250m	>75%	6.96	4.73	-2.23 (-32.0%)
LR500m	**>75%**	7.30	5.28	-2.02 (-27.7%)
LR1km	**>75%**	7.20	5.90	-1.30 (-18.1%)
LR3km	NS	6.59	6.23	-0.36 (-5.4%)
LR3-6km	NS	6.18	6.13	-0.05 (-0.8%)
LLMIX	NS	11.26	11.90	0.64 (5.7%)
PWAT	NS	1.28	1.34	0.06 (5.0%)
FZL	NS	3521.08	3603.05	81.97 (2.3%)
WBZ	NS	3170.86	3300.12	129.25 (4.1%)
STP	NS	0.83	1.27	0.44 (53.5%)
SCP	>75%	3.63	6.61	2.97 (81.9%)
SHERB	NS	1.15	1.24	0.08 (7.1%)

Figure 3.8: Table showing all variables listed in Table 3.1 and their statistical significance as in Fig. 3.7 but for QLCS.

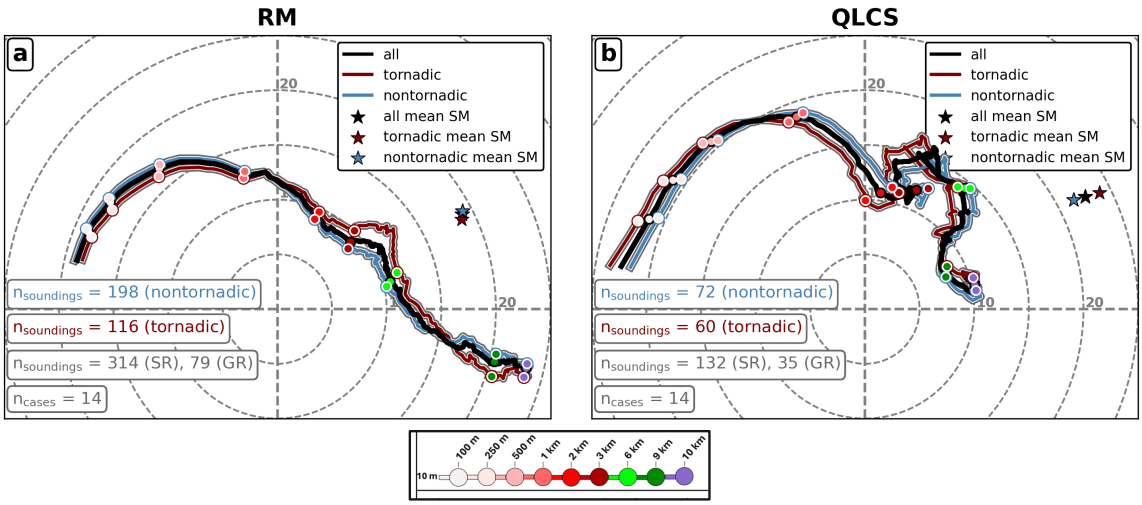


Figure 3.9: Composite SR hodographs of (a) RM and (b) QLCS environments where both a tornadic and nontornadic mesocyclone are present in the inflow of the sounding. The RM and QLCS mode classifications are the same as in Fig. 3.1. The solid black line "all" is the composite SR hodograph using all mesocyclones present in the mixed tornadic and nontornadic environment. The blue hodograph is created using the nontornadic mesocyclones and the red hodograph is for the tornadic mesocyclones. The colored dots to represent the height levels are the same as in Fig.3.1 and shown in the legend, with all mesocyclones having a black outline, tornadic having a red outline, and nontornadic having a blue outline. The mean storm motion (SM) is plotted on the hodograph with a star and color coded as the hodographs are. The n_{cases} and $n_{soundings}$ (GR) will remain the same, as each sounding is required to have both a tornadic and nontornadic mesocyclone. The $n_{soundings}$ (SR) varies because there may be multiple tornadic and/or nontornadic mesocyclones associated with one sounding. The SR $n_{soundings}$ included in the tornadic composite is shown in red and the $n_{soundings}$ included in the nontornadic composite is shown in blue.

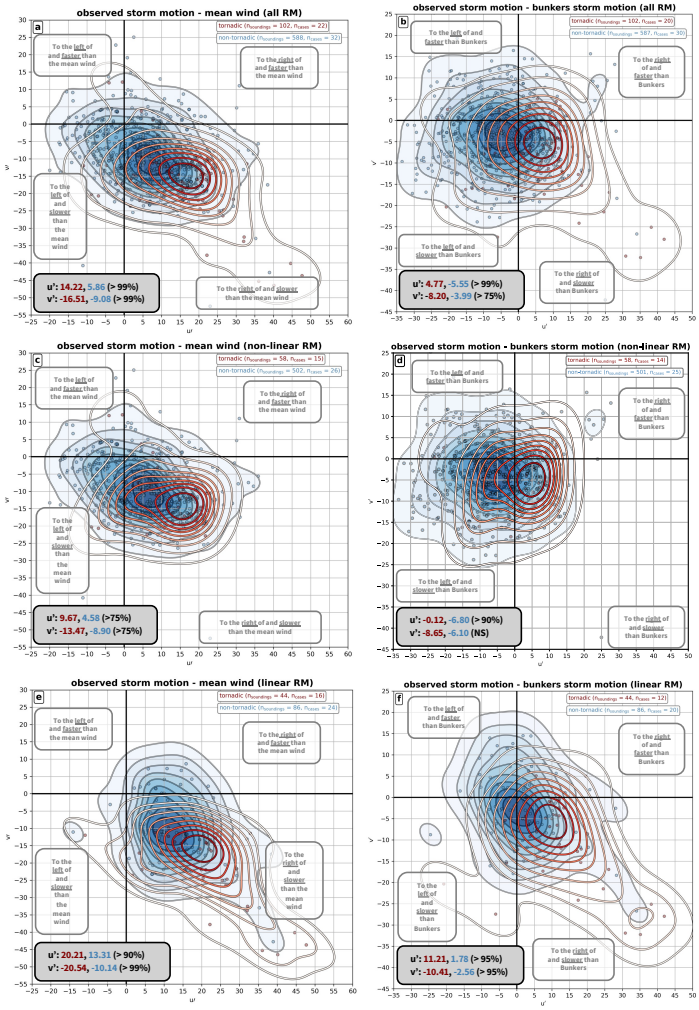


Figure 3.10: Kernel Density Estimation plots of tornadic (reds with no fill) and nontornadic (color-filled blues) observed storm motion deviation from the a,c,e) mean wind (GRW6km) and from b,d,f) Bunkers right storm motion for a,b) all RMs, c,d) nonlinear RMs (modes 4-1, 4-2, 5-1, and 5-2 in Fig. 2.2) and e,f) linear RMs (modes 2-2, 4-3, and 5-3 in Fig. 2.2). The x-axis is the deviation in v (v′) and the y-axis is the deviation in u (u′), therefore, points within the upper (lower) quadrants have a faster (slower) observed storm motion than the mean wind or Bunkers, and points in the left (right) quadrants have a more leftward (rightward) observed storm motion than the mean wind or Bunkers. The values for $n_{soundings}$ and n_{cases} for tornadic (red) and nontornadic (blue) are in the top right quadrant of each subplot. In the bottom right quadrant is the mean value for u′ and v′ in red for tornadic and blue for nontornadic. The value in parentheses is the significance of u′ and v′ between the tornadic and nontornadic subsets using n_{cases}.

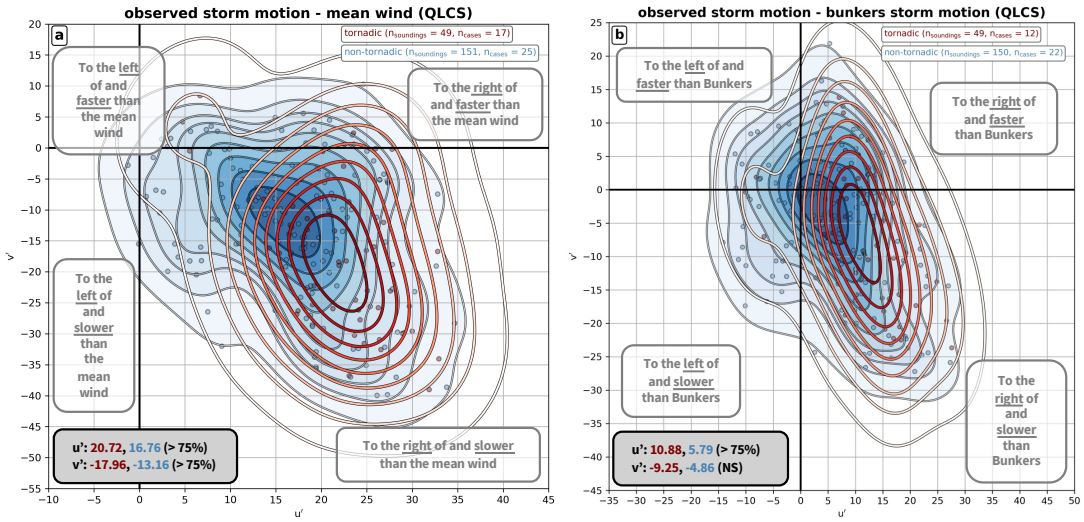


Figure 3.11: KDE plots of tornadic (reds with no fill) and nontornadic (color-filled blues) observed storm motion deviation from the a) mean wind (SH6km) and from b) Bunkers right storm motion for all QLCS modes (modes 1-1, 1-2, and 2-1, see Fig. 2.2). The other aspects of the plot are the same as the panels described in Fig. 3.10.

Chapter 4

Comparison of Model Sounding Profiles to Field-Project Soundings in the Southeast United States: Implications for Southeast U.S. Environmental Studies

4.1 Introduction

Soundings, whether observed of model-derived, are a valuable tool for assessing severe weather potential via environmental conditions. Historically, observed soundings are routinely launched at 0000 and 1200 UTC daily from select National Weather Service (NWS) locations, although many sites in the Great Plains and Intermountain West now launch at 1800 UTC instead of 1200 UTC. Special soundings are possible if hazardous weather is expected. During intensive operating periods (IOPs) of field projects, additional soundings are launched for research purposes, but are also disseminated to operational forecasters. However, the vast majority of convective storms are not sampled by routine or special (NWS or research) soundings. Thus, forecasters rely on gridded analyses from numerical weather prediction models to diagnose the ambient environment. Sounding profiles generated from gridded analyses allow for more detailed temporal and spatial diagnosis of the environment. For a model to run within reasonable bounds of computational expense and time, assumptions and approximations must be made about atmospheric processes that are not fully understood. Many of these assumptions are tied to different boundary layer, microphysics, and radiation parameterization schemes unique to the model, which have shown sensitivity in the SE (e.g., Cohen et al., 2017). Understanding potential systematic and case-dependent biases of the various parameterization schemes provides context to forecasters when incorporating model output into the forecast process. This study uses field observations to quantify environmental characteristics during severe weather events; but given their temporal and spatial confines, we evaluate output from higher-resolution model analyses that forecasters might incorporate into storm-scale prediction: the Storm Prediction Center (SPC) mesoscale surface objective analysis (SFCOA; Bothwell et al., 2022) and High-Resolution Rapid Refresh (HRRR; Dowell et al., 2022) forecast model.

The RAP/RUC (will refer to it solely as "RAP" hereafter) is an analysis and forecast system frequently used in operations. The RAP assimilates available observations (e.g., NWS rawinsonde observations (RAOB), surface station, and aircraft) to generate hourly analyses of current environmental conditions and short-term forecasts (21-51 hours). RAP soundings have previously been used to create tornadic vs. nontornadic storm, storm mode, or storm report-based environmental climatologies (Thompson et al., 2003, 2012; Grams et al., 2012; Smith et al., 2012; Coffer et al., 2019). SFCOA assimilates observations and replaces the RAP 2-m temperature, humidity, and wind, and the 10–m wind with current surface observations via a two-pass Barnes analysis. Given that SFCOA is essentially the RAP with a more realistic depiction of surface conditions, SFCOA has been found to produce smaller mean errors in commonly used forecast parameters (Coniglio, 2012). However, SFCOA near-ground winds have been found to be too slow compared to observations, which can bias calculations of forecast parameters such as storm-relative helicity (SRH) (Coffer et al., 2019). In this study, we focus on SFCOA analyses to diagnose severe environments in the SE.

The HRRR is a convection-allowing model (CAM) run every hour, resulting in analyses every hour. The frequent HRRR cycles are a useful tool for forecasters in fast-evolving environments. The convection-allowing nature of the HRRR allows for the HRRR to capture small-scale storm-induced environmental modification (Coffer et al., 2025), whereas SFCOA cannot. However, profiles extracted for the HRRR can be convectively contaminated, so caution must be taken to ensure profiles represent the ambient environment. Primarily, the HRRR is used as an operational forecasting tool. Few environmental climatologies use the HRRR (Katona et al., 2016; Coffer et al., 2025), but the findings of Coffer et al. (2025) make it an appealing alternative to RAP/SFCOA based climatologies.

Both Coniglio and Jewell (2022) and Coffer et al. (2025) used large supercell

datasets to explore potential biases in soundings from gridded analyses, the downstream impacts on environmental parameter calculations, and skillfulness of some of the more commonly used parameters. Coniglio and Jewell (2022) used a Great Plains field project sounding dataset (Coniglio and Jewell, 2022) to compare observed profiles to SFCOA profiles. The dataset featured 902 observed soundings launched in the vicinity of 216 different supercells on 109 unique days. Coffer et al. (2025) used a larger supercell dataset (n = 6397/8637 nontornadic, 764/9114 weakly tornadic, and 255/1890 significantly tornadic supercells, for HRRR/SFCOA, respectively) spanning the entire U.S., obtained via objective tracking using the GridRad-Severe dataset (Murphy et al., 2023), to compare SFCOA and HRRR profiles. Despite including supercells outside of the Great Plains, Coffer et al. (2025) mentioned their sample (especially for nontornadic supercells) could be lacking in SE cases due to a weakness of the GridRad storm tracking algorithm in capturing low-topped supercells. As a result, how applicable the environmental analyses from these two studies are to SE convective environments remains an open question. This is a primary motivation for this study.

Creation of a database of observed field-project and National Weather Service (NWS) soundings from Southeast-focused field projects is detailed in Chapter 2. The database includes 2497 soundings from 39 different events in the SE during field campaigns from 2016–2023. We use this dataset to compare observed sounding profiles to both SFCOA and HRRR profiles. We also compare environments for both RMs and QLCSs, rather than just RMs as in Coniglio and Jewell (2022) and Coffer et al. (2025).

A primary finding in Chapter 3 was that tornadic storms were characterized by significantly higher SRW than nontornadic ones, regardless of storm mode—corroborating Coniglio and Parker (2020)'s finding of larger low- and mid-level SRW for tornadic supercells. These conclusions were reached using observed soundings with observed storm motions; this differs from RAP-based studies that used Bunkers storm motion

(Bunkers et al., 2000) and found minor, insignificant differences in SRW between tornadic and nontornadic storms (e.g., Thompson et al., 2003; Markowski et al., 2003; Nowotarski and Jensen, 2013; Coffer et al., 2019). While Coniglio and Jewell (2022) found large kinematic errors in SFCOA/RAP profiles, they concluded the errors were not the reason for why they found SRW to be significantly higher for tornadic storms. RAP/SFCOA based climatologies do not register storm-induced or mesoscale (e.g., outflow boundaries) environmental modifications as observed soundings can, but Coniglio and Jewell (2022) concluded environmental modification is also not the sole reason Coniglio and Parker (2020) found larger SRW in tornadic environments. Coniglio and Thompson (2024) further explored potential causes for the discrepancies between tornadic and nontornadic SRWs, including: 1) regionality, seasonality, and time of day, 2) field-campaign bias (i.e., the sample consisting of mostly stronger, nearly tornadic storms), or 3) use of observed rather than Bunkers storm motion impacting the skill of SRW. They found both the field campaign bias (e.g., sampling the stronger part of the nontornadic supercell distribution) and the use of observed storm motions played a role in why SFCOA/RAP SRWs were significantly different in tornadic vs. nontornadic environments in Coniglio and Parker (2020).

Coniglio and Parker (2020) found that deviation of tornadic storms to the right of the mean wind (which tends to be enhanced using observed storm motions) results in greater SRWs aloft (e.g., above 500 m AGL). This yields enhanced deeper-layer SRH while low-level SRH remains more constant (Coniglio and Parker, 2020, see their Fig. 11). This finding motivated Coniglio and Jewell (2022) and Coffer et al. (2025) to further investigate discrepancy between past works finding shallower layers of SRH to be more skillful in tornado forecasting (Rasmussen, 2003; Esterheld and Giuliano, 2008; Nowotarski and Jensen, 2013; Parker, 2014; Coffer et al., 2019) vs. the more recent findings that deeper layers of SRH may be more skillful when using observed

storm motion (Coniglio and Parker, 2020). The dataset created by Coffer et al. (2025) was designed to negate the field-campaign bias that is present in Coniglio and Parker (2020), so they could confidently conclude the use of observed storm motions are the likely cause of deeper-layer SRH being more skillful. The Coffer et al. (2025) study further affirmed the importance of observed storm motion on deeper-layer SRH found in Coniglio and Jewell (2022). In the Coniglio and Thompson (2024) exploration of the difference between Bunkers storm motion and observed storm motion on skill of storm-relative parameters, they found 0–500 m SRW, 0–1 km SRW, 0–1 km SRH, 0–3 km SRH, and effective SRH were much more skillful when observed storm motions were used.

Our motivation is to determine if the results from Coniglio and Jewell (2022), Coniglio and Thompson (2024), and Coffer et al. (2025), which are generally Plains-centric, are applicable in SE environments. In particular, we explore if incorporating observed storm motions emphasizes the importance of SRH in the 1–3 km layer and if the HRRR is more similar to the observations than SFCOA (e.g. Coffer et al., 2025). This will yield information about the biases of the HRRR and SFCOA in the SE, which can then be used as precautionary information for forecasters during operations. Despite the HRRR being retired in the coming years, more climatologies are using the HRRR over SFCOA/RAP, further motivating its usage herein. There has been work done to evaluate HRRR biases in the SE, however, these studies have primarily focused on near surface conditions (Lee et al., 2019, 2023; Wade et al., 2023a). Since SFCOA and HRRR are used operationally for real-time diagnostics prior to convective initiation when storm motion information is unavailable, quantifying biases in Bunkers storm-motion-derived parameters is essential for evaluating tornado potential. Comparing the observed sounding dataset in the Southeast from Chapter 3 to SFCOA and HRRR profiles, we will explore the following for both RM and QLCS storm modes:

1. What are the biases found in SFCOA/HRRR profiles relative to observed profiles?

2. Does the skill of various forecasting parameters in distinguishing between tornadic and nontornadic environments change for SFCOA/HRRR vs. observed profiles?

3. Does the skill of various storm-relative parameters change if observed storm motions or Bunkers storm motions are used? Does the skill of storm-motion-dependent parameters change for SFCOA/HRRR vs. observed profiles?

4.2 Data and methods

4.2.1 SFCOA and HRRR data

SFCOA has 36 vertical levels (every 25 hPa) on a 40–km horizontal grid across the CONUS. SFCOA has only three levels below 500 m, which Coniglio and Jewell (2022) mentioned could be a contributor to the SFCOA near-surface negative bias in ground-relative wind speed. The native RAP has more vertical levels (51) and is on a 13–km grid, but it has not been used in climatological studies as much as the SFCOA has been—warranting comparison of SFCOA to observations rather than the native RAP. Coniglio and Jewell (2022) found no systematic differences between 40–km SFCOA and 13–km RAP data, but did find modest improvement in RAP for some cases in the lowest 500 m.

The 00-h HRRR analyses are used for the HRRR soundings. The HRRR has 51 vertical levels (as in the native RAP) and 3–km grid spacing. The vertical spacing in the lowest levels is 15–30 m, increases to approximately 400 m in the troposphere, and approximately 700 m near the tropopause (Dowell et al., 2022). As with SFCOA, the HRRR also uses 2–m temperature and dew point field and 10–m winds as surface values, however, these are not obtained via the same observational data assimilation

techniques in SFCOA used to improve the accuracy of the near-surface values. The HRRR has been updated throughout our dataset period (2016–2023) (see Fig. 1 of James et al. (2022) for a timeline of HRRR modifications and Table 4 of Dowell et al. (2022) for details of the changes). Katona et al. (2016) noted large, possibly nonphysical variability due to HRRR updates between 2015–2016, however, any variability within our dataset would come from the configuration updates in 2018 and 2021. There is no systematic fix to account for the configuration updates, but we acknowledge the limitation.

4.2.2 Interpolation

To directly compare the observational dataset (hereafter, this dataset will be referred to as "OBS") from Chapters 2 and 3 to HRRR and SFCOA, we first create a single representative HRRR and SFCOA profile for each OBS profile. First, the HRRR and SFCOA profiles are obtained for the four surrounding grid points of each OBS sounding (i.e., the grid points that make up the 3–km × 3–km or 40–km × 40–km box that encloses the OBS sounding). Profiles are obtained for both the time before and after OBS launch—totaling up to 8 profiles each for HRRR and SFCOA that will be used for interpolation (Fig. 4.1). Before interpolation of the profiles to one representative sounding, all 16 profiles must be regridded to the OBS height grid (i.e., 10 m surface, 50 m for the second level, and then every 50 m up to 10 km for the winds). SFCOA is interpolated using a Gaussian-weighted vertical interpolation function (see Chapter 3) with a $\sigma = 100$ m. Since HRRR is on native levels, distance between height levels increases with increasing height, so to ensure consistent interpolation across all levels, a height-dependent σ was applied to scale with increasing distance between available levels: 50 m below 500 m, 100 m from 500 m to 1 km, 300 m from 1—6 km, and 500 m above 6 km. Upscaling the SFCOA and the HRRR profiles allows for direct

comparison of the modeled profiles and OBS (as in Coniglio and Jewell, 2022).

The eight profiles can then be combined into a single representative profile using a Gaussian weighting function in both space and time. The spatial weighting uses $\sigma = 28$ km for SFCOA $\sigma = 2$ km for HRRR. We explore two different methods for the temporal interpolation, where 1) the two spatial interpolated profiles are temporally interpolated at the hour before and after sounding time and 2) only the spatially interpolated profile at the hour prior to sounding time is used. The second method follows Coffer et al. (2025) and Thompson et al. (2012), who expressed concern that using profiles after a storm event (here, after sounding launch time since mesocyclone characteristics are recorded relative to sounding launch time) could result in an unrepresentative profile due to either storm contamination or capturing an undesired post-storm environment. However, this method could also lead to unrepresentative environments because of how rapidly environments can evolve in one hour. A majority of these soundings were launched within a 10-minute period on either side of the top of the hour. Therefore, we do not want soundings that are intended to represent the 1800 UTC environment but were launched at 1802 UTC to be represented in this dataset by the 1900 UTC sounding[1]. Since both methods we tested had negligible differences, we opted to interpolated temporally using a temporal $\sigma = 30$ min. This spatial-temporal interpolation yielded a model profile representative of the observed sounding location and launch time.

4.2.3 Spatial and temporal criteria

Coniglio and Jewell (2022) did not include soundings within 10 km of an updraft because 1) many soundings within 10 km of the updraft entered the updraft and

[1]There are occurrences where neither the hour immediately before or after were available, and in that case, the analysis time 2-hr prior is used. For example, if a sounding occurred at 20:12:19 UTC, but the 20Z and 21Z were both unavailable, the 19Z is used for the time prior.

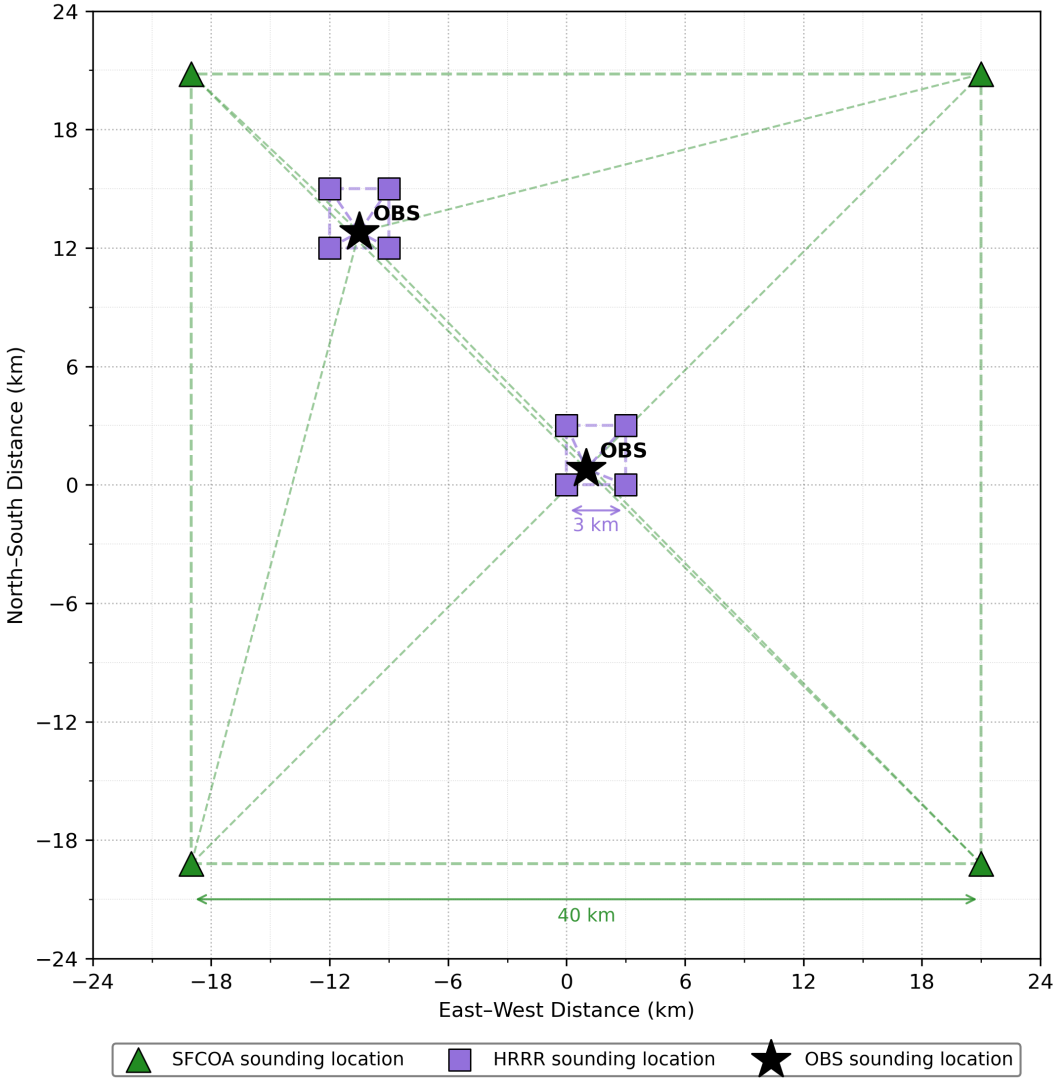


Figure 4.1: Schematic illustrating the grid point selection method for HRRR (purple squares, 3–km grid) and SFCOA (green triangles, 40–km grid) model profiles relative to two example OBS sounding locations (black stars). For each OBS sounding, profiles at the four surrounding model grid points are extracted at the hour before and after the OBS time. Dashed lines connect each sounding location to its four surrounding model grid points.

sampled the storm itself, and 2) storm-induced modification would likely be sampled within 10 km (Potvin et al., 2010). Since our quality control process removes any part of the sounding profile that entered an updraft—and we wish to retain any storm-scale

modifications present in the HRRR—we do not impose a 10–km threshold. Other studies have defined near-field and far-field representative soundings (e.g., Coniglio and Parker, 2020). For the purposes of this study, we focus on mean 0—100–km soundings to define tornadic vs. nontornadic and RM vs. QLCS environments, as the entire 0–100–km subset shows little variation compared to the smaller far-field subset (not shown).

4.2.4 Composite profiles

Composite hodographs are generated for SFCOA and HRRR as they are for OBS, following the methods described in Chapter 3 and are briefly described herein. Both the ground-relative (GR) and storm-relative storm-rotated (SR) hodographs are composited. The SR composites are often comprised of a greater number of hodographs because a single sounding can be used more than once if it samples the environment of multiple mesocyclones (with different motions). The tornadic, nontornadic, RM, and QLCS subsets are the same as in Chapter 3. A mesocyclone is characterized as tornadic if it produced a tornado between 40 min prior to and 90 min after the sounding launch time (similar to Coniglio and Parker, 2020). The tornadic bin includes all tornadic storms in the inflow, including 1) if there are multiple tornadic storms or 2) if there is also a nontornadic storm(s) present. Nontornadic is defined as only a nontornadic storm, or multiple nontornadic storms, present in the inflow. RM is defined as only RM storm(s) being present in the inflow, and QLCS as only QLCS storm(s) present in the inflow. Cases where there are both RM and QLCS storms present in the inflow are deemed "RM+QLCS" in Chapter 3, but will not be further explored here due to a limited sample size of such cases. There are a few number of cases (9 for RM nontornadic and 14 for QLCS nontornadic) where either HRRR and/or SFCOA profiles were not available. To perform a direct comparison between OBS, SFCOA, and HRRR,

soundings where all three are not available are discarded, ensuring a missing case does not bias the results.

4.2.5 Statistical analysis

OBS is compared to SFCOA and HRRR directly by calculating the mean error (ME), which is defined as SFCOA or HRRR minus OBS. The ME provides information on SFCOA and HRRR bias with information on the direction of overestimation (i.e., warm/fast bias) or underestimation (i.e., slow/cool bias). The mean absolute error (MAE) is calculated, and gives a measure of HRRR and SFCOA accuracy (using OBS as truth) without considering the direction of bias. A two-tailed Monte Carlo test is performed to determine the 95% confidence interval on the MEs and MAEs (represented by shading in subsequent figures).

To understand if certain forecast parameters show significance between tornadic and nontornadic samples as well as between OBS, SFCOA, and HRRR, we perform significance testing following the methods described in Chapter 3 (as done for tornadic vs. nontornadic for OBS). The variables used in the significance testing are shown in Table 3.1. The statistical significance of the difference in means between two subsets at four different significance levels (75%, 90%, 95%, and 99%) is determined using a two-tailed Monte Carlo test with 10000 iterations. Two different effective sample sizes are used in Chapter 3, including the number of soundings in a subset ($n_{soundings}$) and the number of cases in a subset (n_{cases}). Since they primarily focused on results using n_{cases}, we only use n_{cases} as the effective sample size for statistical testing. As with the composites, when comparing different data sources (e.g., OBS vs. SFCOA or OBS vs. HRRR), if a sounding is unavailable for one source, it is excluded from the other maintain a one-to-one comparison.

4.3 Results

We evaluate errors in SFCOA and HRRR composite environments for the tornadic, nontornadic, and combined (tornadic+nontornadic) subset for both RM and QLCS. We compute statistics on the tornadic vs. nontornadic subsets within OBS, HRRR, and SFCOA to understand if one data source shows greater differences between their tornadic vs. nontornadic environments. The RM analysis for OBS vs. SFCOA can be compared to the findings of Coniglio and Jewell (2022), who used similar methods to compare OBS vs. SFCOA in the Great Plains. Since they subset their data by far-field and near-field, it is not a one to one comparison, but our results are most similar to their far-field results. Understanding how SFCOA biases may differ in the SE compared to the GP is one of the main motivators of this work. We are also motivated by Coffer et al. (2025) in examining HRRR environments. The thermodynamic results are explored in section 4.3.1 and ground-relative wind results explored in section 4.3.2.

The storm-relative results are detailed in section 4.3.3. For storm-relative winds and associated parameters, the statistics on the tornadic vs. nontornadic subsets within OBS, HRRR, and SFCOA are calculated using both observed storm motions and Bunkers estimated storm motion to answer the third question outlined in the Introduction. For both storm-relative wind calculations, the OBS soundings with observed storm motion are used as the subtrahend (i.e., the truth) whenever calculating the errors.

4.3.1 Thermodynamic errors

Below 850 hPa, SFCOA/HRRR both overestimate dewpoint (Figs. 4.3a,c and 4.4), with greater overestimation in tornadic environments. MLLCL heights are significantly lower for the tornadic subset in SFCOA (673 m) and lower in HRRR (724 m) compared

to OBS (814 m) (Fig. 4.5a). Coniglio and Jewell (2022) did not find much variation in low-level moisture below 850 hPa between OBS and SFCOA (and HRRR) like we find in the SE, and consequently found little variation in MLLCL heights. Comparing MLLCL heights for tornadic vs. nontornadic environments within each data source, SFCOA has the largest (and most significant) difference between MLLCL heights for tornadic vs. nontornadic (673 m vs. 875 m, respectively) followed closely by HRRR (722 m vs. 900 m) and then OBS (814 m vs. 931 m) (Fig. 4.6a). Lower MLLCL heights for tornadic storms is well documented (Rasmussen and Blanchard, 1998; Thompson et al., 2003; Craven and Brooks, 2004; Wade et al., 2018; Coniglio and Parker, 2020), but the fact that SFCOA/HRRR shows greater significance for MLLCL heights than OBS is worth noting—and is likely due to SFCOA and HRRR overestimating low-level dewpoints (Fig. 4.4c). Up to 1 km, QLCS dewpoints have minimal error, with the exception of HRRR tornadic having a less than 1 °C warm bias (Fig. 4.4d). The lower discrepancy in low-level moisture for QLCS compared to RM tornadic and nontornadic environments results in no significant difference in MLLCL heights for QLCSs (Figs. 4.5b and 4.6).

Temperature errors are minimal for both HRRR and SFCOA for RM with MAEs not exceeding the 0.75 °C to −1 °C range (Fig. 4.4a) through 6 km, evident also via the skew-Ts (Fig. 4.3a and c). Albeit small errors, SFCOA and HRRR do underestimate low-level temperatures, agreeing with the cooler tornado inflow Wade et al. (2023a) found for a suit of CAMs in the SE. Given the relatively small low-level temperature and dewpoint errors for RM, 3CAPE (and 6CAPE) shows no significant differences between data sources (Fig. 4.5a). 3CAPE tells a different story for QLCS, having larger values for OBS (Fig. 4.5b), likely due the QLCS warm temperature bias peak at 2 km (i.e., decreasing the CAPE) (Fig. 4.4b). The 1–4–km warm bias does exist, but is less pronounced for RM (Fig. 4.4a) compared to QLCS (Fig. 4.4b). 3CAPE is not

a significant distinguisher between tornadic and nontornadic environments (Fig. 4.6a) like it is in the Great Plains (Coniglio and Jewell, 2022).

MLCAPE for both RM and QLCS tells a different story, with significantly larger values for SFCOA compared to OBS (55–65% for RM and 70–80% for QLCS) (Fig. 4.5a–b). More positive temperature biases in the HRRR compared to SFCOA (Fig. 4.4a–b) results in lower MLCAPE for HRRR compared to SFCOA. The larger MLCAPE than OBS in both SFCOA/HRRR is likely resultant from an increasing low dewpoint (Fig. 4.4c–d) bias with height (e.g., Benjamin et al., 2004b; Coniglio, 2012; Evans et al., 2018; Coniglio and Jewell, 2022; MacDonald and Nowotarski, 2023), resulting in larger MLCAPE for SFCOA/HRRR with increasing height. The reason why HRRR is more similar to OBS for MLCAPE than SFCOA for both RM and QLCS is likely because HRRR overestimates temperature in the 1–4–km range for tornadic and nontornadic subsets (e.g., increasing temperature and decreasing CAPE), whereas SFCOA does not (Fig. 4.4a–b). Coffer et al. (2025) contributes the larger warm bias in the 1–4–km range for HRRR to mid-level latent heating not captured by coarser horizontal resolution models (i.e., SFCOA). MLCAPE for QLCS is also much larger for QLCS for SFCOA/HRRR compared to OBS (with HRRR being larger than SFCOA) due to the large cool bias in dewpoints aloft (Fig. 4.3b,d). Using observations from the Atmospheric Emitted Radiance Interferometer (AERI; Knuteson et al., 2004; Turner and Blumberg, 2019) (which compares well to radiosonde observations Blumberg et al., 2017b), Wagner et al. (2019) found HRRR CAPE lagged CAPE AERI observations by 2–4 h due to HRRRv1 constraint on resolving subgrid scale clouds leading to an overestimation in surface temperatures, which has since been improved in later versions (Lee et al., 2019), leading to less overestimation, especially in the cool season.

LR100m has the greatest difference in means between OBS and SFCOA/HRRR, where for RM OBS is larger than SFCOA for tornadic (7.0 °C km^{-1} OBS, 3.6 °C km^{-1}

SFCOA) (significantly so) and nontornadic (5.8 °C km^{-1} OBS, 3.1 °C km^{-1} SFCOA) (Fig. 4.5a). OBS is also 65–80% larger than HRRR for both the tornadic and nontornadic subsets (Fig. 4.5a). For QLCS, LR100m shows a similar difference in means for OBS vs. SFCOA/HRRR (Fig. 4.5b). The ME profiles indicate HRRR/SFCOA are underestimating temperature at the surface for RM and QLCS (Fig. 4.4a–b), but OBS may actually be underestimating in this instance. A near-surface lapse rate check was employed in the QC (see Chapter 2 for more information) to remove erroneous near-surface data, which is commonly found in observed soundings. The near-surface lapse rates have the most significant errors for the tornadic subset (see the triangles for LR100m in Fig. 4.5), which are likewise the largest errors in Coniglio and Jewell (2022). Despite more significant errors in the tornadic subsets, the difference in means for LR100m between the tornadic and nontornadic subsets for SFCOA (3% RM, 9% QLCS), HRRR (36% RM, $\leq$1% QLCS), and OBS (32% RM, 58% QLCS) (Fig. 4.6) are insignificant and smaller than between data sources. We can not confidently conclude LR100m are physically much larger for OBS vs. HRRR/SFCOA.

All other lapse rates (LR250m, LR500m, LR1km, and LR3km) show minor, insignificant differences for OBS vs. SFCOA/HRRR (not shown) for both RM and QLCS, with the one exception of LR3km-6km (Fig. 4.5). Given temperature errors show an increasingly cool bias between 3–6 km compared to OBS for RM (Fig. 4.4a) and QLCS (Fig. 4.4b), and the largest MAEs are near 6–km, HRRR/SFCOA have larger LR3km-6km than OBS. Despite the small difference in means for LR3km-6km the HRRR nontornadic subset (6.8 °C km^{-1} RM, 6.6 °C km^{-1} QLCS) is significantly larger compared to the OBS nontornadic subset (6.3 °C km^{-1} RM, 6.2 °C km^{-1} QLCS) (Fig. 4.5). When comparing tornadic vs. nontornadic within data sources neither OBS, SFCOA, or HRRR for either RM or QLCS, have significant differences in any lapse rates (Fig. 4.6).

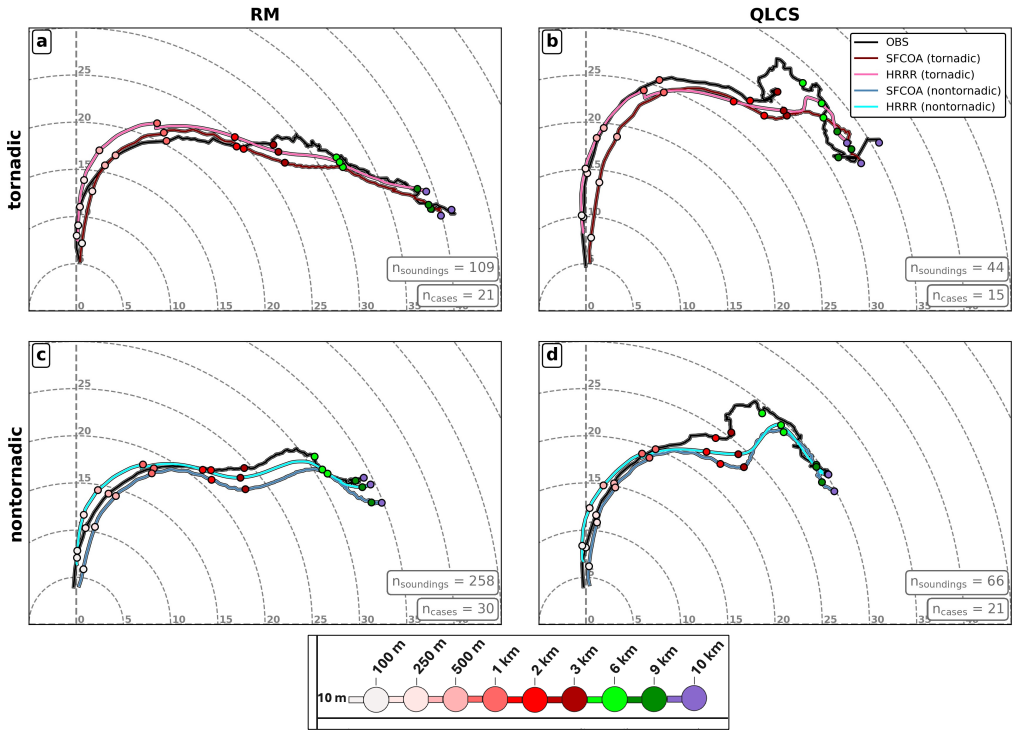


Figure 4.2: Composite ground-relative (GR) hodographs of (a) RM tornadic, (b) QLCS tornadic, (c) RM nontornadic, and (d) QLCS nontornadic mesocyclones. The soundings included in the RM composite requires only RM modes present within the search radius and inflow of the sounding and the QLCS composite requires only QLCS modes present. The modes in RM consist of storm modes 4-1, 5-1, 4-2, 5-2, 2-2, 4-3, and 5-3 and modes in QLCS consist of storm modes 1-1, 1-2, and 2-1 (see Fig. 2.2 and the associated text in Chapter 2 for more information on each storm mode). The number of hodographs making up each composite is found in gray text in the bottom left corner of each plot. The colored-coded circles indicate certain height levels, as shown in the legend.

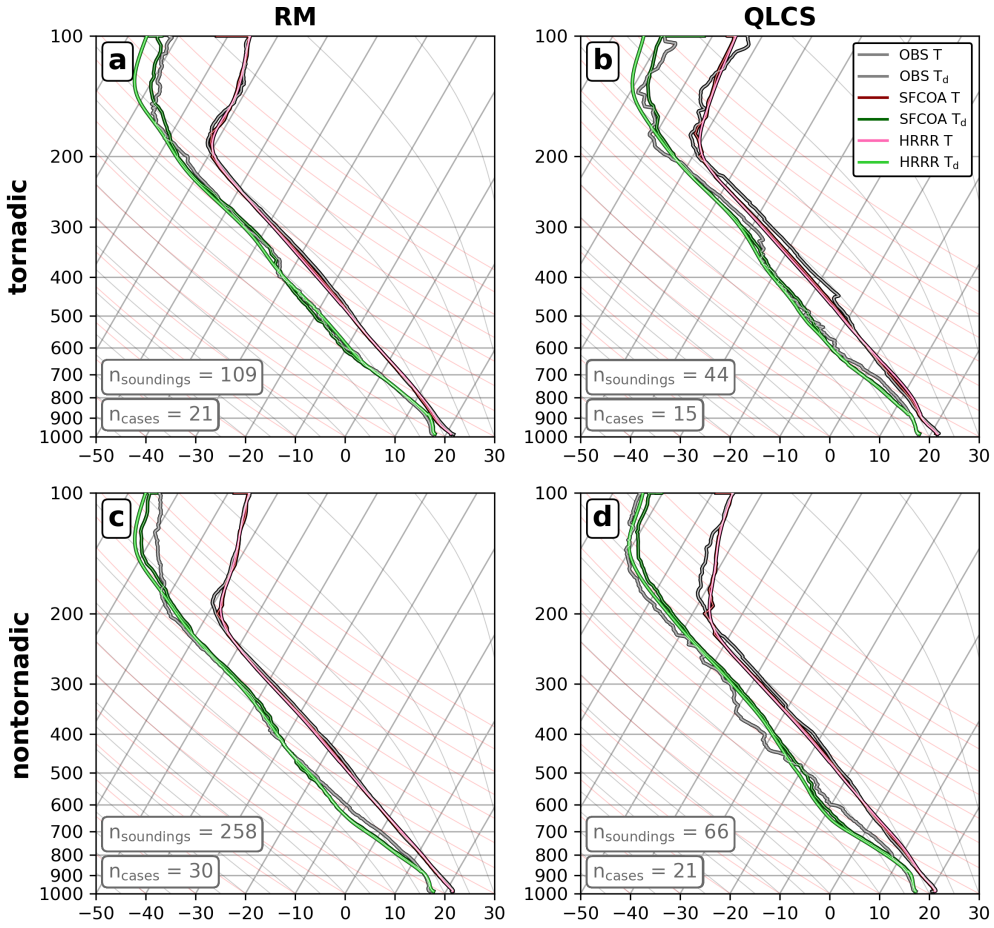


Figure 4.3: Composite skew-Ts of (a) RM tornadic, (b) QLCS tornadic, (c) RM nontornadic, and (d) QLCS nontornadic mesocyclones. The soundings included in the RM and QLCS modes are as described in Fig. 4.2. Since there are no SR thermodynamic parameters, the $n_{soundings}$ and n_{cases} will match the GR values in Fig. 4.2. The grey outlined lines are the temperature (T) and dew point (T_d) for OBS. The SFCOA T is shown in maroon while HRRR T is shown in pink. The SFCOA T_d is shown in dark green while HRRR T_d is shown in lime green.

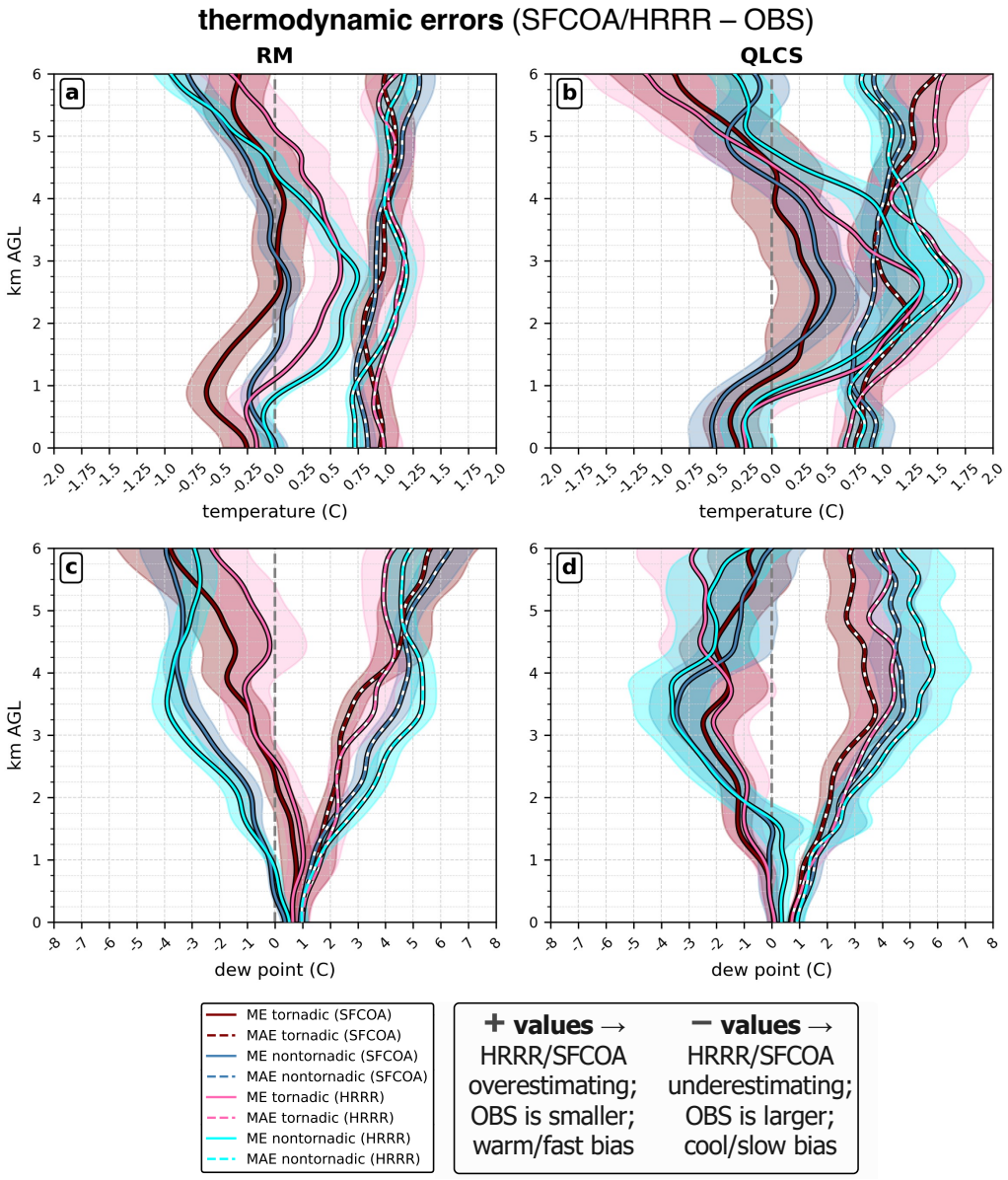


Figure 4.4: The SFCOA and HRRR mean errors (ME) and mean absolute errors (MAE) for a,c) RMs (left) and b,d) QLCSs (right) for a-b) temperature (°C) (top) and c-d) dewpoint (°C). The errors are obtained by subtracting either SFCOA (blue and red lines) or HRRR (cyan and pink lines) from OBS. The red/pink lines are for the tornadic subset and the blue/cyan lines are for the nontornadic subset. Positive MEs mean HRRR/SFCOA are overestimating, or OBS is smaller, indicative of a warm/fast bias. Negative MEs mean HRRR/SFCOA are underestimating, or OBS is larger, indicative of a cool/slow bias.

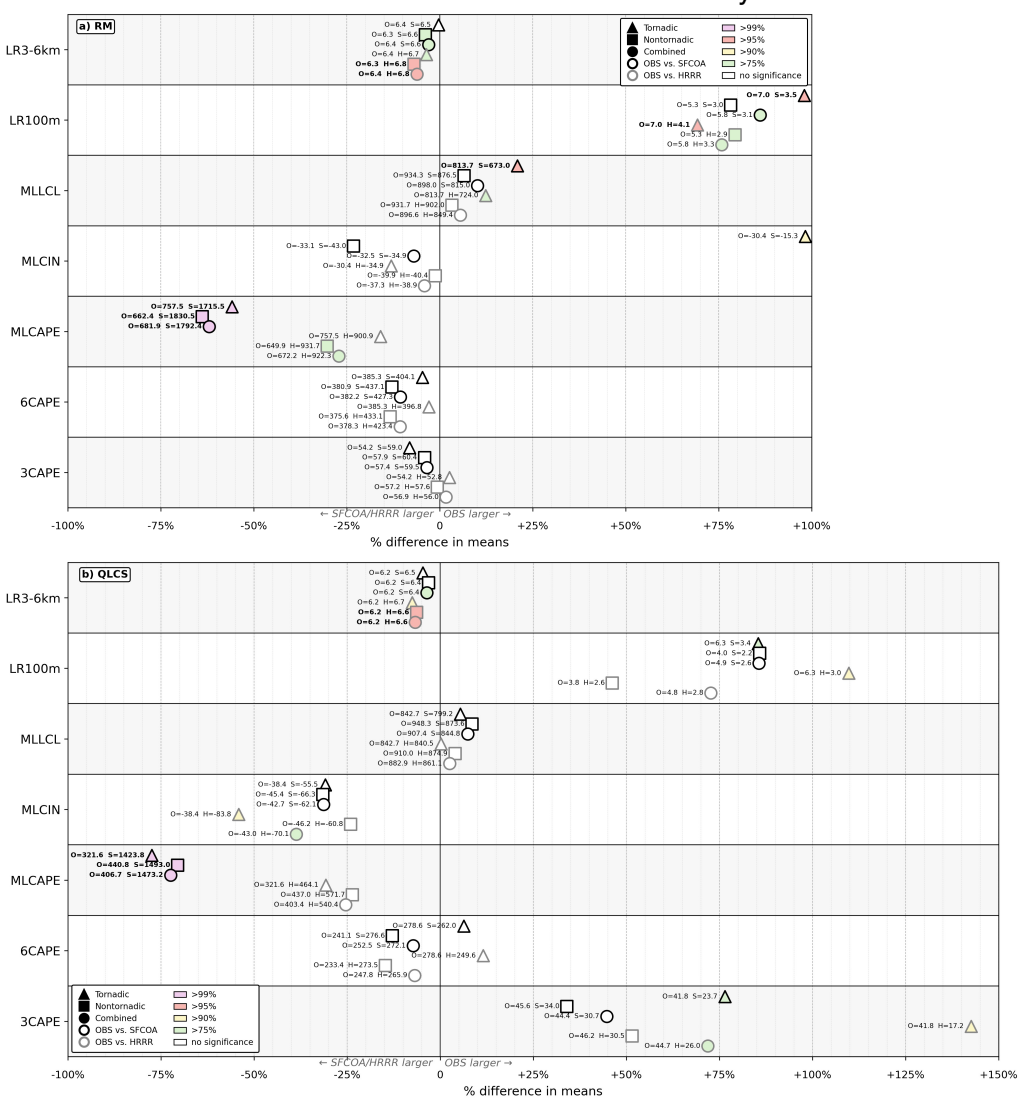

OBS vs. HRRR/SFCOA differences – thermodynamics
a) RM
b) QLCS
LR3-6km
LR100m
MLLCL
MLCIN
MLCAPE
6CAPE
3CAPE
Tornadic
Nontornadic
Combined
OBS vs. SFCOA
OBS vs. HRRR
>99%
>95%
>90%
>75%
no significance
← SFCOA/HRRR larger OBS larger →
% difference in means

Figure 4.5: The percent difference in means between OBS and SFCOA/HRRR for various thermodynamic parameters for (a) RM and (b) QLCS storm modes. The thermodynamic parameters included are (from bottom to top): 3CAPE, 6CAPE, MLCAPE, MLCIN, MLLCL, LR100m, and LR3-6km. There are three subsets used to compare OBS vs. HRRR and OBS vs. SFCOA represented by different shaped symbols, including tornadic storms (triangles), nontornadic storms (squares) cases and both tornadic and nontornadic combined (circles). The fill color denotes statistical significance from Monte Carlo permutation testing, where significance at a confidence interval $\geq 75\%$ is green, $\geq 90\%$ is yellow, $\geq 95\%$ is red, $\geq 99\%$ is purple, and no significance has no fill (white). Black edge coloring on the symbol represents the OBS vs. SFCOA comparisons and gray edge coloring represents the OBS vs. HRRR comparisons. The numbers to the left of the symbol represent the means of the two subsets that are being compared. For all points, the "O =" represents OBS, and "H =" is used when comparing to the HRRR and "S =" is used when comparing to SFCOA. The text is displayed in bold if it is significant at $\geq 95\%$ or 99%. Positive percent difference values (right of 0) indicate the OBS mean is larger than HRRR/SFCOA and a negative percent difference (left of 0) means the HRRR/SFCOA mean is larger than the OBS mean.

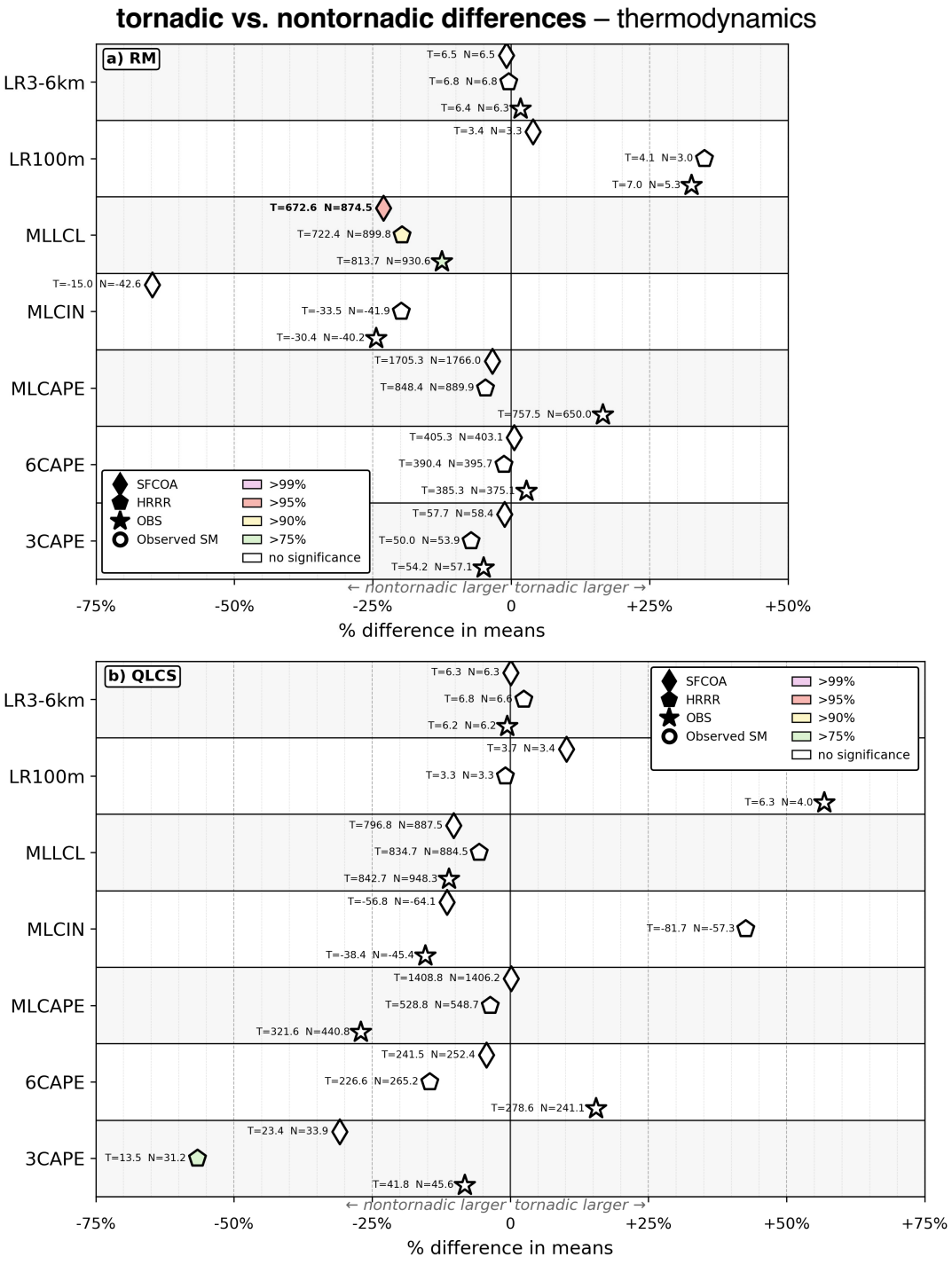

tornadic vs. nontornadic differences – thermodynamics
a) RM
LR3-6km
LR100m
MLLCL
MLCIN
MLCAPE
6CAPE
3CAPE
T=6.5 N=6.5
T=6.8 N=6.8
T=6.4 N=6.3
T=3.4 N=3.3
T=4.1 N=3.0
T=7.0 N=5.3
T=672.6 N=874.5
T=722.4 N=899.8
T=813.7 N=930.6
T=-15.0 N=-42.6
T=-33.5 N=-41.9
T=-30.4 N=-40.2
T=1705.3 N=1766.0
T=848.4 N=889.9
T=757.5 N=650.0
T=405.3 N=403.1
T=390.4 N=395.7
T=385.3 N=375.1
T=57.7 N=58.4
T=50.0 N=53.9
T=54.2 N=57.1
SFCOA
HRRR
OBS
Observed SM
>99%
>95%
>90%
>75%
no significance
← nontornadic larger tornadic larger →
-75%
-50%
-25%
0
+25%
+50%
% difference in means
b) QLCS
LR3-6km
LR100m
MLLCL
MLCIN
MLCAPE
6CAPE
3CAPE
T=6.3 N=6.3
T=6.8 N=6.6
T=6.2 N=6.2
T=3.7 N=3.4
T=3.3 N=3.3
T=6.3 N=4.0
T=796.8 N=887.5
T=834.7 N=884.5
T=842.7 N=948.3
T=-56.8 N=-64.1
T=-81.7 N=-57.3
T=-38.4 N=-45.4
T=1408.8 N=1406.2
T=528.8 N=548.7
T=321.6 N=440.8
T=241.5 N=252.4
T=226.6 N=265.2
T=278.6 N=241.1
T=23.4 N=33.9
T=13.5 N=31.2
T=41.8 N=45.6
SFCOA
HRRR
OBS
Observed SM
>99%
>95%
>90%
>75%
no significance
← nontornadic larger tornadic larger →
-75%
-50%
-25%
0
+25%
+50%
+75%
% difference in means

Figure 4.6: The percent difference in means between the tornadic and the nontornadic subset for various thermodynamic parameters for (a) RM and (b) QLCS storm modes. The thermodynamic parameters included are (from bottom to top): 3CAPE, 6CAPE, MLCAPE, MLCIN, MLLCL, LR100m, and LR3-6km. The difference in means between tornadic and nontornadic is compared for all three data sets, with each being represented by different shaped symbols, OBS (starts), SFCOA (diamonds), and HRRR (pentagons). The fill color denotes statistical significance from Monte Carlo permutation testing, where significance at a confidence interval $\geq$ 75% is green, $\geq$ 90% is yellow, $\geq$95% is red, $\geq$ 99% is purple, and no significance has no fill (white). The numbers to the left of the symbol represent the means of the two subsets that are being compared (i.e., tornadic vs. nontornadic). For all points, the "T =" represents the tornadic mean and "N =" represents the nontornadic mean. The text is displayed in bold if it is significant at $\geq$ 95% or 99%. Positive percent difference values (right of 0) indicate the tornadic mean is larger than the nontornadic mean and a negative percent difference (left of 0) means the nontornadic mean is larger than the tornadic mean.

4.3.2 Ground-relative kinematic errors

The GR zonal of the wind (u) has relatively small errors for RM (MEs $\leq$ 2 m s^{-1} and MAEs $\leq$ 5 m s^{-1}, see Fig. 4.7a) with the HRRR tornadic/nontornadic having a slow bias below 2 km and SFCOA tornadic/nontornadic having a fast bias below 2 km (Fig. 4.7a). For QLCS, errors in u resemble those of RM below 2 km and above (Fig. 4.7b). The fast bias above 2 km for QLCS (Fig. 4.7b) is much larger than RM (Fig. 4.7a), with QLCS nontornadic SFCOA/HRRR MEs between 1–2 m s^{-1} and tornadic MEs between 2–5 m s^{-1} (Fig. 4.7b). RM SFCOA/HRRR tornadic MAEs are larger than the nontornadic (and significantly so between 0–3 km for RM), whereas tornadic MAEs are only consistently larger for QLCS above 3 km (Fig. 4.7b). The tornadic errors are larger for tornadic than nontornadic in u throughout the atmosphere for RM, but not as consistently for QLCS.

For RM, the GR meridional of the wind (v) has a fast bias below 2 km for SFCOA/HRRR tornadic and HRRR nontornadic while SFCOA nontornadic has a slow

bias (Fig. 4.7c). Above 2 km, both SFCOA/HRRR and tornadic/nontornadic samples have a slow bias for RM peaking between 4–5 km (Fig. 4.7c). For QLCS, HRRR and SFCOA are largely different in low-level v, with SFCOA tornadic/nontornadic underestimating below 500 m and HRRR tornadic/nontornadic largely overestimating (Fig. 4.7d). Above 2 km, both SFCOA/HRRR tornadic/nontornadic have an increasing slow bias with height (Fig. 4.7d).

The layer averaged GRWs show differences for SFCOA/HRRR vs. OBS for GRW100m and GRW250m, but there is less than a 10% difference between the means of SFCOA/HRRR vs. OBS for all subsets, for both RM and QLCS for all layers of GRW (Fig. 4.8). OBS is larger than SFCOA but HRRR is larger than OBS for GRW100m, GRW250m, GRW500m, and GRW1km (Fig. 4.8). The OBS larger GRWs compared to SFCOA can be partially attributed to the low-level slow bias of SFCOA in v (with the exception of RM tornadic) (Fig. 4.7c–d). This results in smaller SFCOA low-level hodographs below 1 km (Fig. 4.2) (e.g., Coniglio and Jewell, 2022, albiet the slow bias they find in low-levels for SFCOA is much larger). For both RM and QLCS, HRRR has much stronger inflow (see the starting point of the hodograph compared to OBS/SFCOA in Fig. 4.2) and overestimates v in the low-levels (Fig. 4.7c–d). These errors results in larger GRWs (Fig. 4.8) and hodographs (Fig. 4.2) in the low-levels compared to OBS (also evident in Coffer et al., 2025). SFCOA inflow is more similar to OBS, likely due to the SFCOA surface point being derived from observations.

GRWs have been shown to be a skillful discriminator between tornadic and nontornadic environments (Markowski et al., 2003; Nowotarski and Jensen, 2013; Coniglio and Parker, 2020; Saba et al., 2026; Pounds et al., 2026). All GRW layers starting at the surface show some level of significance between tornadic and nontornadic environments for OBS, SFCOA, and HRRR for both RM and QLCS (Fig. 4.9). For RM and QLCS, SFCOA shows the greatest difference in means and highest significance

between tornadic and nontornadic for GRW100m (e.g., Saba et al., 2026), GRW250m, and GRW500m (Fig. 4.9a). Both SFCOA and HRRR show significant differences between the tornadic and nontornadic (RM and QLCS) subset for GRW1km, GRW3km, and GRW6km (Fig. 4.9a). For the upper-level GRWs, GRW6km-10km is not significant for RM or QLCS, but GRW3km-6km is still significant for QLCS (Fig. 4.9). To summarize, for both RM and QLCS, SFCOA shows the greatest significance in most layers, and greatest in the low-levels, while HRRR shows increased significance between 1–6 km. Since HRRR overestimates inflow, it is reasonable those errors are washed out with increasing layer depth, explaining why HRRR shows more significance in the mid-levels.

As in the GRWs, significant differences in shear between OBS and SFCOA/HRRR are only present in the lowest levels for RM and QLCS (Fig. 4.10). However, SH100m is significantly larger for OBS than for SFCOA and HRRR (Fig. 4.10a–b, for both RM and QLCS) (as in Coniglio and Jewell, 2022), differing from the GRWs where OBS is only significantly larger for SFCOA (and OBS is smaller compared to HRRR, see Fig. 4.8). Since HRRR overestimates the surface and low-level GRWs, the surface point in hodograph space is more similar to the 100 m and 250 m point, reducing the magnitude of the low-level shear vectors, resulting in an underestimation of low to mid-level shear (with significant underestimation for the combined tornadic and nontornadic subsets for RM and QLCS for SH500m, see Fig. 4.10). Coffer et al. (2025) found larger shear for HRRR compared to SFCOA, whereas that is not the case herein. The reasoning for the underestimation of SH100m for SFCOA differs, with the underestimation attributed to the slow bias in v (Fig. 4.7c–d), as with the underestimation of GRWs. Coniglio and Jewell (2022) mentions multiple reasons for the under-representation of near-ground wind speeds and $\leq$ 500 m errors in SFCOA vs. OBS (as this was also one of their findings). First, the difference in vertical resolution could be a factor, where there are

not enough data points below 500 m to accurately represent the near-surface winds. Secondly, they mention the deficiencies in depicting subgrid turbulent mixing in the RAP/SFCOA leading to near-ground wind speed errors, especially in strong synoptic regimes (which are more common in the SE than in the Great Plains, especially for late May-early June in the Great Plains when most field campaigns take place).

For RM, low to mid-level shear (i.e., SH100m–SH3km) shows higher significance between tornadic and nontornadic subsets in SFCOA and HRRR compared to OBS (Fig. 4.11a). For RM, tornadic means compared to OBS in SH500m, SH1km, SH3km, and SH6km are significantly higher for SFCOA, and tornadic means in SH1km and SH3km are significantly higher for HRRR (Fig. 4.11a). SH1km and SH3km are the only shear parameters that show significance with QLCS, and only for SFCOA (Fig. 4.11b). In other words, shear is a more significant distinguisher between tornadic and nontornadic environments in HRRR/SFCOA than OBS in the low and mid-levels for RM, but only in the mid-levels for QLCS.

For upper-level shear, SH3–6km is significantly larger for RM and larger for QLCS for nontornadic than tornadic for HRRR and SFCOA (Fig. 4.11). There is notable backing aloft, between 3–6 km, which is more prevalent in the tornadic (Fig. 4.12a–b) environments (Fig. 4.12c–d). The backing results in a reduced 3–6 km shear vector in OBS, which is why SH3–6km in OBS is larger than in SFCOA and HRRR for the tornadic subset (triangles on Fig. 4.10). While HRRR/SFCOA do not depict this backing, the 3–6 km shear vector is shorter for the tornadic subsets than nontornadic (significantly so for RM), as it is in OBS (Fig. 4.11).

On the other hand, the HRRR has larger GRWs than OBS and larger low-level hodographs, attributable to the overestimation of v in the low-levels (Fig. 4.7c–d). However, both SFCOA and HRRR significantly underestimate SH100m. The underestimation of low-level shear for SFCOA can be traced back to the smaller GRWs.

Since smaller GRWs in the HRRR is not the reason for the underestimation of low-level shear, there must be another cause. HRRR underestimates SH250m and SH500m while SFCOA is much closer to OBS (for QLCS) (Fig. 4.10), providing insight into why the HRRR leads to underestimation of shear. With increasing layer depth, HRRR continues to underestimate because the surface point on the HRRR is overestimated, making the difference between the 100 m and 250 m point smaller.

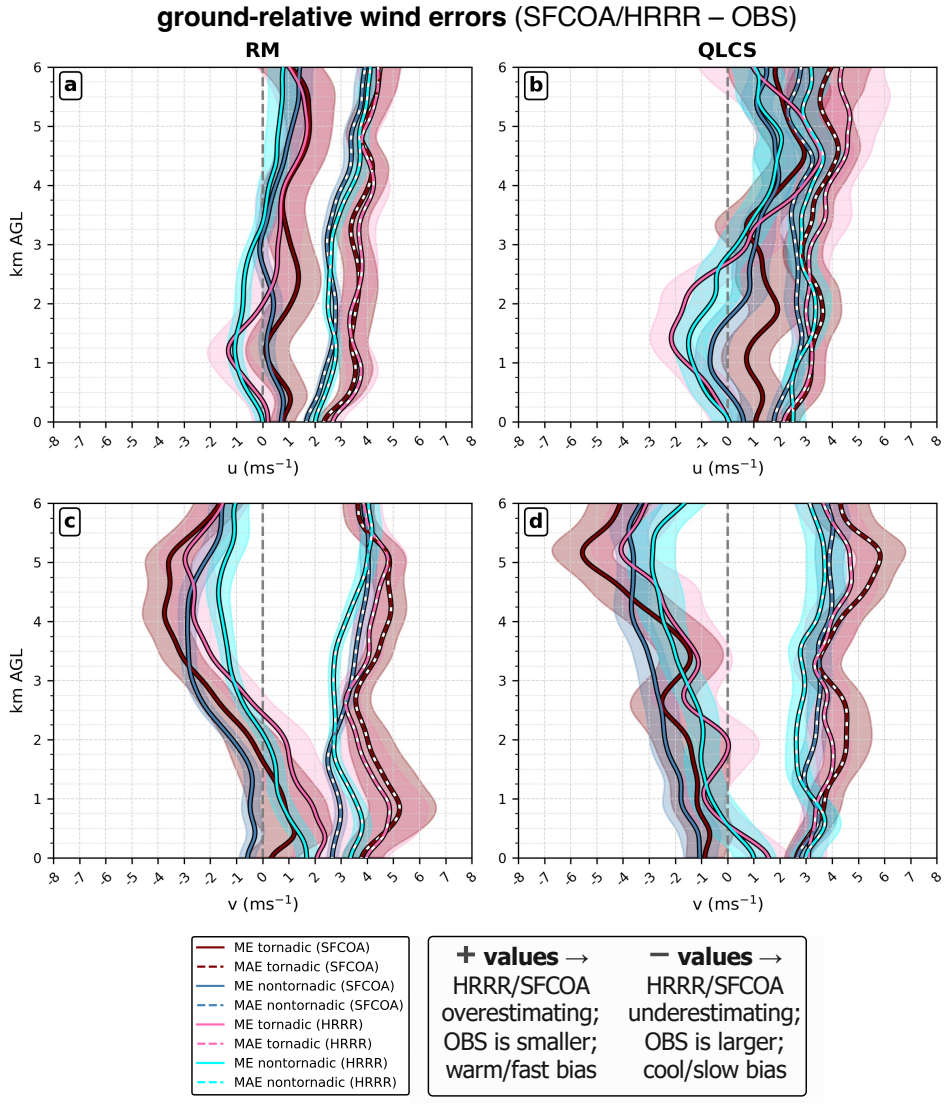


Figure 4.7: Same as Fig. 4.4, but for the errors in the ground-relative a-b) u component of the wind (ms^{-1}) and c-d) v component of the wind (ms^{-1}).

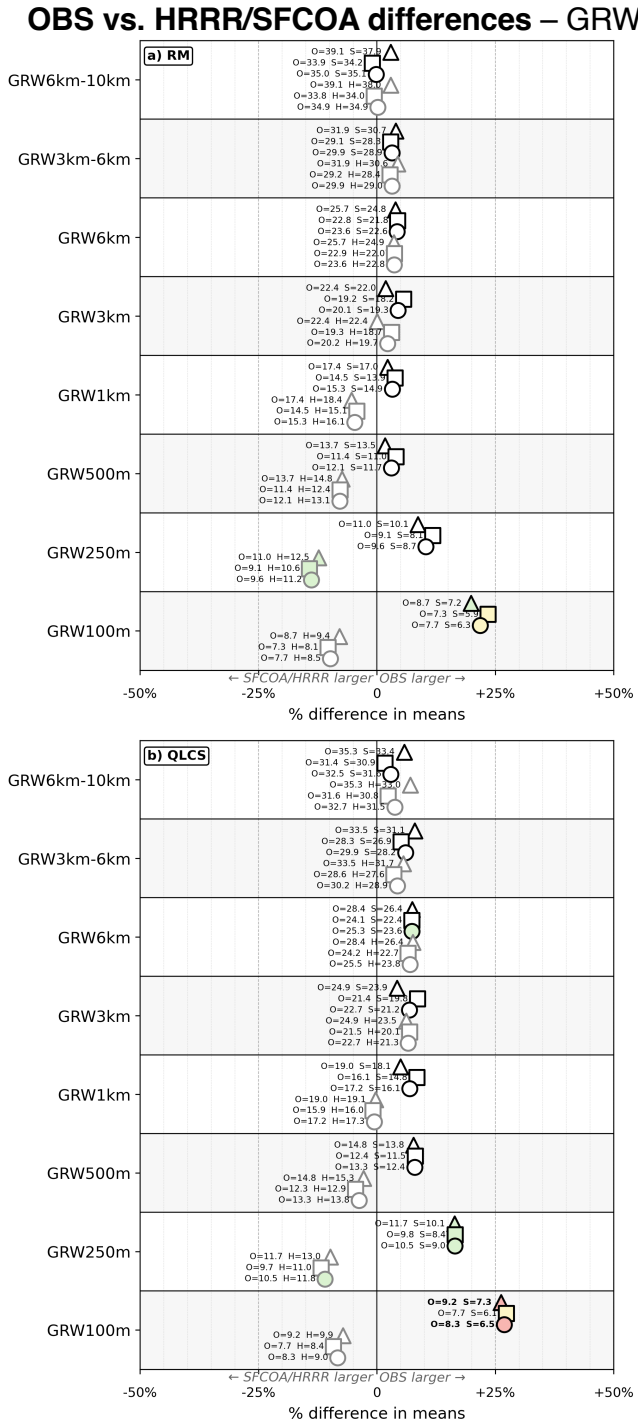


Figure 4.8: The same as in Fig. 4.5, but for GRW. The GRW parameters included are (from bottom to top): GRW100m, GRW250m, GRW500m, GRW1km, GRW3km, GRW6km, GRW3km-6km, and GRW6km-10km.



Figure 4.9: The same as in Fig. 4.6, but for GRW. The GRW parameters included are (from bottom to top): GRW100m, GRW250m, GRW500m, GRW1km, GRW3km, GRW6km, GRW3km-6km, and GRW6km-10km.

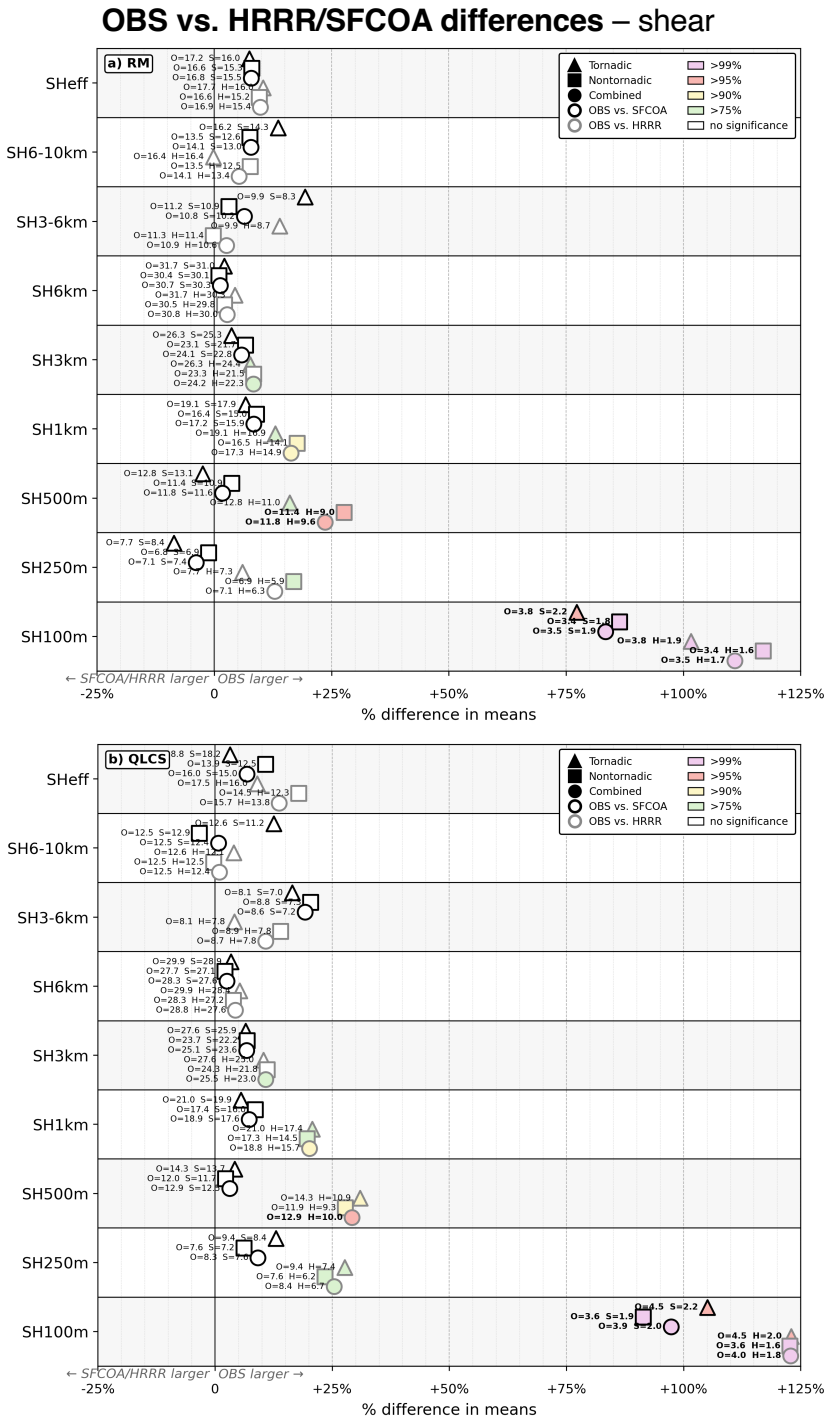


Figure 4.10: The same as in Fig. 4.5, but for shear. The shear parameters included are (from bottom to top): SH100m, SH250m, SH500m, SH1km, SH3km, SH6km, SH3km-6km, SH6km-10km, and SHeff.

4.3.3 Storm-relative kinematic errors

The SR u-component of the wind (ustm) has a different shape to the MEs than for u, but similar magnitudes in the MAEs for both RM and QLCS (Figs. 4.13a and 4.14a). Conversely, there are minor difference in the shape of the MEs in v (Fig. 4.7c–d) and the SR v-component of the wind (vstm) for both RM/QLCS (Figs. 4.13d and 4.14d). Meaning, the errors in v between OBS and SFCOA/HRRR do not change, but the errors in u do change when converted to a storm-relative reference frame.

The use of Bunkers storm motion amplifies the biases (increases in MAEs) in both ustm and vstm for RM (Fig. 4.13c,f) and more dramatically for QLCS (Fig. 4.14c,f)—note the increase in the x-axis from Fig. 4.13 to Fig. 4.14. Using observed storm motion, SFCOA/HRRR ustm overestimates for the RM tornadic subset, and underestimates (MEs ≤ 2 m s^{-1}) for the RM nontornadic subset (Fig. 4.13a). When Bunkers storm motion is used to calculate ustm, the SFCOA/HRRR tornadic MEs shift left (Fig. 4.13b), resulting in lower overestimation below 1 km and underestimation above 1 km. The nontornadic MEs shift right (Fig. 4.13b), leading to an underestimation of ustm. To summarize, the use of Bunkers storm motion rather than observed storm motion to calculate ustm for RM storms results in a decrease of the slow bias in low-levels and an increasing fast bias aloft for tornadic storms, and a transition from a slow bias to a fast bias for nontornadic storms. For QLCS (Fig. 4.14c), Bunkers increases the biases for ustm, but has minor impacts on the sign of the MEs (Fig. 4.14a–c). For QLCS, there is an increasing slow bias in vstm when Bunkers is used for the HRRR tornadic/nontornadic subsets and the SFCOA tornadic (SFCOA nontornadic has minimal change) (Fig. 4.14d–f).

For Bunkers calculated vstm, there are significant differences in errors between the tornadic SFCOA/HRRR and nontornadic SFCOA/HRRR subsets, opposed to sep-

aration between SFCOA tornadic/nontornadic and HRRR tornadic/nontornadic, as seen for observed calculated vstm (Figs. 4.13b and 4.14b). For RM, tornadic SFCOA/HRRR errors in Bunkers calculated vstm are minimal, so the large separation between tornadic and nontornadic subsets must come from the nontornadic subset having a large fast bias *only* when Bunkers is used (MEs of 2–4 ms^{-1}, Fig. 4.13e). The separation of the low-level vstm MEs between SFCOA tornadic/nontornadic and HRRR tornadic/nontornadic (Figs. 4.13d and 4.14d) are a key contributor to the larger storm-relative flow in the HRRR (Coffer et al., 2025, see their Fig. 7), and thus larger SR hodographs for the HRRR (Fig. 4.12). Coniglio and Jewell (2022) found OBS and Coffer et al. (2025) found HRRR to both have faster storm-relative flow than SFCOA, again, resulting in a larger SR hodograph for OBS and HRRR compared to SFCOA (Fig. 4.12). The ustm and vstm errors in Coffer et al. (2025, their Fig. 9) resemble (at least in sign) Coniglio and Jewell (2022, their Figs. 3 and 7). However, we do notice differences in sign in the errors, particularly in low-level vstm (Figs. 4.13d and 4.14d). Both Coniglio and Jewell (2022) and Coffer et al. (2025) found a low-level slow bias in vstm, whereas, vstm has a low-level fast bias in HRRR, however the bias is faster for RMs than QLCSs (Figs. 4.13d and 4.14d).

There is an underestimation bias for all subsets in vstm aloft for both RM/QLCS (Figs. 4.13a and 4.14a), as seen in the Great Plains (Coniglio and Jewell, 2022). Despite little difference between observed and Bunkers vstm for RM tornadic storms (difference in MAEs of 1 ms^{-1}, see Fig 4.13f), the vstm MEs between 4–5 km do reach the -3 to -4 ms^{-1} range for observed (Fig. 4.13d) and -4 to -5 ms^{-1} range for Bunkers (Fig. 4.13e). These are much larger than the MEs at the same level for nontornadic storms, despite nontornadic storms having the most variation with Bunkers usage.

The differences in means between OBS and SFCOA/HRRR for various SRW measures increase, although insignificantly, with increasing layer depth (Fig. 4.15) for both

RM and QLCS. While not significant, OBS has larger SRW values than SFCOA for all SRW layers. The HRRR is more similar to OBS, with slightly larger (insignificant) values at deeper-layers (i.e., SRW1km and SRW3km). The HRRR overestimates vstm below 2 km and SFCOA underestimates vstm in both RM (Fig. 4.13d) and QLCS (Fig. 4.14d) causing these differences in SRW compared to OBS. These results are consistent with HRRR underestimating and SFCOA overestimating the GRWs compared to OBS (see Fig. 4.8 or Section 4.3 4.3.2). These differences in SRWs between data sources are small, but the differences in tornadic and nontornadic SRW means remain significant (as in Chapter 3) whether HRRR or SFCOA are used (with observed storm motions) (Fig. 4.16).

The difference in tornadic and nontornadic means are more similar between OBS/SFCOA/HRRR for Bunkers calculated SRWs (Fig. 4.16, gray outlined symbols) compared to observed calculated SRWs (Fig. 4.16, black outlined symbols), in part due to the similarities of tornadic similarities of nontornadic errors in SFCOA/HRRR in Bunkers calculated ustm and vstm (Figs. 4.13b,e and 4.14b,e). Conversely, when using observed storm motion, OBS has the highest difference in means between tornadic and nontornadic environments for nearly all layers of SRWs for RM and QLCS (Fig. 4.16, black outlined symbols). This differs from Coniglio and Jewell (2022), who found when using SFCOA, the difference in means between tornadic and nontornadic SRWs are larger than for OBS. The difference in means for Bunkers calculated SRW decreases between tornadic and nontornadic environments with increasing layer depth (Fig. 4.16)—only showing significance in layers below 250 m for QLCS (Fig. 4.16b) and below 1 km for RM (Fig. 4.16a). In brief, Bunkers decreases the skill SRW has in distinguishing tornadic environments from nontornadic when observed storm motion is used.

Much like for GRWs and shear, only low-level SRH (i.e., SRH100m) shows no-

table difference in means between OBS and SFCOA/HRRR, where OBS is larger for RM, and significantly larger for QLCS (Fig. 4.17). The underestimation in low-level shear (Fig. 4.10) is likely the main contributor to the underestimation of SRH100m for SFCOA/HRRR. Deeper-layer SRH (i.e., SRH500m, SRH1km, and SRH3km) has greater statistical importance and greater difference between the means of tornadic vs. nontornadic environments (Fig. 4.18) (Coniglio and Jewell, 2022; Coffer et al., 2025, Pounds et al., 2026). For RM, SFCOA using observed storm motions has the largest difference in means and is significant between tornadic and nontornadic environments for all layers of SRH shown (Fig. 4.18a). Using Bunkers, SFCOA is also the most significant data source compared to OBS/HRRR (when using Bunkers, see Fig. 4.17). For both RM and QLCS, using observed storm motion compared to Bunkers results in higher differences in means between tornadic vs. nontornadic environments for OBS/SFCOA/HRRR (Fig. 4.18), consistent with Coniglio and Jewell (2022) and Coffer et al. (2025). Bunkers motion underestimates the tornadic vtsm (Figs. 4.13 and 4.14), and thus having small separation in the Bunkers calculated SRWs between tornadic and nontornadic storms could contribute to smaller differences in means for Bunkers calculated SRH (Fig. 4.18).

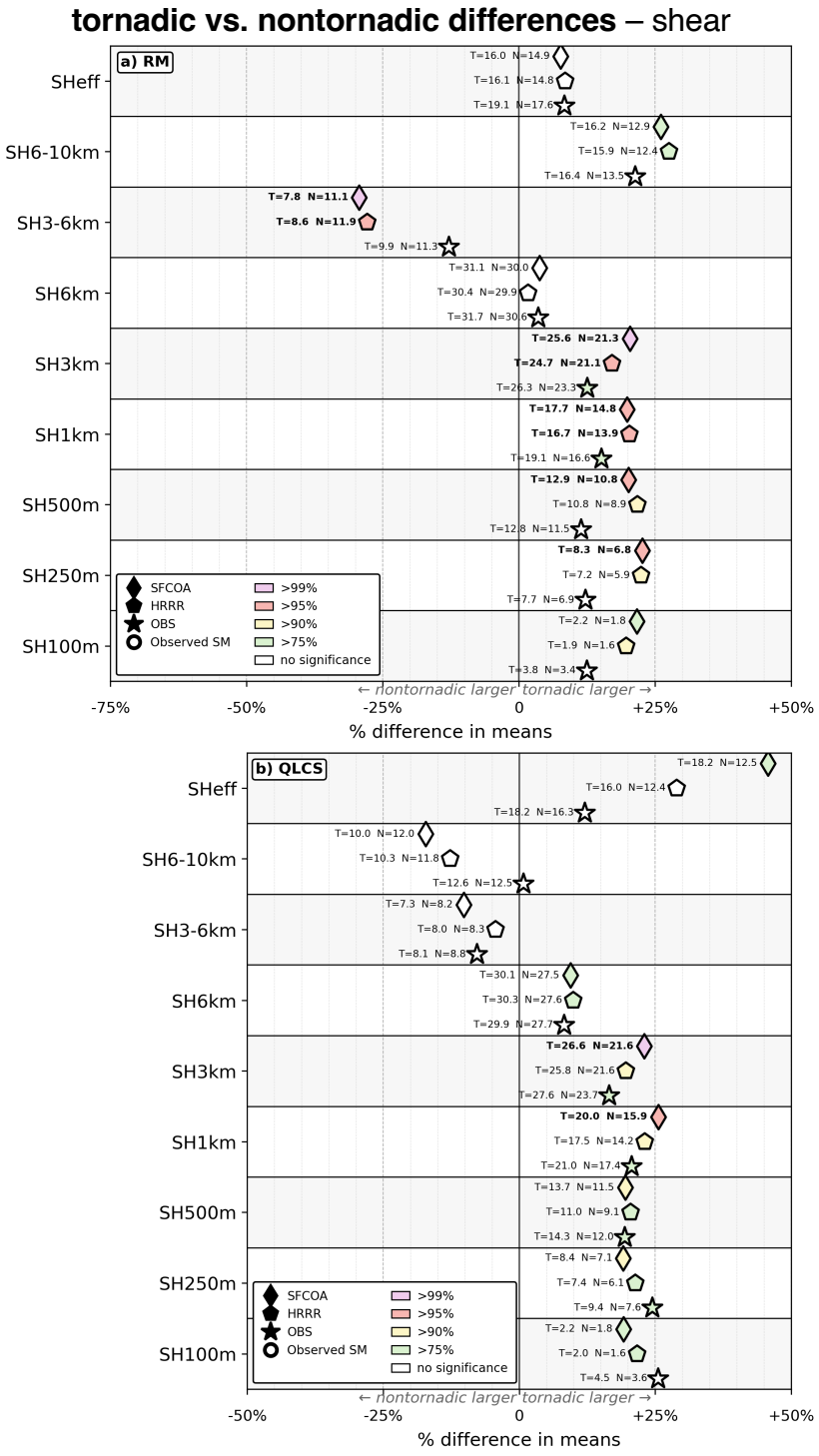


Figure 4.11: The same as in Fig. 4.6, but for shear. The shear parameters included are (from bottom to top): SH100m, SH250m, SH500m, SH1km, SH3km, SH6km, SH3km-6km, SH6km-10km, and SHeff.

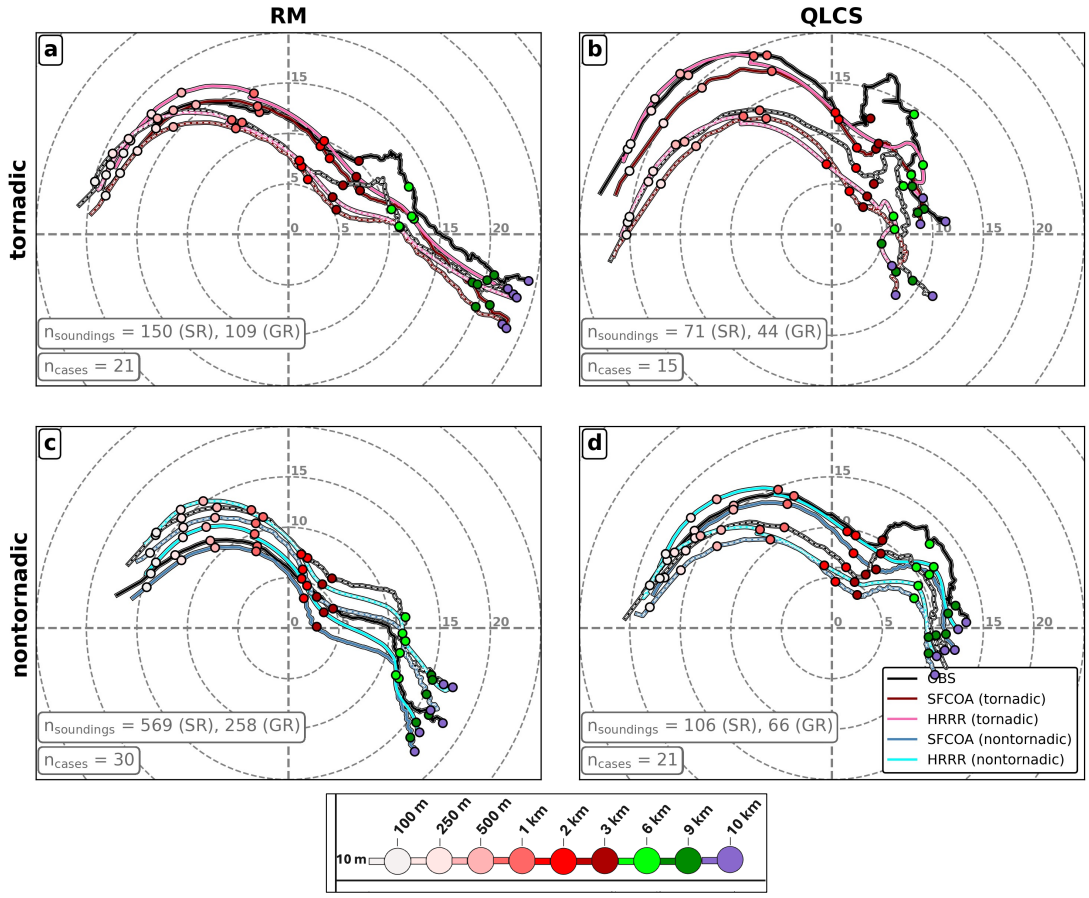


Figure 4.12: Same as in Fig. 4.2, but for SR hodographs, using both observed storm motion and Bunkers storm motion. The $n_{soundings}$ is displayed for both ground-relative (GR) and storm-relative (SR) while and n_{cases} remains the same for both. While there is no GR hodograph plotted, this number tells us the number of unique hodographs in each composite. The SR $n_{soundings}$ minus the SR $n_{soundings}$ gives the number of hodographs that are used more than once, but for a different mesocyclone (with a different storm motion). The solid colored lines represent the composite mean SR hodographs using observed storm motion, and the colored hodographs with white dashes overlaid are the SR hodographs using Bunker storm motion.

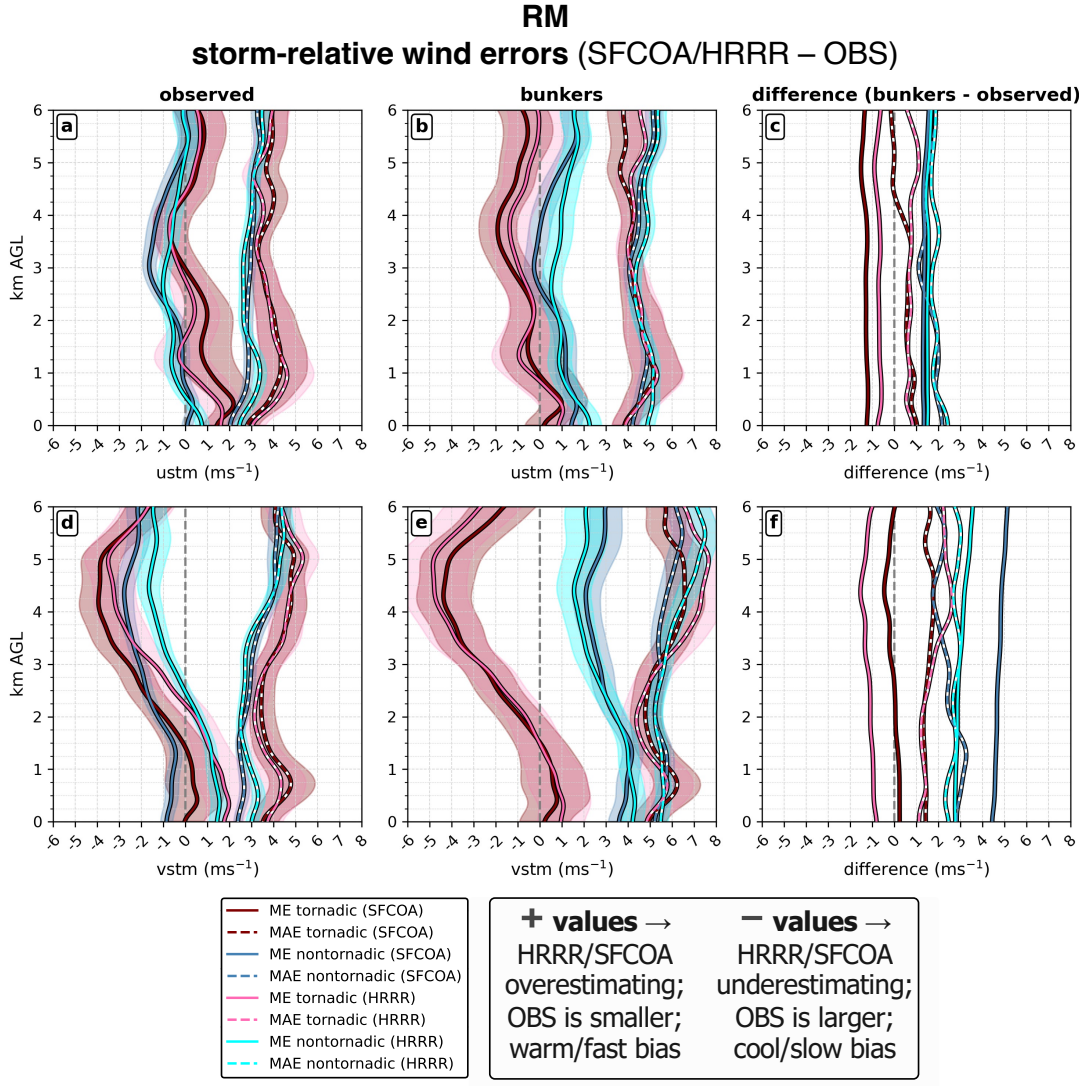


Figure 4.13: The SFCOA and HRRR mean errors (ME) and mean absolute errors (MAE) for the RM (a–b) SR u-component (ustm) (ms^{-1}) and (d–e) SR v-component (vstm) (ms^{-1}) using a,d) observed storm motion and b,e) Bunkers estimated storm motion. The errors are obtained by subtracting either SFCOA (blue and red lines) or HRRR (cyan and pink lines) from the OBS sounding (using observed storm motion for all). The red/pink lines are for the tornadic subset and the blue/cyan lines are for the nontornadic subset. The errors using the observed storm motion (b,e) are then subtracted from the errors using Bunkers storm motion (a,d) to obtain the difference in errors (c,f) when using Bunkers rather than observed storm motion. Positive MEs mean HRRR/SFCOA are overestimating, or OBS is smaller, indicative of a fast bias. Negative MEs mean HRRR/SFCOA are underestimating, or OBS is larger, indicative of a slow bias.

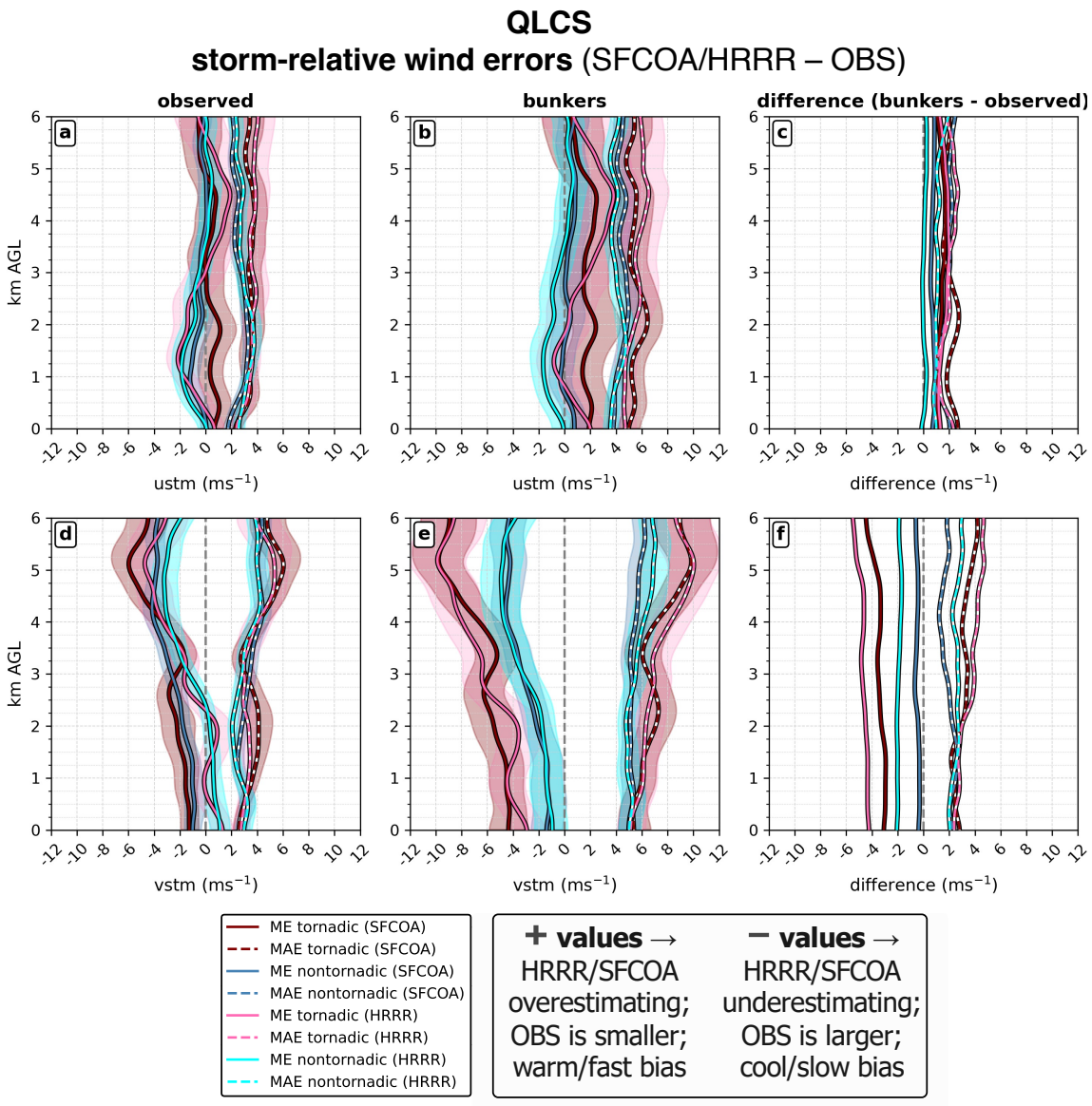


Figure 4.14: The same as in Fig. 4.13, but for QLCS.

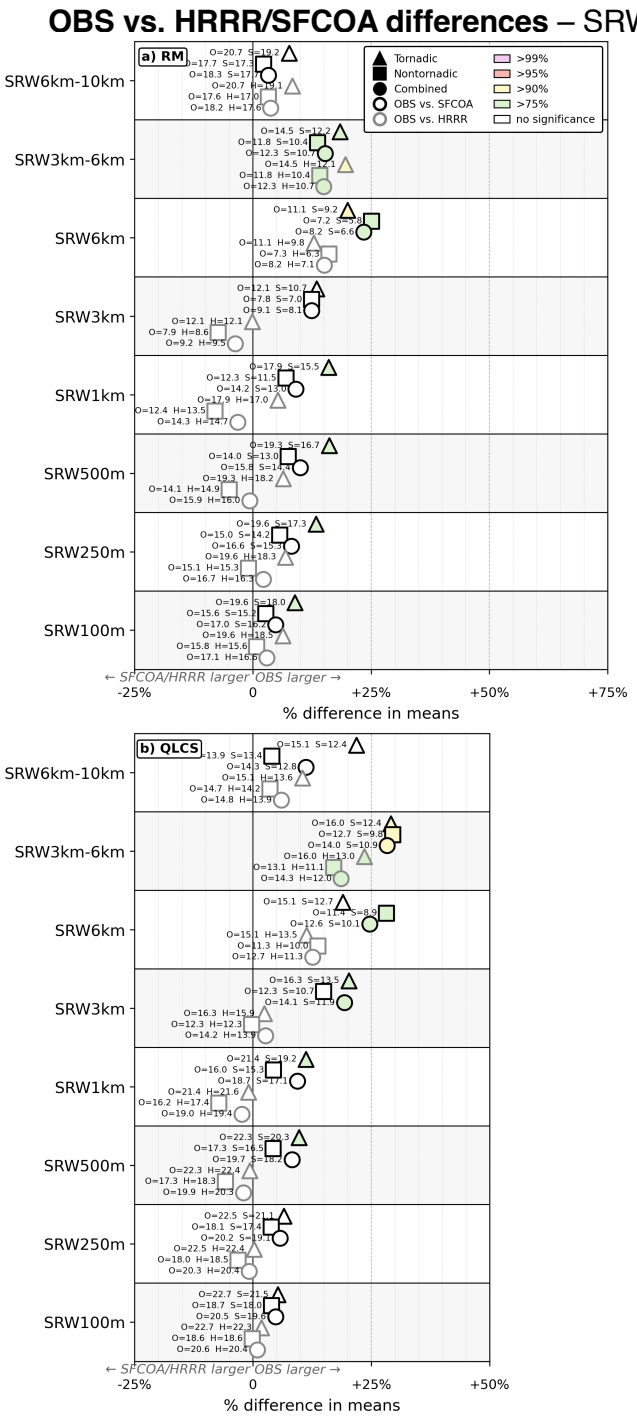


Figure 4.15: The same as in Fig. 4.5, but for SRW. The SRW parameters included are (from bottom to top): SRW100m, SRW250m, SRW500m, SRW1km, SRW3km, SRW6km, SRW3km-6km, and SRW6km-10km.

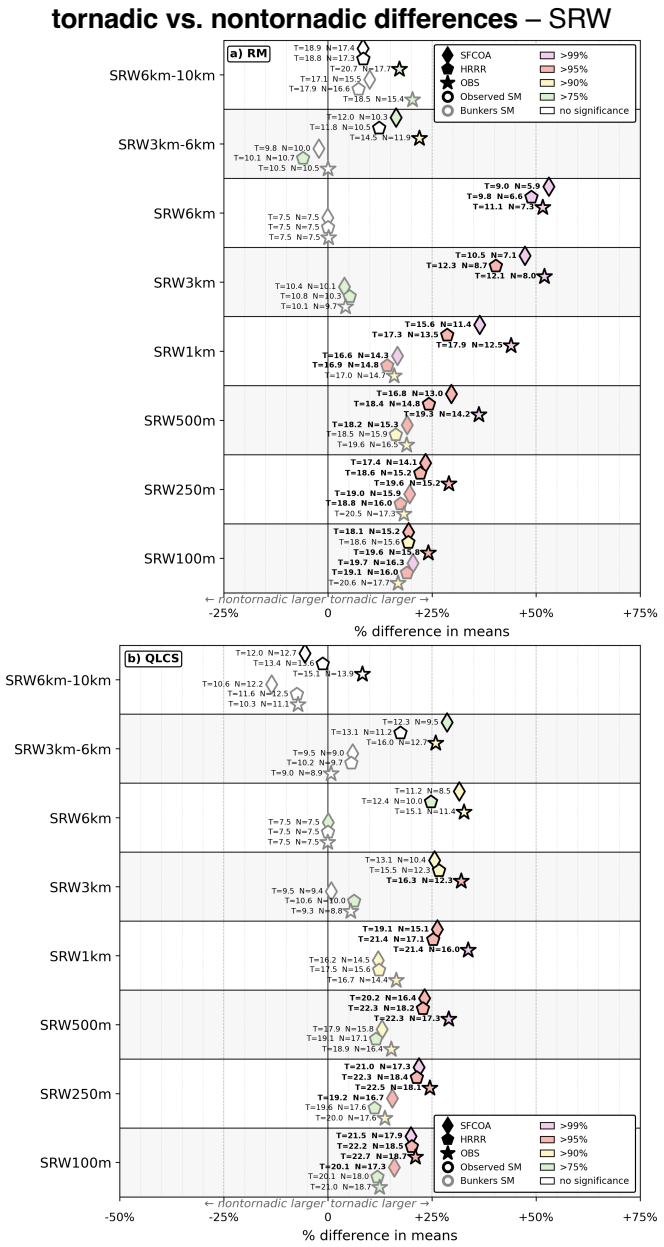


Figure 4.16: The same as in Fig. 4.6, but for SRW. The SRW parameters included are (from bottom to top): SRW100m, SRW250m, SRW500m, SRW1km, SRW3km, SRW6km, SRW3km-6km, and SRW6km-10km. The one addition here from the contents in Fig. 4.6 is an additional set of symbols representing the means using Bunkers storm motion since SRW is a storm-relative parameter. Black edge coloring on the symbol represents the tornadic vs. nontornadic comparisons when observed storm motion is used and gray edge coloring represents the tornadic vs. nontornadic comparisons when Bunkers storm motion is used.

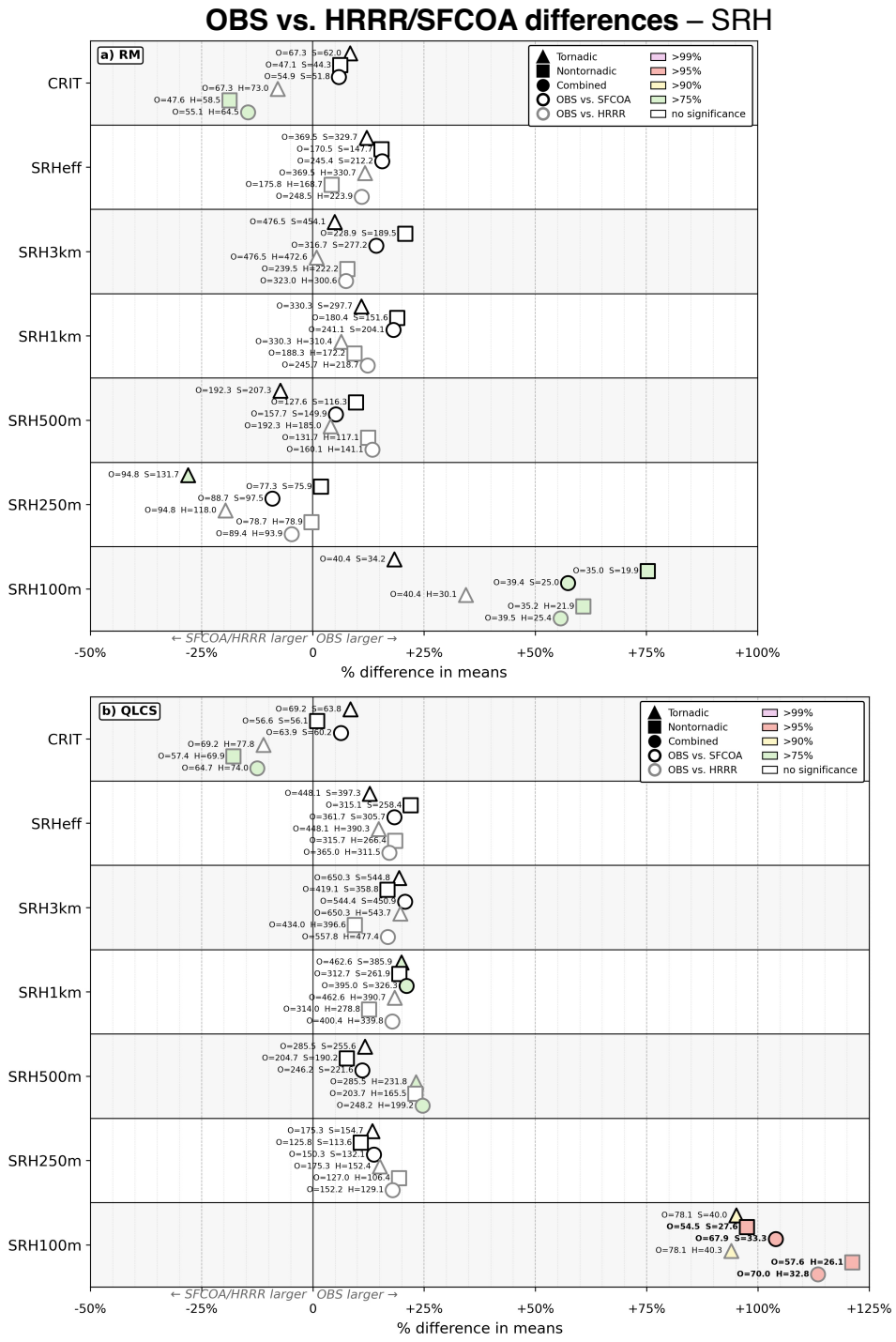


Figure 4.17: The same as in Fig. 4.5, but for SRH. The SRH parameters included are (from bottom to top): SRH100m, SRH250m, SRH500m, SRH1km, SRH3km, SRHeff, and CRIT.

4.4 Conclusions and discussion

Motivated by the wealth of Great Plains climatological studies (e.g., Parker, 2014; Wade et al., 2018; Coniglio and Parker, 2020; Coniglio and Jewell, 2022) and relative lack of understanding of SE environments, we examined the depiction of observed (OBS) SE environments in SFCOA and HRRR analysis fields. SFCOA—the most commonly used gridded-analyses for environmental climatologies—does not capture storm-induced environmental modification due to the coarse, 40–km grid spacing. The HRRR—most commonly used in real-time operational forecasting—can at least partially depict storm-environmental influences (e.g., Coffer et al., 2025). In evaluating biases in OBS vs. SFCOA and OBS vs. HRRR (for both RM and QLCS storm modes), we find:

- SFCOA and HRRR both have an increasingly negative dewpoint bias with height, resulting in an increasing overestimation of CAPE compared to OBS with increasing height. The HRRR does not overestimate MLCAPE as much in SFCOA because the HRRR has a mid-level warm bias that acts to decrease CAPE and offset the increases due to the low dewpoint bias.

- The HRRR overestimates inflow at the surface for both RM and QLCS, which is why there is an overestimation of low-level GRWs and an underestimation of low-level shear. The HRRR overestimates v and vstm, resulting in an slight overestimation of SRWs—but SRWs that are most similar to OBS (as in Coffer et al., 2025).

- SFCOA has an underestimation bias in the ground- and storm-relative wind component orthogonal to storm motion (i.e., v and vstm) for both RM (e.g., Coniglio and Jewell, 2022) and QLCS, resulting in underestimation of low-level

GRWs, shear, and SRWs.

- Despite different signs and magnitudes of kinematic errors for SFCOA and HRRR, as found in Coffer et al. (2025), we found HRRR was more similar to SFCOA than either SFCOA or HRRR are to OBS for common severe weather indices.

The near-surface layers (i.e., 0–100 m and 0–250 m) are where the most kinematic discrepancy exists between OBS profiles and SFCOA/HRRR profiles. Both Coniglio (2012) and Coffer et al. (2019) found that the low-level winds were too fast in RUC/RAP soundings, whereas SFCOA mitigates near-surface biases in comparison. Since the surface layer in the HRRR is model-derived, it overestimates the true surface conditions. The impact of overestimation of GRWs in the HRRR and underestimation in SFCOA is an important bias for forecasters to be aware of, given recent studies relating environmental, near-surface flow characteristics to supercell tornado production. Markowski (2024) noted the influence of coherent vorticity streaks in the inflow environment in seeding simulated tornadogenesis. They have since been observed by a mobile lidar platform in the inflows of tornadic and nontornadic supercells (Gebauer et al., 2026).

We also wanted to understand how the skill of various forecast parameters in distinguishing tornadic and nontornadic environments and if the skill changed when using SFCOA or HRRR compared to OBS. We found:

- SFCOA/HRRR both overestimated low-level dewpoints, with a larger warm bias for tornadic storms. This resulted in higher significance of MLLCL heights between RM tornadic and RM nontornadic environments in SFCOA/HRRR than in OBS.

- The GRWs are more skillful in distinguishing tornadic and nontornadic environments using SFCOA rather than OBS/HRRR in both RM and QLCS en-

vironments. This is a testament to the success of incorporating surface wind observations into SFCOA.

- In RM environments, HRRR and SFCOA showed more significant differences than OBS between tornadic and nontornadic environments in low-level shear (i.e., layers shallower than 3 km).

- The 3–6 km shear magnitudes are smaller for nontornadic than tornadic in OBS, SFCOA, and HRRR. For OBS, the smaller, but insignificant 3–6 km shear is due to backing from 3–6 km (evident in the tornadic hodographs), but this backing is not depicted in the composite SFCOA/HRRR hodographs. Due to the lack of backing, the 3–6 km shear in SFCOA/HRRR significantly smaller for tornadic RMs than nontornadic RMs.

- SRWs exhibit more skill in distinguishing tornadic vs. nontornadic RM and QLCS environments in OBS than in SFCOA or HRRR.

- SFCOA has increased skill for GRWs, shear, and SRH compared to OBS/HRRR in distinguishing tornadic and nontornadic RM environments.

Given the primary usage of modeled profiles for forecasting (i.e., prior to ongoing convention), interpretation of the storm-relative variables in the SFCOA/HRRR soundings are calculated using Bunkers storm motion as well as observed storm motion. The differences are relevant to forecasters who use Bunkers from both OBS soundings and model soundings prior to convection initiation (i.e., before there is an ongoing storm) when an observed storm motion cannot be calculated. Studies in the Great Plains (e.g., Coniglio and Jewell, 2022), across the entire U.S. (e.g., Coffer et al., 2025), and in the SE (Chapter 3) find that observed storm motions for tornadic storms are slower and to the right of Bunkers. However, unique to the SE, nontornadic storms are also

slower than Bunkers (and to the left, as found in other studies in different regions). Storm motions in the SE are much faster than in the Great Plains on average and the previously mentioned studies were unable to conclude if their findings would hold in the SE. The motivating studies for this work have confirmed that observed storm motion results in an increase in skillfulness of deeper-layer SRW and SRH, as seen here (Coniglio and Parker, 2020; Coniglio and Jewell, 2022; Coniglio and Thompson, 2024; Coffer et al., 2025). Coniglio and Thompson (2024) noted that near-ground variables did not show higher skill when observed storm motion was used rather than Bunkers, and that holds true in our dataset for RMs, but not for QLCSs. We find larger significance in low-level (0–100 m and 0–250 m) SRW and SRH for QLCS when observed storm motions are used.

Coffer et al. (2025) mentions that forecasters may be better off using SRH500m rather than the more skillful SRH3km when forecasting hours to days in advance. Without observed storm motion and observed soundings, SRH shows similar skill across layer depths. However, we agree with their recommendation, because when using Bunkers storm motion estimates and SFCOA/HRRR profiles, the difference between tornadic and nontornadic means is closest to the difference in means when using observed soundings and observed storm motions. Coffer et al. (2025) also mentions that the skill increase in the deeper-layer SRH is due to deviant motion (i.e., tornadic storms have a larger SRH due to increased rightward motion compared to Bunkers) that could be due to internal storm dynamics and cannot be readily anticipated prior to convection initiation.

The significant difference in HRRR and SFCOA bias between tornadic and nontornadic storms was not present whenever Bunkers storm motion was calculated for each individual sounding. We found the use of Bunkers storm motion leads to a large faster bias in ustm and vstm for nontornadic storms and a small slower bias for tornadic

storms compared to the use of observed storm motion. These biases led to smaller differences in the means of storm relative parameters (e.g., SRW and SRH) when using Bunker storm motion. Various SRW layers that are significant in OBS still show significance when using SFCOA/HRRR profiles for both QLCS and RM. However, when Bunkers storm motion is used, significance of SRW and the difference in means between tornadic and nontornadic subsets decreases with increasing layer depth, rather than increase as it does when observed storm motion is used.

Another unique aspect of our study is the comparison for QLCS, whereas previous studies have focused on supercells. Primarily, we find QLCS environments have much higher environmental variability and thus larger errors than RM environments. The variability present in QLCS environments is more pronounced when using Bunkers storm motion over observed. This finding is not surprising, as the Bunkers estimate is not designed to be used on QLCS MVs, despite it being done in some cases due to the absence of any other method (e.g., Thompson et al., 2012; Anderson-Frey et al., 2019). Our findings highlight the need for storm motion estimation based on a given wind profile from QLCS MVs, as exists for RMs (e.g., Bunkers et al., 2000). A QLCS-specific storm motion estimate would allow for reduction in errors storm-relative parameters calculated from model data (e.g., SFCOA or HRRR, among many other models). Reduction of these errors would greatly improve accuracy of storm-relative variables such as SRW, which have significant skill in distinguishing between tornadic and nontornadic environments for QLCSs (Chapter 3).

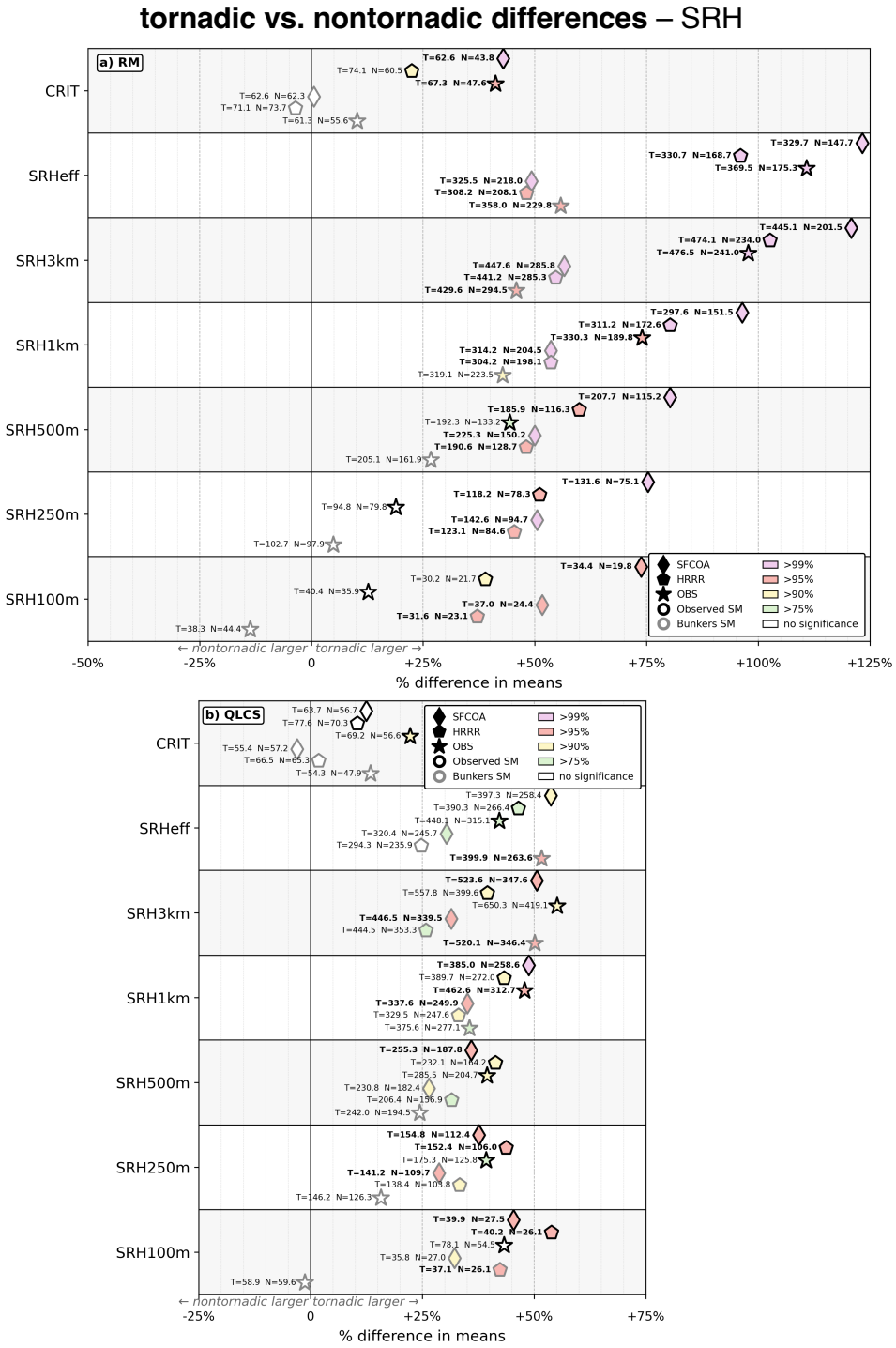


Figure 4.18: The same as in Fig. 4.6, but for SRH. The SRH parameters included are (from bottom to top): SRH100m, SRH250m, SRH500m, SRH1km, SRH3km, SRHeff, and CRIT. Both Bunkers storm motion and observed storm motion mean calculations are included as in Fig. 4.16.

Chapter 5

Conclusions

5.1 Conclusions

The overarching motivation for this Dissertation was to answer questions about Southeast U.S. (SE) severe storm environments—primarily questions that have been addressed in the Great Plains (GP) but not in the SE. Tornadic environments in the SE can happen at all hours of the day, year-round, rather than being more confined to late afternoon and evening hours in the late Spring months. The larger temporal range of tornadic activity in the SE, combined with the increased vulnerability of the population make it one of the most deadly regions for tornadoes—on top of being one of the most understudied. Recent field campaigns in the SE provided the necessary data to further explore what forecast parameters have skill in distinguishing between various SE environments (e.g., RM vs. QLCS, weak vs. strong mesocyclones, and tornadic vs. nontornadic). As detailed in Chapter 2, we created a database of observed soundings in the SE from recent (2016–2023) field campaigns. Atmospheric soundings in proximity (0–100 km) to an existing mesocyclone were used to characterize environments by classifications such as storm mode, mesocyclone strength, and tornado production in Chapter 3. The varying environments were evaluated for possible significance of common forecast parameters. Complementing efforts of Coniglio and Jewell (2022) and Coffer et al. (2025), we compared the findings of observed soundings to SFCOA

and HRRR soundings in Chapter 4.

The main goal of this work was to provide forecasters with insights on which forecasting parameters are most skillful in the SE, and to provide researchers with a baseline SE climatology to guide future efforts to improve forecasting skill in the region. With the goal in mind, and in combining the research questions we addressed in each chapter, the overarching questions we sought to answer in this Dissertation and their associated findings are as follows:

Understanding the differences between the SE and the GP was the primary motivator for the first question: *How do observed SE environments compare to the commonly studied Great Plains? Do SFCOA/HRRR soundings (and their associated errors) differ greatly in the SE?* Overall, we found larger separation between tornadic and nontornadic environments in the GP compared to the SE. Some parameters, primarily thermodynamic variables, on the low end of favorable in the GP were more similar to the mean tornadic value in the SE. This particularly applies to composite parameters, as CAPE is a large component of STP and SCP. Since SE tornadic events often occur in HSLC regimes, CAPE is much lower, skewing composite parameters to the lower end of favorable, despite a conducive environment. For example, the STP nontornadic mean in the SE is 0.7 and the tornadic mean is 1.8, but in the GP, 1.8 is the nontornadic mean and 4.6 is the tornadic mean (Coniglio and Parker, 2020, their Fig. 8). Additionally, lapse rates for tornadic storms can be an entire $^{\circ}$C km^{-1} steeper in the SE compared to the GP. Biases of SFCOA/HRRR compared to OBS do also differ in some aspects in the SE compared to the GP. Primarily, the overall magnitude of kinematic errors between OBS and SFCOA/HRRR are larger in the SE compared to the GP. This could be in part due to the overall faster storm motions and faster winds throughout the troposphere for SE tornado events.

A large proportion of severe/tornado climatologies focus primarily on supercells

rather than linear modes as well, motivating our second question: *How do the environments for RM and QLCS storm modes vary? Are some forecasting parameters more skillful for one storm mode? Does this vary for SFCOA/HRRR profiles?* Deeper-layer SRH shows much higher skill in distinguishing between RM tornadic and nontornadic environments than QLCS. Deeper-layer SRW is more skillful in distinguishing between tornadic and nontornadic environments for RM modes, while shallower layers of SRW are more skillful for QLCS modes. These results remain true for SFCOA/HRRR profiles, but skill of shallow-layer SRH in distinguishing QLCS tornadic and nontornadic environments and skill of all layers of SRH in distinguishing tornadic and nontornadic RM environments increases when using SFCOA/HRRR compared to OBS.

A large proportion of severe/tornado climatologies focus primarily on tornadic vs. nontornadic environments, as we do as well. Our third question is as follows: *What forecast parameters are the most skillful distinguishers of tornadic and nontornadic environments in the SE? Does this change for SFCOA/HRRR profiles?* For both RM and QLCS storm modes, the SRWs and GRWs were the most significant distinguishers between tornadic and nontornadic environments. Even when only considering strong mesocyclones, SRW and GRWs still showed significant differences between environments. These results do change for SFCOA/HRRR profiles. Specifically, when using observed storm motion, SRWs exhibit more skill in distinguishing between tornadic and nontornadic environments for SFCOA/HRRR compared to OBS. For SRH, SFCOA shows more skill in distinguishing between tornadic and nontornadic environments compared to OBS/HRRR.

A large proportion of severe/tornado climatologies focus primarily on differences in tornadic vs. nontornadic environments, as mentioned above, but fewer explore differences in environments supporting strong vs. weak mesocyclones. Our third question is as follows: *What forecast parameters are the most skillful distinguishers of strong vs.*

weak mesocyclone environments in the SE? When comparing weak and strong mesocyclones, we find there are more significant differences between the two subsets for QLCSs, most notably in upper-level SRW. This question was not explored for SFCOA/HRRR profiles given the minor differences found in Chapter 3 and a limited sample size.

Coniglio and Jewell (2022), Coniglio and Thompson (2024), and Coffer et al. (2025) found storm-relative variables, and their skill in distinguishing between tornadic and nontornadic environments, increase when using observed storm motions rather than Bunkers estimated storm motion. To confirm whether their findings are applicable to the SE, we ask: *How do observed storm motions vs. estimated storm motions impact the overall skill of various forecasting parameters? Does it change the skill when using SFCOA/HRRR profiles?* Much like in the GP, when using observed storm motions, deeper-layers of SRW and SRH were more skillful in distinguishing between tornadic and nontornadic environments for RM. Bunkers storms motion reduced the skill of storm-relative parameters, especially for parameters calculated over deeper-layers.

5.2 Forecasting implications

The overall goal of this Dissertation was to provide forecasters with information that could improve their forecasting capabilities in the SE. This goal is motivated by the fact that HSLC environments——most prevalent in the SE——are associated with lower probability of detection (POD) and higher false-alarm ratios (FAR) tornado warnings (Dean and Schneider, 2008; Schneider and Dean, 2008; Brotzge et al., 2013; Dean and Schneider, 2012; Anderson-Frey et al., 2016, 2019). The mean values of various forecasting parameters detailed throughout provide forecasters with reference values and associated significance in differentiating between environments (e.g., tornadic vs. nontornadic) in the SE. As is, the composite profiles presented in this dissertation can

serve as reference hodographs for forecasters when evaluating an environment's severe potential. We are working towards the composite hodographs being implemented in NSHARP, the workflow used by forecasters at the Storm Prediction Center.

I recognize that this dissertation contains copious amount of information, much of which is not directly pertinent to routine operational forecasting. Instead, a significant portion of the findings are intended to inform and guide future research efforts, and it is hoped that these insights will be considered and incorporated in future studies. Acknowledging this, we conclude by highlighting five operationally-relevant findings for forecasters to takeaway from this work. These are:

1. The three variables with the largest significant difference in means between tornadic and nontornadic RM environments in the SE are: 0–3 km SRH (473 m^2s^{-2} vs. 242 m^2s^{-2}), effective layer SRH (373 m^2s^{-2} vs. 174 m^2s^{-2}), and 0–6 km SRW (10.9 ms^{-1} vs. 7.3 m s^{-1}).

2. The three variables with the largest significant difference in means between tornadic and nontornadic QLCS environments in the SE are: 0–250 m SRW (22.3 m s^{-1} vs. 18.2 m s^{-1}), 0–500 m SRW (21.8 m s^{-1} vs. 17.3 m s^{-1}), and 0–1 km SRW (20.6 m s^{-1} vs. 16.0 m s^{-1}). These values are less significant for SFCOA/HRRR and when using Bunkers storm motion rather than observed storm motion.

3. Composite values such as STP (0.7 nontornadic vs. 1.8 tornadic) and SCP (3 nontornadic vs. 7.5 tornadic) are great predictors of RM tornadic environmental favorability. However, it is worth noting the STP and SCP values are much different than the favorable values in the GP. In the GP, mean nontornadic is STP is 1.8 (which is mean tornadic in the SE) and mean tornadic is 4.6 (Coniglio and Parker, 2020).

4. GRWs are skillful in distinguishing between tornadic and nontornadic environments, and more so when using HRRR/SFCOA profiles. When using observed profiles with observed storm motions, SRWs are more skillful.

5. Near surface shear and SRH are underestimated and MLCAPE is largely overestimated in the HRRR/SFCOA in the SE.

5.3 Future work

The differences we find between tornadic and nontornadic environments answer the question of, "is this environment supportive of tornadic or nontornadic storms" rather than if a storm in a given environment will produce a tornado. As previously mentioned, small environmental heterogeneities could be responsible in part for varying mesocyclone strength and tornado production (e.g., Richardson et al., 2007; Davenport and Parker, 2015; Davenport et al., 2019; Flournoy et al., 2020; Markowski, 2020) and can exist in similar environments (Markowski et al., 1998; Parker, 2014; Coffer et al., 2017; Wade et al., 2018; Flournoy et al., 2020; Markowski, 2020; Coniglio and Parker, 2020). One of the most prolific tornado outbreaks in the SE, occurring in an extremely volatile environment, 27–28 April 2011, had supercells that were significant tornado producers and supercells that had dormant periods in close spatiotemporal proximity (Lyza et al., 2022a). We found that the differences in storm motion did not result in large differences in the hodographs (and thus storm-relative parameters such as SRW and SRH) between tornadic and nontornadic storms occurring in the same environment. Even with small environmental heterogeneity, Anderson-Frey et al. (2016) mentioned the difficulties in determining which storm in similar environments may become tornadic. Additionally, inter-storm structure may also play a role in if a storm will/will not produce a tornado. While some of these inter-storm structures

(e.g., updraft shape or tilt, precipitation distributions) may be controlled by the environment, further investigation was beyond the scope of this study, but would be an advantageous avenue for future research. Specifically, if inter-storm characteristics and their environment controls can be identified, it would be of interest to see if any of those characteristics can be inferred from the environment.

As mentioned in Chapter 3, it would be worthwhile to explore what the main contributing factors to increased SRW are. Further, it would be interesting to further explore how increasing SRW contributes to increasing tornado probability. As mentioned in the prior paragraph, storm characteristics such as updraft shape and tilt may depend on the environment. Specifically, stronger SRWs have been shown to increase updraft width (e.g., Peters et al., 2020, 2023) and updraft tilt (e.g., Brown and Nowotarski, 2019) (see Chapter 3 for further discussion). However, the controls on increasing SRW are not as clear. While deviate storm motions are a control, increasing GRWs can also increase the SRWs. Given GRWs are larger in the SE, especially near the surface, their impact should be further explored. Thus, it is possible exploration of why larger GRWs exists in some environments could provide clues to why SRWs are larger as well.

However, storm motion also plays a role in the strength of the SRWs and other storm relative parameters. Analysis in both Chapters 3 and 4 explored differences in observed storm motion vs. Bunkers storm motion. Our finding reveal that Bunkers storm motion is too fast in the SE compared to observed storm motions for both tornadic and nontornadic mesocyclones. However, nontornadic storms have observed storm motions left of Bunkers and tornadic storms have observed storm motions right of Bunkers, with the difference in means between tornadic and nontornadic storm motions being significant. While, Bunkers is not as accurate as observed storm motions, if we use the information we have on how Bunkers compares to observed, it has potential

to be used as a forecast tool. For example, if a forecaster can in real-time compare the observed storm motion to Bunkers storm motion, and they see that a storm is left of Bunkers, they could possibly infer that that storm is less likely to be tornadic. This potential operational usage could be further explored in future works. For example, we could take a large sample of tornado warnings in the SE, use the associated observed storm motions, and compare to the estimated Bunkers motion via the nearest observed sounding or a SFCOA/HRRR sounding. If the tornado warned storms that are verified are consistently right of Bunkers and unverified warnings are consistently left of Bunkers, then that quick calculation could have operational relevance.

While the deviation from Bunkers might provide useful information on tornadic potential, Bunkers still has limitations. In strong SRH environments (i.e., those seen in the SE and herein), and environments with strong clockwise low-level hodograph curvature, Bunkers underestimates SRH (Bunkers, 2018). As shown in Chapter 4, Bunkers does lead to underestimation of SRH in the SE, especially for deeper-layer SRH (and mostly for RMs). Additionally, Bunkers is not designed to be used on QLCSs, but is used in some climatologies due to the absence of a better estimate. Future work should explore other methods of storm motion calculations, as mentioned in Chapter 3. While Bunkers is based on the wind profile, certain wind profiles, such as those of QLCSs or with high SRH, may benefit from modifications to Bunkers. Improvement to storm motion estimates could lead to improvement in calculations of parameters such as SRH and SRW, which have significant skill in distinguishing between tornadic and nontornadic environments.

Reference List

Anderson-Frey, A. K., Y. P. Richardson, A. R. Dean, R. L. Thompson, and B. T. Smith, 2016: Investigation of Near-Storm Environments for Tornado Events and Warnings. *Weather and Forecasting*, **31 (6)**, 1771–1790, https://doi.org/10.1175/WAF-D-16-0046.1, URL https://journals.ametsoc.org/view/journals/wefo/31/6/waf-d-16-0046_1.xml.

Anderson-Frey, A. K., Y. P. Richardson, A. R. Dean, R. L. Thompson, and B. T. Smith, 2019: Characteristics of Tornado Events and Warnings in the Southeastern United States. *Weather and Forecasting*, **34 (4)**, 1017–1034, https://doi.org/10.1175/WAF-D-18-0211.1.

Ashley, W. S., 2007: Spatial and Temporal Analysis of Tornado Fatalities in the United States: 1880–2005. *Weather and Forecasting*, **22 (6)**, 1214–1228, https://doi.org/10.1175/2007WAF2007004.1, URL https://journals.ametsoc.org/view/journals/wefo/22/6/2007waf2007004_1.xml.

Ashley, W. S., A. M. Haberlie, and J. Strohm, 2019: A Climatology of Quasi-Linear Convective Systems and Their Hazards in the United States. *Weather and Forecasting*, **34 (6)**, 1605–1631, https://doi.org/10.1175/WAF-D-19-0014.1, URL https://journals.ametsoc.org/view/journals/wefo/34/6/waf-d-19-0014_1.xml.

Ashley, W. S., A. J. Krmenec, and R. Schwantes, 2008: Vulnerability due to Nocturnal Tornadoes. *Weather and Forecasting*, **23 (5)**, 795–807, https://doi.org/10.1175/2008WAF2222132.1.

Atkins, N. T., J. M. Arnott, R. W. Przybylinski, R. A. Wolf, and B. D. Ketcham, 2004: Vortex Structure and Evolution within Bow Echoes. Part I: Single-Doppler and Damage Analysis of the 29 June 1998 Derecho. *Monthly Weather Review*, **132 (9)**, 2224–2242, https://doi.org/https://doi.org/10.1175/1520-0493(2004)132⟨2224:VSAEWB⟩2.0.CO;2, URL https://journals.ametsoc.org/view/journals/mwre/132/9/1520-0493_2004_132_2224_vsaewb_2.0.co_2.xml.

Atkins, N. T., and M. S. Laurent, 2009a: Bow Echo Mesovortices. Part I: Processes That Influence Their Damaging Potential. *Monthly Weather Review*, **137 (5)**, 1497–1513, https://doi.org/10.1175/2008MWR2649.1.

Atkins, N. T., and M. S. Laurent, 2009b: Bow Echo Mesovortices. Part II: Their Genesis. **137 (5)**, 1514–1532, https://doi.org/10.1175/2008MWR2650.1.

Beebe, R. G., 1958: Tornado Proximity Soundings. *Bulletin of the American Meteorological Society*, **39 (4)**, 195–201, https://doi.org/10.1175/1520-0477-39.4.195.

Benjamin, S. G., G. A. Grell, J. M. Brown, T. G. Smirnova, and R. Bleck, 2004a: Mesoscale Weather Prediction with the RUC Hybrid Isentropic–Terrain-Following Coordinate Model. *Monthly Weather Review*, **132 (2)**, 473–494.

Benjamin, S. G., and Coauthors, 2004b: An Hourly Assimilation–Forecast Cycle: The RUC. *Monthly Weather Review*, **132 (2)**, 495–518, URL https://journals.ametsoc.org/view/journals/mwre/132/2/1520-0493_2004_132_0495_ahactr_2.0.co_2.xml.

Benjamin, S. G., and Coauthors, 2016: A North American Hourly Assimilation and Model Forecast Cycle: The Rapid Refresh. *Monthly Weather Review*, **144 (4)**, 1669–1694, https://doi.org/10.1175/MWR-D-15-0242.1.

Bessardon, G. E. Q., K. Fosu-Amankwah, A. Petersson, and B. J. Brooks, 2019: Evaluation of Windsond S1H2 performance in Kumasi during the 2016 DACCIWA field campaign. *Atmospheric Measurement Techniques*, **12 (2)**, 1311–1324, https://doi.org/10.5194/amt-12-1311-2019, URL https://amt.copernicus.org/articles/12/1311/2019/.

Blair, S. F., and Coauthors, 2017: High-Resolution Hail Observations: Implications for NWS Warning Operations. *Weather and Forecasting*, **32 (3)**, 1101–1119, https://doi.org/10.1175/WAF-D-16-0203.1.

Blumberg, W. G., K. T. Halbert, T. A. Supinie, P. T. Marsh, R. L. Thompson, and J. A. Hart, 2017a: SHARPpy: An Open-Source Sounding Analysis Toolkit for the Atmospheric Sciences. *Bulletin of the American Meteorological Society*, **98**, 1625–1636, https://doi.org/10.1175/BAMS-D-15-00309.1.

Blumberg, W. G., T. J. Wagner, D. D. Turner, and J. Correia, 2017b: Quantifying the Accuracy and Uncertainty of Diurnal Thermodynamic Profiles and Convection Indices Derived from the Atmospheric Emitted Radiance Interferometer. *Journal of Applied Meteorology and Climatology*, **56 (10)**, 2747–2766, https://doi.org/10.1175/JAMC-D-17-0036.1, URL https://journals.ametsoc.org/view/journals/apme/56/10/jamc-d-17-0036.1.xml.

Bothwell, P. D., J. A. Hart, and R. L. Thompson, 2022: An integrated three-dimensional objective analysis scheme in use at the Storm Prediction Center. *21st Conf. on Severe Local Storms*, Amer. Meteor. Soc., San Antonio, TX, j117-J120.

Brandes, E. A., R. P. Davies-Jones, and B. C. Johnson, 1988: Streamwise Vorticity Effects on Supercell Morphology and Persistence. **45 (6)**, 947–

963, URL https://journals.ametsoc.org/view/journals/atsc/45/6/1520-0469_1988_045_0947_sveosm_2_0_co_2.xml.

Britt, K. C., P. S. Skinner, P. L. Heinselman, and K. H. Knopfmeier, 2020: Effects of Horizontal Grid Spacing and Inflow Environment on Forecasts of Cyclic Mesocyclogenesis in NSSL's Warn-on-Forecast System (WoFS). *Weather and Forecasting*, **35 (6)**, 2423–2444, https://doi.org/10.1175/WAF-D-20-0094.1, URL https://journals.ametsoc.org/view/journals/wefo/35/6/waf-d-20-0094.1.xml.

Brooks, H. E., C. A. Doswell, and J. Cooper, 1994: On the Environments of Tornadic and Nontornadic Mesocyclones. *Weather and Forecasting*, **9 (4)**, 606–618, https://doi.org/10.1175/1520-0434(1994)009⟨0606:OTEOTA⟩2.0.CO;2, URL https://journals.ametsoc.org/view/journals/wefo/9/4/1520-0434_1994_009_0606_oteota_2_0_co_2.xml.

Brooks, H. E., C. A. Doswell, and C. A. D. Iii, 2002: Deaths in the 3 May 1999 Oklahoma City Tornado from a Historical Perspective. *Weather and Forecasting*, **17**, 354–361, https://doi.org/10.1175/1520-0434(2002)017⟨0354:ditmoc⟩2.0.co;2, URL https://zenodo.org/records/1234651.

Brotzge, J. A., S. E. Nelson, R. L. Thompson, and B. T. Smith, 2013: Tornado probability of detection and lead time as a function of convective mode and environmental parameters. *Weather and forecasting*, **28 (5)**, 1261–1276.

Brown, M. C., and C. J. Nowotarski, 2019: The Influence of Lifting Condensation Level on Low-Level Outflow and Rotation in Simulated Supercell Thunderstorms. *Journal of the Atmospheric Sciences*, **76 (5)**, 1249–1372, https://doi.org/10.1175/JAS-D-18-0216.1.

Brown, M. C., and C. J. Nowotarski, 2020: Southeastern U.S. Tornado Outbreak Likelihood Using Daily Climate Indices. *Journal of Climate*, **33 (8)**, 3229–3252, https://doi.org/10.1175/JCLI-D-19-0684.1.

Brown, M. C., C. J. Nowotarski, A. R. Dean, B. T. Smith, R. L. Thompson, and J. M. Peters, 2021: The Early Evening Transition in Southeastern U.S. Tornado Environments. *Weather and Forecasting*, **36 (4)**, 1431–1452, https://doi.org/10.1175/WAF-D-20-0191.1.

Browning, K. A., 1962: Cellular structure of convective storms. *The Meteorological Magazine*, **91 (1085)**, 341–350.

Browning, K. A., 1964: Airflow and precipitation trajectories within severe local storms which travel to the right of the winds. *Journal of Atmospheric Sciences*, **21 (6)**, 634–

639.

Bunkers, M. J., 2018: Observations of Right-Moving Supercell Motion Forecast Errors. *Weather and Forecasting*, **33 (1)**, 145–159, https://doi.org/10.1175/WAF-D-17-0133.1.

Bunkers, M. J., B. A. Klimowski, J. W. Zeitler, R. L. Thompson, and M. L. Weisman, 2000: Predicting Supercell Motion Using a New Hodograph Technique. *Weather and Forecasting*, **15 (1)**, 61–79, https://doi.org/https://doi.org/10.1175/1520-0434(2000)015⟨0061:PSMUAN⟩2.0.CO;2.

Bunkers, M. J., M. B. Wilson, M. S. V. D. Broeke, and D. J. Healey, 2022: Scan-by-Scan Storm-Motion Deviations for Concurrent Tornadic and Nontornadic Supercells. *Weather and Forecasting*, **37 (5)**, 749–770, https://doi.org/10.1175/WAF-D-21-0153.1.

Childs, S. J., and R. S. Schumacher, 2018: Cold-season Tornado Risk Communication: Case Studies from November 2016 to February 2017. *Weather, Climate, and Society*, **10 (3)**, 419–433, https://doi.org/10.1175/WCAS-D-17-0073.1, URL https://journals.ametsoc.org/view/journals/wcas/10/3/wcas-d-17-0073_1.xml.

Ciesielski, P. E., P. T. Haertel, R. H. Johnson, J. Wang, and S. M. Loehrer, 2012: Developing High-Quality Field Program Sounding Datasets. *Bulletin of the American Meteorological Society*, **93 (3)**, 325–336, https://doi.org/10.1175/BAMS-D-11-00091.1.

Coffer, B. E., and P. M. Markowski, 2018: Comments on "The Regulation of Tornado Intensity by Updraft Width". *Journal of the Atmospheric Sciences*, **75 (11)**, 4049–4056, https://doi.org/10.1175/JAS-D-18-0170.1.

Coffer, B. E., and M. D. Parker, 2015: Impacts of Increasing Low-Level Shear on Supercells during the Early Evening Transition. *Monthly Weather Review*, **143 (5)**, 1945–1969, https://doi.org/10.1175/MWR-D-14-00328.1, URL https://journals.ametsoc.org/view/journals/mwre/143/5/mwr-d-14-00328.1.xml.

Coffer, B. E., and M. D. Parker, 2017: Simulated Supercells in Nontornadic and Tornadic VORTEX2 Environments. **145 (1)**, 149–180, https://doi.org/10.1175/MWR-D-16-0226.1.

Coffer, B. E., M. D. Parker, M. C. Coniglio, and C. R. Homeyer, 2025: Supercell environments using GridRad-Severe and the HRRR: Addressing discrepancies between prior tornado datasets. https://doi.org/10.1175/WAF-D-24-0251.1.

Coffer, B. E., M. D. Parker, J. M. L. Dahl, L. J. Wicker, and A. J. Clark, 2017:

Volatility of Tornadogenesis: An Ensemble of Simulated Nontornadic and Tornadic Supercells in VORTEX2 Environments. *Monthly Weather Review*, **145 (11)**, 4605–4625, https://doi.org/10.1175/MWR-D-17-0152.1, URL https://journals.ametsoc.org/view/journals/mwre/145/11/mwr-d-17-0152.1.xml.

Coffer, B. E., M. D. Parker, R. L. Thompson, B. T. Smith, and R. E. Jewell, 2019: Using Near-Ground Storm Relative Helicity in Supercell Tornado Forecasting. *Weather and Forecasting*, **34 (5)**, 1417–1435, https://doi.org/10.1175/WAF-D-19-0115.1.

Cohen, A. E., S. M. Cavallo, M. C. Coniglio, H. E. Brooks, and I. L. Jirak, 2017: Evaluation of Multiple Planetary Boundary Layer Parameterization Schemes in Southeast U.S. Cold Season Severe Thunderstorm Environments. *Weather and Forecasting*, **32 (5)**, 1857–1884, https://doi.org/10.1175/WAF-D-16-0193.1, URL https://journals.ametsoc.org/view/journals/wefo/32/5/waf-d-16-0193_1.xml.

Coleman, T. A., and P. G. Dixon, 2014: An Objective Analysis of Tornado Risk in the United States. *Weather and Forecasting*, **29 (2)**, 366–376, https://doi.org/10.1175/WAF-D-13-00057.1, URL https://journals.ametsoc.org/view/journals/wefo/29/2/waf-d-13-00057_1.xml.

Coniglio, M. C., 2012: Verification of RUC 0–1-h Forecasts and SPC Mesoscale Analyses Using VORTEX2 Soundings. *Weather and Forecasting*, **27 (3)**, 667–683, https://doi.org/10.1175/WAF-D-11-00096.1.

Coniglio, M. C., and R. E. Jewell, 2022: SPC Mesoscale Analysis Compared to Field-Project Soundings: Implications for Supercell Environment Studies. *Monthly Weather Review*, **150 (3)**, 567–588, https://doi.org/10.1175/MWR-D-21-0222.1.

Coniglio, M. C., and M. D. Parker, 2020: Insights into supercells and their environments from three decades of targeted radiosonde observations. *Monthly Weather Review*, **148 (12)**, 4893–4915.

Coniglio, M. C., and R. L. Thompson, 2024: Impacts of Sampling and Storm-Motion Estimates on RUC/RAP-Based Discriminations of Nontornadic and Tornadic Supercell Environments. *Weather and Forecasting*, **39 (10)**, 1417–1434, https://doi.org/10.1175/WAF-D-24-0027.1, URL https://journals.ametsoc.org/view/journals/wefo/39/10/WAF-D-24-0027.1.xml.

Craven, J. P., and H. E. Brooks, 2004: Baseline Climatology of Sounding Dervied Parameters Associated with Deep Moist Convection. *National Weather Digest*, **28 (1)**, 13–24.

Crowe, C. C., C. J. Schultz, M. Kumjian, L. D. Carey, and W. A. Petersen, 2012:

Use of dual-polarization signatures in diagnosing tornadic potential. *Electron. J. Oper. Meteor*, **13 (5)**, 57–78, URL https://scholar.google.com/scholar?cluster=5254162868629937234&hl=en&oi=scholarr.

Darkow, G. L., 1969: An analysis of over sixty tornado proximity soundings. *10th Conf. on Severe Local Storms*, Omaha, NE, 218–221.

Darkow, G. L., and D. W. McCann, 1977: Relative environmental winds for 121 tornado bearing storms. *Sixth Conf. on Severe Local Storms*, Chicago, IL, 413–417.

Davenport, C. E., and M. D. Parker, 2015: Impact of Environmental Heterogeneity on the Dynamics of a Dissipating Supercell Thunderstorm. https://doi.org/10.1175/MWR-D-15-0072.1, URL https://journals.ametsoc.org/view/journals/mwre/143/10/mwr-d-15-0072.1.xml.

Davenport, C. E., C. L. Ziegler, and M. I. Biggerstaff, 2019: Creating a More Realistic Idealized Supercell Thunderstorm Evolution via Incorporation of Base-State Environmental Variability. *Monthly Weather Review*, **147 (11)**, 4177–4198, https://doi.org/10.1175/MWR-D-18-0447.1, URL https://journals.ametsoc.org/view/journals/mwre/147/11/mwr-d-18-0447.1.xml.

Davies, J. M., and R. H. Johns, 1993: Some Wind and Instability Parameters Associated With Strong And Violent Tornadoes: 1. Wind Shear And Helicity. *The Tornado: Its Structure, Dynamics, Prediction, and Hazards*, American Geophysical Union (AGU), 573–582, https://doi.org/10.1029/GM079p0573, URL https://onlinelibrary.wiley.com/doi/abs/10.1029/GM079p0573, _eprint: https://agupubs.onlinelibrary.wiley.com/doi/pdf/10.1029/GM079p0573.

Davies-Jones, R., 1984: Streamwise Vorticity: The Origin of Updraft Rotation in Supercell Storms. *Journal of the Atmospheric Sciences*, **41 (20)**, 2991–3006.

Davies-Jones, R. P., D. W. Burgess, and M. P. Foster, 1990: Test of helicity as as forecast parameter. *16th Conf. on Severe Local Storms*, Amer. Meteor. Soc., Kananaskis Park, AB, Canada, 588–592.

Davis, J. M., and M. D. Parker, 2014: Radar Climatology of Tornadic and Nontornadic Vortices in High-Shear, Low-CAPE Environments in the Mid-Atlantic and Southeastern United States. *Weather and Forecasting*, **29 (4)**, 828–853, https://doi.org/10.1175/WAF-D-13-00127.1.

Dawson, D. T., E. R. Mansell, Y. Jung, L. J. Wicker, M. R. Kumjian, and M. Xue, 2014: Low-Level ZDR Signatures in Supercell Forward Flanks: The Role of Size Sorting and Melting of Hail. *Journal of the Atmospheric Sciences*, **71 (1)**, 276–299,

https://doi.org/10.1175/JAS-D-13-0118.1.

Dean, A. R., and R. S. Schneider, 2008: Forecast challenges at the NWS Storm Prediction Center relating to the frequency of favorable severe storm environments. *24th Conf. on Severe Local Storms*, Amer. Meteor. Soc., Savannah, GA, 9A.2, URL https://ams.confex.com/ams/24SLS/techprogram/paper_141743.htm.

Dean, A. R., and R. S. Schneider, 2012: No. 60, 60. An examination of tornado environments, events, and impacts from 2003-2012. Amer. Meteor. Soc., URL https://ams.confex.com/ams/26SLS/webprogram/Paper211580.html.

Diedrichsen, M. R., M. C. Coniglio, and S. Waugh, 2025: An Intercomparison of the Sparv Windsond S1H2 and Vaisala RS41-SGP in Severe Weather Environments. *Journal of Atmospheric and Oceanic Technology*, **42 (12)**, 1601–1615, https://doi.org/10.1175/JTECH-D-25-0006.1, URL https://journals.ametsoc.org/view/journals/atot/42/12/JTECH-D-25-0006.1.xml.

Doswell III, C. A., and D. W. Burgess, 1993: Tornadoes and Toraadic Storms: a Review of Conceptual Models. *The Tornado: Its Structure, Dynamics, Prediction, and Hazards*, American Geophysical Union (AGU), 161–172.

Dowell, D. C., and Coauthors, 2022: The High-Resolution Rapid Refresh (HRRR): An Hourly Updating Convection-Allowing Forecast Model. Part I: Motivation and System Description. *Weather and Forecasting*, **37 (8)**, 1371–1395, https://doi.org/10.1175/WAF-D-21-0151.1.

Droegemeier, K. K., S. M. Lazarus, and R. Davies-Jones, 1993: The Influence of Helicity on Numerically Simulated Convective Storms. *Monthly Weather Review*, **121 (7)**, 2005–2029, URL https://journals.ametsoc.org/view/journals/mwre/121/7/1520-0493_1993_121_2005_tiohon_2_0_co_2.xml.

Duda, J. D., and W. A. Gallus, 2010: Spring and Summer Midwestern Severe Weather Reports in Supercells Compared to Other Morphologies. *Weather and Forecasting*, **25 (1)**, 190–206, https://doi.org/10.1175/2009WAF2222338.1.

Edwards, R., and R. L. Thompson, 2000: RUC-2 Supercell Proximity Soundings, Part II: An Independent Assessment of Supercell Forecast Parameters. *20th Conf. on Severe Local Storms*, Amer. Meteor. Soc., Orlando, FL, URL https://ams.confex.com/ams/Sept2000/webprogram/Paper16314.html.

EOL, 2019: Meso18-19 Field Catalog. Earth Observing Labratory, URL https://www.eol.ucar.edu/field_projects/meso18-19.

Esterheld, J. M., and D. J. Giuliano, 2008: Discriminating between Tornadic and Non-Tornadic Supercells: A New Hodograph Technique. *E-Journal of Severe Storms Meteorology*, **3 (2)**, 1–50, https://doi.org/10.55599/ejssm.v3i2.15.

Evans, C., S. J. Weiss, I. L. Jirak, A. R. Dean, and D. S. Nevius, 2018: An Evaluation of Paired Regional/Convection-Allowing Forecast Vertical Thermodynamic Profiles in Warm-Season, Thunderstorm-Supporting Environments. *Weather and Forecasting*, **33 (6)**, 1547–1566, https://doi.org/10.1175/WAF-D-18-0124.1.

Faletti, W. L., C. C. Weiss, P. S. Skinner, and B. C. Ancell, 2026: Using Ensemble Sensitivity to Diagnose Environmental Modulation of Mesocyclone Intensity in the Warn-on-Forecast System. *Monthly Weather Review*, https://doi.org/10.1175/MWR-D-25-0123.1, URL https://journals.ametsoc.org/view/journals/mwre/aop/MWR-D-25-0123.1/MWR-D-25-0123.1.xml.

Fawbush, E. J., and R. C. Miller, 1953: A Method for Forecasting Hailstone Size at the Earth's Surface. *Bulletin of the American Meteorological Society*, **34 (6)**, 235–244, https://doi.org/10.1175/1520-0477-34.6.235.

Fawbush, W. J., and R. C. Miller, 1952: A Mean Sounding Representative of the Tornadic Airmass Environment. *Bulletin of the American Meteorological Society*, **33 (7)**, 303–307, https://doi.org/10.1175/1520-0477-33.7.303.

Fischer, A., and J. M. Davies, 2009: Significant Nighttime Tornadoes in the Plains Associated with Relatively Stable Low-Level Conditions. *E-Journal of Severe Storms Meteorology*, **10**, 2009–EJ3, URL http://www.nwas.org/ej/pdf/2009-EJ3.pdf.

Fischer, J., and J. M. L. Dahl, 2020: The Relative Importance of Updraft and Cold Pool Characteristics in Supercell Tornadogenesis Using Highly Idealized Simulations. *Journal of the Atmospheric Sciences*, **77 (12)**, 4089–4107, https://doi.org/10.1175/JAS-D-20-0126.1, URL https://journals.ametsoc.org/view/journals/atsc/77/12/jasD200126.xml.

Flournoy, M. D., M. C. Coniglio, and E. N. Rasmussen, 2021: Examining Relationships between Environmental Conditions and Supercell Motion in Time. *Weather and Forecasting*, **36 (3)**, 737–755, https://doi.org/10.1175/WAF-D-20-0192.1, tex.ids=flournoyExaminingRelationshipsEnvironmental2021a.

Flournoy, M. D., M. C. Coniglio, E. N. Rasmussen, J. C. Furtado, and B. E. Coffer, 2020: Modes of Storm-Scale Variability and Tornado Potential in VORTEX2 Near- and Far-Field Tornadic Environments. *Monthly Weather Review*, **148 (10)**, 4185–4207, https://doi.org/10.1175/MWR-D-20-0147.1, URL https://journals.ametsoc.org/view/journals/mwre/148/10/mwrD200147.xml.

Flournoy, M. D., A. W. Lyza, M. A. Satrio, M. R. Diedrichsen, M. C. Coniglio, and S. Waugh, 2022: A Climatology of Cell Mergers with Supercells and Their Association with Mesocyclone Evolution. *Monthly Weather Review*, **150 (2)**, 451–461, https://doi.org/10.1175/MWR-D-21-0204.1.

Flournoy, M. D., A. W. Lyza, A. R. Wade, and J. Fischer, 2024: Observed Relationships between Supercell Mesocyclone Intensity and Evolution, Background Environmental Characteristics, and Cell Mergers. https://doi.org/10.1175/MWR-D-23-0199.1, URL https://journals.ametsoc.org/view/journals/mwre/152/8/MWR-D-23-0199.1.xml.

Forbes, G. S., and R. M. Wakimoto, 1983: A Concentrated Outbreak of Tornadoes, Downbursts and Microbursts, and Implications Regarding Vortex Classification. *Monthly Weather Review*, **111 (1)**, 220–236, https://doi.org/10.1175/1520-0493(1983)111⟨0220:ACOOTD⟩2.0.CO;2, URL https://journals.ametsoc.org/view/journals/mwre/111/1/1520-0493_1983_111_0220_acootd_2_0_co_2.xml.

French, M. M., D. W. Burgess, E. R. Mansell, and L. J. Wicker, 2015: Bulk Hook Echo Raindrop Sizes Retrieved Using Mobile, Polarimetric Doppler Radar Observations. *Journal of Applied Meteorology and Climatology*, **54 (2)**, 423–450, https://doi.org/10.1175/JAMC-D-14-0171.1, URL https://journals.ametsoc.org/view/journals/apme/54/2/jamc-d-14-0171.1.xml.

Fujita, T. T., 1978: Manual of downburst identification for Project NIMROD. Satellite and Mesometeorology Research Paper 156 NASA-CR-156953, Department of Geophysical Sciences, University of Chicago, 104 pp. URL https://ntrs.nasa.gov/citations/19780022828, nTRS Author Affiliations: Chicago Univ. NTRS Document ID: 19780022828 NTRS Research Center: Legacy CDMS (CDMS).

Gallus, W. A., N. A. Snook, and E. V. Johnson, 2008: Spring and Summer Severe Weather Reports over the Midwest as a Function of Convective Mode: A Preliminary Study. *Weather and Forecasting*, **23 (1)**, 101–113, https://doi.org/10.1175/2007WAF2006120.1.

Galway, J. G., and A. Pearson, 1981: Winter Tornado Outbreaks. *Monthly Weather Review*, **109 (5)**, 1072–1080, URL https://journals.ametsoc.org/view/journals/mwre/109/5/1520-0493_1981_109_1072_wto_2_0_co_2.xml.

Gebauer, J. G., M. C. Coniglio, R. A. Saba, T. M. Bell, E. N. Smith, D. J. Bodine, R. M. Frost, and P. M. Markowski, 2026: Will a Worm Turn? Observations of Coherent Surface-Layer Vertical Vorticity in Supercell Inflow. *Bulletin of the American Meteorological Society*, **107 (3)**, E675–E695, https://doi.org/10.1175/BAMS-D-24-0350.1, URL https://journals.ametsoc.org/view/journals/bams/107/3/BAMS-D-24-0350.1.

xml.

Goldacker, N. A., and M. D. Parker, 2021: Low-Level Updraft Intensification in Response to Environmental Wind Profiles. *Journal of the Atmospheric Sciences*, **78 (9)**, 2763–2781, https://doi.org/10.1175/JAS-D-20-0354.1.

Grams, J. S., R. L. Thompson, D. V. Snively, J. A. Prentice, G. M. Hodges, and L. J. Reames, 2012: A Climatology and Comparison of Parameters for Significant Tornado Events in the United States. *Weather and Forecasting*, **27 (1)**, 106–123, https://doi.org/10.1175/WAF-D-11-00008.1.

Guarriello, F., C. J. Nowotarski, and C. C. Epifanio, 2018: Effects of the Low-Level Wind Profile on Outflow Position and Near-Surface Vertical Vorticity in Simulated Supercell Thunderstorms. *Journal of the*, **75 (3)**, 731–753, https://doi.org/10.1175/JAS-D-17-0174.1.

Gutierrez, R. E., and M. R. Kumjian, 2021: Environmental and Radar Characteristics of Gargantuan Hail–Producing Storms. *Monthly Weather Review*, **149 (8)**, 2523–2538, https://doi.org/10.1175/MWR-D-20-0298.1.

Guyer, J. L., and A. R. Dean, 2010: Tornadoes within weak CAPE environments across the continental United States. *25th Conf. on Severe Local Storms*, Amer. Meteor. Soc., Denver, CO, 1.5, URL https://ams.confex.com/ams/25SLS/webprogram/Paper175725.html, 1.5.

Hill, A. J., C. C. Weiss, and D. C. Dowell, 2021: Influence of a Portable Near-Surface Observing Network on Experimental Ensemble Forecasts of Deep Convection Hazards during VORTEX-SE. *Weather and Forecasting*, **36 (4)**, 1141–1167, https://doi.org/10.1175/WAF-D-20-0237.1, URL https://journals.ametsoc.org/view/journals/wefo/36/4/WAF-D-20-0237.1.xml.

Hitchcock, S. M., R. S. Schumacher, G. R. Herman, M. C. Coniglio, M. D. Parker, and C. L. Ziegler, 2019: Evolution of Pre- and Postconvective Environmental Profiles from Mesoscale Convective Systems during PECAN. *Monthly Weather Review*, **147 (7)**, 2329–2354, https://doi.org/10.1175/MWR-D-18-0231.1.

Homeyer, C. R., M. J. Bunkers, J. T. Allen, and A. M. Murphy, 2025: United States Supercell Storms and Their Severity: A 14-Year Radar-Based Climatology. *Journal of Applied Meteorology and Climatology*, **64 (8)**, 959–970, https://doi.org/10.1175/JAMC-D-24-0185.1.

Homeyer, C. R., E. M. Murillo, and M. R. Kumjian, 2023: Relationships between 10 Years of Radar-Observed Supercell Characteristics and Hail Potential. *Monthly*

Weather Review, **151 (10)**, 2609–2632, https://doi.org/10.1175/MWR-D-23-0019.1.

Hosek, M. J., C. L. Ziegler, M. I. Biggerstaff, T. A. Murphy, and Z. Wang, 2023: Relation between Baroclinity, Horizontal Vorticity, and Mesocyclone Evolution in the 6–7 April 2018 Monroe, Louisiana, Tornadic Supercell during VORTEX-SE. *Monthly Weather Review*, **151 (11)**, 2949–2976, https://doi.org/10.1175/MWR-D-22-0313.1, URL https://journals.ametsoc.org/view/journals/mwre/151/11/MWR-D-22-0313.1.xml.

Houston, A. L., R. L. Thompson, and R. Edwards, 2008: The Optimal Bulk Wind Differential Depth and the Utility of the Upper-Tropospheric Storm-Relative Flow for Forecasting Supercells. **23 (5)**, 825–837, https://doi.org/10.1175/2008WAF2007007.1, URL https://journals.ametsoc.org/view/journals/wefo/23/5/2008waf2007007_1.xml.

Hu, M., S. G. Benjamin, T. T. Ladwig, D. C. Dowell, S. S. Weygandt, C. R. Alexander, and J. S. Whitaker, 2017: GSI Three-Dimensional Ensemble–Variational Hybrid Data Assimilation Using a Global Ensemble for the Regional Rapid Refresh Model. *Monthly Weather Review*, **145 (10)**, 4205–4225, https://doi.org/10.1175/MWR-D-16-0418.1.

Jackson, J. D., and M. E. Brown, 2009: Sounding-Derived Low-Level Thermodynamic Characteristics Associated with Tornadic and Non-Tornadic Supercell Environments in the Southeast United States. *Natl. Wea. Dig.*, **33**, 15–26, URL https://nwafiles.nwas.org/file/nwafiles/digest/papers/2009/Vol33No1/Pg15-JacksonBrown.pdf.

James, E. P., and Coauthors, 2022: The High-Resolution Rapid Refresh (HRRR): An Hourly Updating Convection-Allowing Forecast Model. Part II: Forecast Performance. *Weather and Forecasting*, **37 (8)**, 1397–1417, https://doi.org/10.1175/WAF-D-21-0130.1, URL https://journals.ametsoc.org/view/journals/wefo/37/8/WAF-D-21-0130.1.xml.

Johns, R. H., and C. A. Doswell, 1992: Severe Local Storms Forecasting. *Weather and Forecasting*, **7 (4)**, 588–612.

Katona, B., P. Markowski, C. Alexander, and S. Benjamin, 2016: The Influence of Topography on Convective Storm Environments in the Eastern United States as Deduced from the HRRR. *Weather and Forecasting*, **31 (5)**, 1481–1490, https://doi.org/10.1175/WAF-D-16-0038.1.

Kerr, B. W., and G. L. Darkow, 1996: Storm-Relative Winds and Helicity in the Tornadic Thunderstorm Environment. *Weather and Forecasting*, **11 (4)**, 489–505, https://doi.org/https://doi.org/10.1175/1520-0434(1996)011⟨0489:SRWAHI⟩2.

0.CO;2.

King, J. R., M. D. Parker, K. D. Sherburn, and G. M. Lackmann, 2017: Rapid Evolution of Cool Season, Low-CAPE Severe Thunderstorm Environments. *Weather and Forecasting*, **32 (2)**, 763–779, https://doi.org/10.1175/WAF-D-16-0141.1.

Kis, A. K., and J. M. Straka, 2010: Nocturnal Tornado Climatology. *Weather and Forecasting*, **25 (2)**, 545–561, https://doi.org/10.1175/2009WAF2222294.1.

Knuteson, R. O., and Coauthors, 2004: Atmospheric Emitted Radiance Interferometer. Part II: Instrument Performance. *Journal of Atmospheric and Oceanic Technology*, **21 (12)**, 1777–1789, https://doi.org/10.1175/JTECH-1663.1, URL https://journals.ametsoc.org/view/journals/atot/21/12/jtech-1663_1.xml.

Kosiba, K. A., and Coauthors, 2024: The Propagation, Evolution, and Rotation in Linear Storms (PERiLS) Project. *Bulletin of the American Meteorological Society*, **105 (10)**, E1768–E1799, https://doi.org/10.1175/BAMS-D-22-0064.1, tex.ids=kosibaPropagationEvolutionRotation2024a.

Kumjian, M. R., 2011: Precipitation Properties of Supercell Hook Echoes. *E-Journal of Severe Storms Meteorology*, **6 (5)**, 1–21, https://doi.org/10.55599/ejssm.v6i5.32, URL https://ejssm.com/ojs/index.php/site/article/view/32.

Kumjian, M. R., and A. V. Ryzhkov, 2008: Polarimetric signatures in supercell thunderstorms. *Journal of applied meteorology and climatology*, **47 (7)**, 1940–1961, URL https://journals.ametsoc.org/view/journals/apme/47/7/2007jamc1874.1.xml.

Kumjian, M. R., and A. V. Ryzhkov, 2009: Storm-Relative Helicity Revealed from Polarimetric Radar Measurements. *Journal of the Atmospheric Sciences*, **66 (3)**, 667–685, https://doi.org/10.1175/2008JAS2815.1.

Kumjian, M. R., and A. V. Ryzhkov, 2012: The impact of size sorting on the polarimetric radar variables. *Journal of the Atmospheric Sciences*, **69 (6)**, 2042–2060.

LaFleur, A. T., R. L. Tanamachi, D. T. Dawson, and D. D. Turner, 2023: Factors Affecting the Rapid Recovery of CAPE on 31 March 2016 during VORTEX-Southeast. *Monthly Weather Review*, **151 (6)**, 1459–1477, https://doi.org/10.1175/MWR-D-22-0051.1, URL https://journals.ametsoc.org/view/journals/mwre/151/6/MWR-D-22-0051.1.xml.

Laser, J. J., M. C. Coniglio, P. S. Skinner, and E. N. Smith, 2022: Doppler Lidar and Mobile Radiosonde Observation-Based Evaluation of Warn-on-Forecast System Predicted Near-Supercell Environments during TORUS 2019. *Weather and*

Forecasting, **37 (10)**, 1783–1804, https://doi.org/10.1175/WAF-D-21-0190.1, URL https://journals.ametsoc.org/view/journals/wefo/37/10/WAF-D-21-0190.1.xml.

LeBel, L. J., P. Markowski, and Y. P. Richardson, 2024: How Well Do Small Balloon-Borne Sondes Perform in Heavy Precipitation? *31st Conference on Severe Local Storms*, AMS, URL https://scholar.google.com/scholar?cluster=15405674990117999937&hl=en&oi=scholarr.

Lee, T. R., M. Buban, D. D. Turner, T. P. Meyers, and C. B. Baker, 2019: Evaluation of the High-Resolution Rapid Refresh (HRRR) Model Using Near-Surface Meteorological and Flux Observations from Northern Alabama. *Weather and Forecasting*, **34 (3)**, https://doi.org/10.1175/WAF-D-18-0184.1, URL https://journals.ametsoc.org/view/journals/wefo/34/3/waf-d-18-0184_1.xml.

Lee, T. R., R. D. Leeper, T. Wilson, H. J. Diamond, T. P. Meyers, and D. D. Turner, 2023: Using the U.S. Climate Reference Network to Identify Biases in Near- and Subsurface Meteorological Fields in the High-Resolution Rapid Refresh (HRRR) Weather Prediction Model. *Weather and Forecasting*, **38 (6)**, https://doi.org/10.1175/WAF-D-22-0213.1, URL https://journals.ametsoc.org/view/journals/wefo/38/6/WAF-D-22-0213.1.xml.

Lin, G., Z. Wang, C. Ziegler, X.-M. Hu, M. Xue, B. Geerts, and Y. Chu, 2023: A Comparison of Convective Storm Inflow Moisture Variability between the Great Plains and the Southeastern United States Using Multiplatform Field Campaign Observations. *Journal of Atmospheric and Oceanic Technology*, **40 (5)**, 539–556, https://doi.org/10.1175/JTECH-D-22-0037.1, URL https://journals.ametsoc.org/view/journals/atot/40/5/JTECH-D-22-0037.1.xml.

Lin, Y., and M. R. Kumjian, 2022: Influences of CAPE on Hail Production in Simulated Supercell Storms. *Journal of the Atmospheric Sciences*, **79 (1)**, 179–204, https://doi.org/10.1175/JAS-D-21-0054.1.

Loeffler, S. D., and M. R. Kumjian, 2018: Quantifying the Separation of Enhanced ZDR and KDP Regions in Nonsupercell Tornadic Storms. *Weather and Forecasting*, **33 (5)**, 1143–1157, https://doi.org/10.1175/WAF-D-18-0011.1, URL https://journals.ametsoc.org/view/journals/wefo/33/5/waf-d-18-0011_1.xml.

Loeffler, S. D., and M. R. Kumjian, 2020: Idealized Model Simulations to Determine Impacts of Storm-Relative Winds on Differential Reflectivity and Specific Differential Phase Fields. *Journal of Geophysical Research: Atmospheres*, **125 (24)**, e2020JD033 870, https://doi.org/10.1029/2020JD033870, URL https://onlinelibrary.wiley.com/doi/abs/10.1029/2020JD033870, _eprint: https://agupubs.onlinelibrary.wiley.com/doi/pdf/10.1029/2020JD033870.

Lyza, A. W., A. W. Clayton, K. R. Knupp, E. Lenning, M. T. Friedlein, R. L. Castro, and E. S. Bentley, 2017: Analysis of mesovortex characteristics, behavior, and interactions during the second 30 June-1 July 2014 midwestern derecho event. *E-Journal of Severe Storms Meteorology*, **12 (2)**, 1–33, URL https://ejssm.com/ojs/index.php/site/article/view/67.

Lyza, A. W., M. D. Flournoy, and E. N. Rasmussen, 2022a: Observed Characteristics of the Tornadic Supercells of 27–28 April 2011 in the Southeast United States. **150 (11)**, 2883–2910, https://doi.org/10.1175/MWR-D-21-0274.1.

Lyza, A. W., B. T. Goudeau, and K. R. Knupp, 2022b: Damage Analysis and Close-Range Radar Observations of the 13 April 2019 Greenwood Springs, Mississippi, Tornado during VORTEX-SE Meso18-19. *Monthly Weather Review*, **150 (7)**, 1873–1893, https://doi.org/10.1175/MWR-D-21-0281.1, URL https://journals.ametsoc.org/view/journals/mwre/150/7/MWR-D-21-0281.1.xml.

Lyza, A. W., T. A. Murphy, B. T. Goudeau, P. T. Pangle, K. R. Knupp, and R. A. Wade, 2020: Observed Near-Storm Environment Variations across the Southern Cumberland Plateau System in Northeastern Alabama. *Monthly Weather Review*, **148 (4)**, 1465–1482, https://doi.org/10.1175/MWR-D-19-0190.1, URL https://journals.ametsoc.org/view/journals/mwre/148/4/mwr-d-19-0190.1.xml.

MacDonald, L. M., and C. J. Nowotarski, 2023: Verification of Rapid Refresh and High-Resolution Rapid Refresh Model Variables in Tornadic Tropical Cyclones. *Weather and Forecasting*, **38 (5)**, 655–675, https://doi.org/10.1175/WAF-D-22-0117.1, URL https://journals.ametsoc.org/view/journals/wefo/38/5/WAF-D-22-0117.1.xml.

Maddox, R. A., 1976: An Evaluation of Tornado Proximity Wind and Stability Data. *Monthly Weather Review*, **104 (2)**, 133–142.

Mahalik, M. C., B. R. Smith, K. L. Elmore, D. M. Kingfield, K. L. Ortega, and T. M. Smith, 2019: Estimates of Gradients in Radar Moments Using a Linear Least Squares Derivative Technique. *Weather and Forecasting*, **34 (2)**, 415–434, https://doi.org/10.1175/WAF-D-18-0095.1, URL https://journals.ametsoc.org/view/journals/wefo/34/2/waf-d-18-0095_1.xml.

Mallinson, H. M., and S. G. Lasher-Trapp, 2019: An Investigation of Hydrometeor Latent Cooling upon Convective Cold Pool Formation, Sustainment, and Properties. *Monthly Weather Review*, **147 (9)**, 3205–3222, https://doi.org/10.1175/MWR-D-18-0382.1, URL https://journals.ametsoc.org/view/journals/mwre/147/9/mwr-d-18-0382.1.xml.

Marion, G. R., and R. J. Trapp, 2021: Controls of Quasi-Linear Convective Sys-

tem Tornado Intensity. *Journal of the Atmospheric Sciences*, **78 (4)**, 1189–1205, https://doi.org/10.1175/JAS-D-20-0164.1, URL https://journals.ametsoc.org/view/journals/atsc/78/4/JAS-D-20-0164.1.xml.

Markowski, P., C. Hannon, J. Frame, E. Lancaster, A. Pietrycha, R. Edwards, and R. L. Thompson, 2003: Characteristics of Vertical Wind Profiles near Supercells Obtained from the Rapid Update Cycle. *Weather and Forecasting*, **18 (6)**, 1262–1272.

Markowski, P. M., 2020: What is the Intrinsic Predictability of Tornadic Supercell Thunderstorms? **148 (8)**, 3157–3180, https://doi.org/10.1175/MWR-D-20-0076.1, URL https://journals.ametsoc.org/view/journals/mwre/148/8/mwrD200076.xml.

Markowski, P. M., 2024: A New Pathway for Tornadogenesis Exposed by Numerical Simulations of Supercells in Turbulent Environments. *Journal of the Atmospheric Sciences*, **81 (3)**, 481–518, https://doi.org/10.1175/JAS-D-23-0161.1, URL https://journals.ametsoc.org/view/journals/atsc/81/3/JAS-D-23-0161.1.xml.

Markowski, P. M., N. T. Lis, D. D. Turner, T. R. Lee, and M. S. Buban, 2019: Observations of Near-Surface Vertical Wind Profiles and Vertical Momentum Fluxes from VORTEX-SE 2017: Comparisons to Monin–Obukhov Similarity Theory. *Monthly Weather Review*, **147 (10)**, 3811–3824, https://doi.org/10.1175/MWR-D-19-0091.1, URL https://journals.ametsoc.org/view/journals/mwre/147/10/mwr-d-19-0091.1.xml.

Markowski, P. M., and Y. P. Richardson, 2014: The Influence of Environmental Low-Level Shear and Cold Pools on Tornadogenesis: Insights from Idealized Simulations. *Journal of the Atmospheric Sciences*, **71 (1)**, 243–275, https://doi.org/10.1175/JAS-D-13-0159.1, URL https://journals.ametsoc.org/view/journals/atsc/71/1/jas-d-13-0159.1.xml.

Markowski, P. M., J. M. Straka, and E. N. Rasmussen, 2002: Direct Surface Thermodynamic Observations within the Rear-Flank Downdrafts of Nontornadic and Tornadic Supercells. **130 (7)**, 1692–1721, https://doi.org/10.1175/1520-0493(2002)130⟨1692:DSTOWT⟩2.0.CO;2.

Markowski, P. M., J. M. Straka, E. N. Rasmussen, and D. O. Blanchard, 1998: Variability of Storm-Relative Helicity during VORTEX. *Monthly Weather Review*, **126 (11)**, 2959–2971, https://doi.org/10.1175/1520-0493(1998)126⟨2959:VOSRHD⟩2.0.CO;2.

McCaul, E. W., and M. L. Weisman, 2001: The Sensitivity of Simulated Supercell Structure and Intensity to Variations in the Shapes of Environmental Buoyancy and Shear Profiles. *Monthly Weather Review*, **129 (4)**, 664–687, https://doi.org/10.1175/1520-0493(2001)129⟨0664:TSOSSS⟩2.0.CO;2.

McDonald, J. M., and C. C. Weiss, 2021: Cold Pool Characteristics of Tornadic Quasi-Linear Convective Systems and Other Convective Modes Observed during VORTEX-SE. *Monthly Weather Review*, **149 (3)**, 821–840, https://doi.org/10.1175/MWR-D-20-0226.1, URL https://journals.ametsoc.org/view/journals/mwre/149/3/MWR-D-20-0226.1.xml.

Moller, A. R., C. A. Doswell, M. P. Foster, and G. R. Woodall, 1994: The Operational Recognition of Supercell Thunderstorm Environments and Storm Structures. *Weather and Forecasting*, **9 (3)**, 327–347.

Murphy, A. M., C. R. Homeyer, and K. Q. Allen, 2023: Development and Investigation of GridRad-Severe, a Multiyear Severe Event Radar Dataset. *Monthly Weather Review*, **151 (9)**, 2257–2277, https://doi.org/10.1175/MWR-D-23-0017.1.

Murphy, T. A., T. M. Stetzer, L. Walker, T. Fricker, B. Bryant, and C. Woodrum, 2022: Analysis of the 12 April 2020 Northern Louisiana Tornadic QLCS. *Journal of Operational Meteorology*, 43–62, https://doi.org/10.15191/nwajom.2022.1004, URL http://nwafiles.nwas.org/jom/articles/2022/2022-JOM4/2022-JOM4.pdf.

Nelson, S. P., and N. C. Knight, 1987: The Hybrid Multicellular–Supercellular Storm—an Efficient Hail Producer. Part I: An Archetypal Example. *Journal of the Atmospheric Sciences*, **44 (15)**, 2042–2059, https://doi.org/10.1175/1520-0469(1987)044⟨2042:THMSEH⟩2.0.CO;2.

Newton, C. W., and S. Katz, 1958: Movement of Large Convective Rainstorms in Relation to Winds Aloft. *Bulletin of the American Meteorological Society*, **39 (3)**, 129–136, https://doi.org/10.1175/1520-0477-39.3.129, URL https://journals.ametsoc.org/view/journals/bams/39/3/1520-0477-39_3_129.xml.

Nowotarski, C. J., and A. A. Jensen, 2013: Classifying proximity soundings with self-organizing maps toward improving supercell and tornado forecasting. *Weather and forecasting*, **28 (3)**, 783–801.

Ostaszewski, J. S., C. C. Weiss, J. M. McDonald, M. C. Coniglio, and S. M. Waugh, 2025: Surface Cold Pool Observations near Tornadic and Nontornadic QLCS Mesovortices during PERiLS. *Mon*, **153 (9)**, 1815–1840, https://doi.org/10.1175/MWR-D-24-0166.1.

Pardun, T. J., A. E. Reinhart, and M. C. Coniglio, 2025: A Comparison between Tornadic and Nontornadic QLCS Mesovortices Using a Multiradar Analysis of Operational and Experimental MRMS Products. *Weather and Forecasting*, **40 (6)**, 915–935, https://doi.org/10.1175/WAF-D-24-0050.1, URL https://journals.ametsoc.org/view/journals/wefo/40/6/WAF-D-24-0050.1.xml.

Parker, M. D., 2014: Composite vortex2 supercell environments from near-storm soundings. *Monthly Weather Review*, **142 (2)**, 508–529.

Peters, J. M., B. E. Coffer, M. D. Parker, C. J. Nowotarski, J. P. Mulholland, C. J. Nixon, and J. T. Allen, 2023: Disentangling the influences of storm-relative flow and horizontal streamwise vorticity on low-level mesocyclones in supercells. *Journal of the Atmospheric Sciences*, **80 (1)**, 129–149.

Peters, J. M., C. J. Nowotarski, and H. Morrison, 2019: The Role of Vertical Wind Shear in Modulating Maximum Supercell Updraft Velocities. *Journal of the Atmospheric Sciences*, **76 (10)**, 3169–3189, https://doi.org/10.1175/JAS-D-19-0096.1.

Peters, J. M., C. J. Nowotarski, J. P. Mulholland, and R. L. Thompson, 2020: The Influences of Effective Inflow Layer Streamwise Vorticity and Storm-Relative Flow on Supercell Updraft Properties. *Journal of the Atmospheric Sciences*, **77 (9)**, 3033–3057, https://doi.org/10.1175/JAS-D-19-0355.1.

Potvin, C. K., K. L. Elmore, and S. J. Weiss, 2010: Assessing the Impacts of Proximity Sounding Criteria on the Climatology of Significant Tornado Environments. *Weather and Forecasting*, **25 (3)**, 921–930, https://doi.org/10.1175/2010WAF2222368.1.

Potvin, C. K., and Coauthors, 2019: Systematic Comparison of Convection-Allowing Models during the 2017 NOAA HWT Spring Forecasting Experiment. *Weather and Forecasting*, **34 (5)**, 1395–1416, https://doi.org/10.1175/WAF-D-19-0056.1, URL https://journals.ametsoc.org/view/journals/wefo/34/5/waf-d-19-0056_1.xml.

Pounds, L. E., R. L. Miller, M. D. Flournoy, M. C. Coniglio, A. R. Wade, and K. T. Halbert, 2026: Composite Southeast United States Convective Environments from Field Campaign Sounding Observations. *Monthly Weather Review*, submitted.

Przybylinski, R. W., 1995: The Bow Echo: Observations, Numerical Simulations, and Severe Weather Detection Methods. *Weather and Forecasting*, **10 (2)**, URL https://journals.ametsoc.org/view/journals/wefo/10/2/1520-0434_1995_010_0203_tbeons_2_0_co_2.xml.

Rasmussen, E. N., 2003: Refined Supercell and Tornado Forecast Parameters. *Weather and Forecasting*, **18 (3)**, 530–535.

Rasmussen, E. N., 2015: VORTEX-Southeast Program Overview. Tech. rep., National Severe Storms Laboratory, 36 pp.

Rasmussen, E. N., and D. O. Blanchard, 1998: A Baseline Climatology of Sounding-Derived Supercell andTornado Forecast Parameters. *Weather and Forecasting*,

13 (4), 1148–1164, URL https://journals.ametsoc.org/view/journals/wefo/13/4/1520-0434_1998_013_1148_abcosd_2_0_co_2.xml.

Rasmussen, E. N., J. M. Straka, R. Davies-Jones, C. A. Doswell, F. H. Carr, M. D. Eilts, and D. R. MacGorman, 1994: Verification of the Origins of Rotation in Tornadoes Experiment: VORTEX. *Bulletin of the American Meteorological Society*, **75 (6)**, 995–1006.

Richardson, Y. P., K. K. Droegemeier, and R. P. Davies-Jones, 2007: The Influence of Horizontal Environmental Variability on Numerically Simulated Convective Storms. Part I: Variations in Vertical Shear. *Monthly Weather Review*, **135 (10)**, 3429–3455, https://doi.org/10.1175/MWR3463.1, URL https://journals.ametsoc.org/view/journals/mwre/135/10/mwr3463.1.xml.

Rogers, J. W., B. A. Hagenhoff, A. E. Cohen, R. L. Thompson, B. T. Smith, and E. E. Carpenter, 2016: Lower Mississippi River Valley Quasi-Linear Convective System Tornado Environments and Radar Signatures. *Journal of Operational Meteorology*, **05 (04)**, 42–52, https://doi.org/10.15191/nwajom.2017.0504.

Romine, G. S., D. W. Burgess, and R. B. Wilhelmson, 2008: A Dual-Polarization-Radar-Based Assessment of the 8 May 2003 Oklahoma City Area Tornadic Supercell. *Monthly Weather Review*, **136 (8)**, 2849–2870, https://doi.org/10.1175/2008MWR2330.1.

Rotunno, R., and J. B. Klemp, 1982: The Influence of the Shear-Induced Pressure Gradient on Thunderstorm Motion. *Monthly Weather Review*, **110 (2)**, 136–151, URL https://journals.ametsoc.org/view/journals/mwre/110/2/1520-0493_1982_110_0136_tiotsi_2_0_co_2.xml.

Saba, R. A., 2024: Examining Right-Moving Supercell Environments with Doppler Wind Lidar Observations. M.S. thesis, University of Oklahoma – Graduate College, United States, Oklahoma.

Saba, R. A., M. C. Coniglio, J. G. Gebauer, T. M. Bell, E. N. Smith, and S. Waugh, 2026: Examining Right-Moving Supercell Environments in the Great Plains with Composite Doppler Wind Lidar Observations. *Monthly Weather Review*, **154 (4)**, 767–789, https://doi.org/10.1175/MWR-D-25-0177.1, URL https://journals.ametsoc.org/view/journals/mwre/154/4/MWR-D-25-0177.1.xml.

Schaefer, J. T., and R. L. Livingston, 1988: The typical structure of tornado proximity soundings. *Journal of Geophysical Research: Atmospheres*, **93 (D5)**, 5351–5364, https://doi.org/10.1029/JD093iD05p05351.

Schenkman, A. D., M. Xue, and A. Shapiro, 2012: Tornadogenesis in a Simulated Mesovortex within a Mesoscale Convective System. *Journal of the Atmospheric Sciences*, **69 (11)**, 3372–3390, https://doi.org/10.1175/JAS-D-12-038.1, URL https://journals.ametsoc.org/view/journals/atsc/69/11/jas-d-12-038.1.xml.

Schneider, R. S., and A. R. Dean, 2008: A Comprehensive 5-year Severe Storm Environment Climatology for the Continental United States. Amer. Meteor. Soc., Savannah, GA, URL https://scispace.com/papers/a-comprehensive-5-year-severe-storm-environment-climatology-4062t17uys.

Schneider, R. S., A. R. Dean, S. J. Weiss, and P. D. Bothwell, 2006: Analysis of estimated environments for 2004 and 2005 severe convective storm reports. *23rd Conf. on Severe Local Storms*, Amer. Meteor. Soc., St. Louis, MO, Vol. 3.5, URL https://ams.confex.com/ams/23SLS/techprogram/paper_115246.htm.

Sessa, M., and R. Trapp, 2023: Environmental and Radar-Derived Predictors of TornadoIntensity within Ongoing Convective Storms. *Journal of Operational Meteorology*, 49–71, https://doi.org/10.15191/nwajom.2023.1105, URL http://nwafiles.nwas.org/jom/articles/2023/2023-JOM5/2023-JOM5.pdf.

Sherburn, K. D., and M. D. Parker, 2014: Climatology and Ingredients of Significant Severe Convection in High-Shear, Low-CAPE Environments. *Weather and Forecasting*, **29 (4)**, 854–877, https://doi.org/10.1175/WAF-D-13-00041.1, URL https://journals.ametsoc.org/view/journals/wefo/29/4/waf-d-13-00041_1.xml.

Sherburn, K. D., M. D. Parker, J. R. King, and G. M. Lackmann, 2016: Composite Environments of Severe and Nonsevere High-Shear, Low-CAPE Convective Events. *Weather and Forecasting*, **31 (6)**, 1899–1927, https://doi.org/10.1175/WAF-D-16-0086.1.

Showalter, A. K., 1943: *Preliminary Report on Tornadoes ...: Prepared in Cooperation with the War Advisory Council on Meteorology*. Department of Commerce, google-Books-ID: ofvKQt1DdaoC.

Simmons, K. M., and D. Sutter, 2005: WSR-88D Radar, Tornado Warnings, and Tornado Casualties. *Weather and Forecasting*, **20 (3)**, 301–310, https://doi.org/10.1175/WAF857.1, URL https://journals.ametsoc.org/view/journals/wefo/20/3/waf857_1.xml.

Smith, B. T., R. L. Thompson, J. S. Grams, C. Broyles, and H. E. Brooks, 2012: Convective Modes for Significant Severe Thunderstorms in the Contiguous United States. Part I: Storm Classification and Climatology. *Weather and Forecasting*, **27 (5)**, 1114–1135, https://doi.org/10.1175/WAF-D-11-00115.1.

Smith, T. M., and Coauthors, 2016: Multi-Radar Multi-Sensor (MRMS) Severe Weather and Aviation Products: Initial Operating Capabilities. *Bulletin of the American Meteorological Society*, **97 (9)**, 1617–1630, https://doi.org/10.1175/BAMS-D-14-00173.1.

Snook, N., and M. Xue, 2008: Effects of microphysical drop size distribution on tornadogenesis in supercell thunderstorms. *Geophysical Research Letters*, **35 (24)**, https://doi.org/10.1029/2008GL035866, URL https://onlinelibrary.wiley.com/doi/abs/10.1029/2008GL035866, _eprint: https://onlinelibrary.wiley.com/doi/pdf/10.1029/2008GL035866.

SPC, 2024: Severe weather database. https://www.spc.noaa.gov/wcm/.

Strader, S. M., and W. S. Ashley, 2018: Finescale Assessment of Mobile Home Tornado Vulnerability in the Central and Southeast United States. *Weather, Climate, and Society*, **10 (4)**, 797–812, https://doi.org/10.1175/WCAS-D-18-0060.1, URL https://journals.ametsoc.org/view/journals/wcas/10/4/wcas-d-18-0060_1.xml.

Strader, S. M., W. S. Ashley, T. J. Pingel, and A. J. Krmenec, 2017: Observed and Projected Changes in United States Tornado Exposure. *Weather, Climate, and Society*, **9 (2)**, 109–123, https://doi.org/10.1175/WCAS-D-16-0041.1, URL https://journals.ametsoc.org/view/journals/wcas/9/2/wcas-d-16-0041_1.xml.

Sutter, D., and K. M. Simmons, 2010: Tornado fatalities and mobile homes in the United States. *Natural Hazards*, **53 (1)**, 125–137, https://doi.org/10.1007/s11069-009-9416-x.

Tanamachi, R. L., S. J. Frasier, J. Waldinger, A. LaFleur, D. D. Turner, and F. Rocadenbosch, 2019: Progress toward Characterization of the Atmospheric Boundary Layer over Northern Alabama Using Observations by a Vertically Pointing, S-Band Profiling Radar during VORTEX-Southeast. *Journal of Atmospheric and Oceanic Technology*, **36 (11)**, 2221–2246, https://doi.org/10.1175/JTECH-D-18-0224.1, URL https://journals.ametsoc.org/view/journals/atot/36/11/jtech-d-18-0224.1.xml.

Thompson, R. L., 1998: Eta Model Storm-Relative Winds Associated with Tornadic and Nontornadic Supercells. *Weather and Forecasting*, **13 (1)**, 135–137.

Thompson, R. L., 2023: A Comparison of Right-Moving Supercell and Quasi-Linear Convective System Tornadoes in the Contiguous United States 2003–21. *Weather and Forecasting*, **38 (8)**, 1497–1513, https://doi.org/10.1175/WAF-D-23-0006.1.

Thompson, R. L., R. Edwards, J. A. Hart, K. L. Elmore, and P. Markowski, 2003:

Close Proximity Soundings within Supercell Environments Obtained from the Rapid Update Cycle. *Weather and Forecasting*, **18 (6)**, 1243–1261.

Thompson, R. L., R. Edwards, and C. M. Mead, 2004: An update to the supercell composite and significant tornado parameters. *22nd Conference on Severe Local Storms*, Amer. Meteor. Soc., Hyannis, MA, P8.1, [Available online at https://ams.confex.com/ams/11aram22sls/techprogram/paper_82100.htm.].

Thompson, R. L., C. M. Mead, and R. Edwards, 2007: Effective Storm-Relative Helicity and Bulk Shear in Supercell Thunderstorm Environments. *Weather and Forecasting*, **22 (1)**, 102–115, https://doi.org/10.1175/WAF969.1.

Thompson, R. L., B. T. Smith, J. S. Grams, A. R. Dean, and C. Broyles, 2012: Convective Modes for Significant Severe Thunderstorms in the Contiguous United States. Part II: Supercell and QLCS Tornado Environments. *Weather and Forecasting*, **27 (5)**, 1136–1154, https://doi.org/10.1175/WAF-D-11-00116.1.

Trapp, R. J., G. R. Marion, and S. W. Nesbitt, 2017: The Regulation of Tornado Intensity by Updraft Width. *Journal of the Atmospheric Sciences*, **74 (12)**, 4199–4211, https://doi.org/10.1175/JAS-D-16-0331.1.

Trapp, R. J., S. A. Tessendorf, E. S. Godfrey, and H. E. Brooks, 2005: Tornadoes from Squall Lines and Bow Echoes. Part I: Climatological Distribution. *Weather and Forecasting*, **20 (1)**, 23–34, https://doi.org/10.1175/WAF-835.1.

Trier, S. B., G. S. Romine, D. A. Ahijevych, R. A. Sobash, and M. B. Chasteen, 2021: Relationship of Convection Initiation and Subsequent Storm Strength to Ensemble Simulated Environmental Conditions during IOP3b of VORTEX Southeast 2017. *Monthly Weather Review*, **149 (10)**, 3265–3287, https://doi.org/10.1175/MWR-D-21-0111.1, URL https://journals.ametsoc.org/view/journals/mwre/149/10/MWR-D-21-0111.1.xml.

Turner, D. D., and W. G. Blumberg, 2019: Improvements to the AERIoe Thermodynamic Profile Retrieval Algorithm. *IEEE Journal of Selected Topics in Applied Earth Observations and Remote Sensing*, **12 (5)**, 1339–1354, https://doi.org/10.1109/JSTARS.2018.2874968, URL https://ieeexplore.ieee.org/document/8576572.

Wade, A. R., M. C. Coniglio, and C. L. Ziegler, 2018: Comparison of Near- and Far-Field Supercell Inflow Environments Using Radiosonde Observations. *Monthly Weather Review*, **146 (8)**, 2403–2415, https://doi.org/10.1175/MWR-D-17-0276.1.

Wade, A. R., I. L. Jirak, and A. W. Lyza, 2023a: Regional and Seasonal Biases in Convection-Allowing Model Forecasts of Near-Surface Temperature and

Moisture. *Weather and Forecasting*, **38 (12)**, 2415–2426, https://doi.org/10.1175/WAF-D-23-0120.1, URL https://journals.ametsoc.org/view/journals/wefo/38/12/WAF-D-23-0120.1.xml.

Wade, A. R., and M. D. Parker, 2021: Dynamics of Simulated High-Shear, Low-CAPE Supercells. *Journal of the Atmospheric Sciences*, **78 (5)**, 1389–1410, https://doi.org/10.1175/JAS-D-20-0117.1, URL https://journals.ametsoc.org/view/journals/atsc/78/5/JAS-D-20-0117.1.xml.

Wade, A. R., B. J. Squitieri, and I. L. Jirak, 2023b: 27-Year Climatology of Severe Wind-Producing Mesoscale Convective Systems in the United States. AMS, URL https://ams.confex.com/ams/WAFNWPMS/webprogram/Paper425233.html.

Wagner, T. J., P. M. Klein, and D. D. Turner, 2019: A New Generation of Ground-Based Mobile Platforms for Active and Passive Profiling of the Boundary Layer. *Bulletin of the American Meteorological Society*, **100 (1)**, 137–153, https://doi.org/10.1175/BAMS-D-17-0165.1, URL https://journals.ametsoc.org/view/journals/bams/100/1/bams-d-17-0165.1.xml.

Warren, R. A., H. Richter, and R. L. Thompson, 2021: Spectrum of Near-Storm Environments for Significant Severe Right-Moving Supercells in the Contiguous United States. https://doi.org/10.1175/MWR-D-21-0006.1, URL https://journals.ametsoc.org/view/journals/mwre/149/10/MWR-D-21-0006.1.xml.

Weisman, M. L., and J. B. Klemp, 1982: The Dependence of Numerically Simulated Convective Storms on Vertical Wind Shear and Buoyancy. *Monthly Weather Review*, **110 (6)**, 504–520, https://doi.org/10.1175/1520-0493(1982)110⟨0504:TDONSC⟩2.0.CO;2.

Weisman, M. L., and J. B. Klemp, 1984: The Structure and Classification of Numerically Simulated Convective Stormsin Directionally Varying Wind Shears. *Monthly Weather Review*, **112 (12)**, 2479–2498, https://doi.org/10.1175/1520-0493(1984)112⟨2479:TSACON⟩2.0.CO;2.

Weisman, M. L., and R. J. Trapp, 2003: Low-Level Mesovortices within Squall Lines and Bow Echoes. Part I: Overview and Dependence on Environmental Shear. *Monthly Weather Review*, **131 (11)**, 2779–2803, https://doi.org/10.1175/1520-0493(2003)131⟨2779:LMWSLA⟩2.0.CO;2, URL https://journals.ametsoc.org/view/journals/mwre/131/11/1520-0493_2003_131_2779_lmwsla_2.0.co_2.xml.